EVALUATING THE REPEATABILITY OF FRICTION AND WEAR TESTING ON A LUBRICANT WITH DISPERSED HEXAGONAL-BORON NITRIDE NANOPARTICLES.

Howard Benadé

© University of Pretoria

EVALUATING THE REPEATABILITY OF FRICTION AND WEAR TESTING ON A LUBRICANT WITH DISPERSED HEXAGONAL-BORON NITRIDE NANOPARTICLES.

By

Howard Benadé

A dissertation submitted in partial fulfilment of the requirements of the degree

Master of Engineering (Chemical Engineering)

In the

Department of Chemical Engineering

University of Pretoria

Pretoria

1 March 2015

© University of Pretoria

EVALUATING THE REPEATABILITY OF FRICTION AND WEAR TESTING ON A LUBRICANT WITH DISPERSED HEXAGONAL-BORON NITRIDE NANOPARTICLES.

Synopsis

The SRV test rig was used to evaluate the friction and wear properties of a lubricant in a laboratory setup. Normally, the coefficient of friction and the amount of wear that occurred are measured while the wear scar surface is also evaluated. Special attention was paid to factors that affect the repeatability.

The test fluid was subjected to a friction and wear test on the SRV test rig in order to determine what factors affect the repeatability of the coefficient of friction, the amount of wear that occurred and the wear scar appearance. The test fluid used was based on rapeseed oil and white mineral oil. The fluid also contained an extreme pressure additive in the form of sulphurised ester. This was also compared for the same test fluid with dispersed hexagonal-boron nitride (h-BN) nanoparticles.

The standard test method as described by ASTM D 6425, was used as test method. Instead of the standard temperature, the block temperature was increased to 100 °C in order to simulate harsher operating environments. The load was set at 200 N

It was found that:

- The rapid load increase from 50 to 200 N at the end of the running-in period (as described in the standard test method) caused poor repeatability. The test was modified with a more gradual load application for the duration of the running-in period (30 N/min), which resulted in improvement in the repeatability of the tests conducted.
- The moisture content in the atmosphere also affected the repeatability of the friction and wear tests. This was most likely due to the formation of a corrosion layer that involves water and by keeping the relative humidity constant, a further improvement in the repeatability was observed.

© University of Pretoria

- The addition of the h-BN nanoparticles resulted in an improvement of the repeatability of the coefficient of friction (COF), wear scar surface (WSS) and wear scar volume (WSV), since the wear scar surfaces indicated that the particles remove the corrosion layers. This could have led to more consistent wear surfaces for the duration of the test.
- The particles also influenced the corrosion layer formation. For both fluids, Raman spectroscopy indicated that greigite (Fe_3S_4) and goethite (α-FeOOH) were found on the surface, while additional corrosion products were found on the wear scar surface for the test fluid with dispersed particles. These compounds were melanterite ($FeSO_4.7H_2O$) and rozenite ($FeSO_4.4H_2O$). All these corrosion products were most likely formed due to the reaction of iron from the specimens with sulphurised esters in the test fluid.

KEYWORDS: hexagonal-boron nitride (h-BN), nanoparticles, dispersion, repeatability, friction and wear, SRV test rig, lubricant.

© University of Pretoria

Acknowledgements

I would like to thank Producut Lubrication Technologies for the unlimited supply of metal working fluid as well as the donation of the nanoparticles.

I would also like to thank Mr. Eben du Plessis for his guidance and mentorship prior and during the project and without whom; I would not have considered continuing with my post graduate studies.

I also want to thank Dr. Heidi Rolfes for all the inputs and guidance with regard to particle dispersions. I would also like to thank her for the use of the Emulsion Laboratory at the University of Pretoria.

Finally, I would like to thank my study leader, Prof. Philip de Vaal, for the opportunity to complete my master's degree. I would also like to thank him for his guidance and patience during the project.

© University of Pretoria

Contents

Synopsis iii
Nomenclature viii
1 Introduction 1
2 Literature 4
2.1. Lubricant Evaluation 4
2.2. Running-in 7
2.3. Lubricating Regimes 8
2.4. Functions of Lubricants 10
2.4.1. Control of Friction 10
2.4.2. Control of Wear 11
2.4.3. Control of Temperature 12
2.5. Metal Working Fluids 13
2.5.1. Base Fluids 14
2.5.2. Additives 16
2.6. Corrosion during Wear 17
2.7. Properties of particles that Affect Friction and Wear 18
2.7.1. Composition and Structure of particle 18
2.7.2. particle Size 22
2.7.3. particle Concentration 23
2.8. Operating Conditions that Affect Friction and Wear 24
2.8.1. Temperature 25
2.8.2. Load Carrying capacity 26
2.8.3. Composition of Opposing Bodies 29
2.9. Lubricating Mechanism of Nanofluids 31
2.10. Boron Nitride as a Lubricant Additive 36
2.11. Nanoparticle dispersions 37
2.11.1. Dispersions 37
2.11.2. Dispersion of nanoparticles 39
2.11.3. Viscosity 40
3. Experimental 43
3.1. Dispersion of Nanoparticles 43
3.1.1. Apparatus: Dispersion 44
3.1.1.1. Ultrasonic Cleaner 45
3.1.1.2. Viscometer 46
3.1.1.3. Zeta Sizer 47
3.1.1.4. Thermogravimetric Analysis (TGA) 48
3.1.2. Measured variables: Dispersion 49
3.1.3. Method: Dispersion 50
3.2. Friction and wear testing 50
3.2.1. Apparatus: Friction and wear testing 50
3.2.1.1. Friction and wear testing rig: SRV 51

© University of Pretoria

3.2.1.2. Surface analysis: raman spectroscopy 52
3.2.2. Measured variables: Friction and wear testing 52
3.2.3. Method: Friction and wear testing 53
4. Results 57
4.1. Physical properties 57
4.1.1. Physical properties: lubricating fluid 57
4.1.2. Particle size analysis: boron nitride nanoparticles 60
4.2. Dispersion of particles 61
4.2.1. Dispersant screening 61
4.2.2. Dispersant optimization 63
4.2.3. Verification: Zeta sizing 64
4.3. Dispersion stability 65
4.4. Repeatability of friction and wear testing with Test fluid without particles. 66
4.4.1. Standard test method. 66
4.4.2. Modified test method. 70
4.4.3. Surface analysis. 74
4.4.4. Modified test method with constant humidity 77
4.5. Repeatability of friction and wear testing of test fluid with particles 83
4.5.1. Standard test method 83
4.5.2. Surface analysis 86
4.5.3. Modified test method with constant humidity 89
4.6. Influence on Repeatability with addition of particles 92
5. Conclusions and Recommendations 97
5.1. Physical Properties 97
5.2. Particle Dispersion 97
5.3. Friction and Wear Testing 97
6. References 100
Appendix A: Dispersions 107
A.1. Dispersion Formation: Comminution 109
A.2. Dispersion Formation Mechanism 112
A2.1. Surface Wetting 112
A.2.2.2. Stability of Dispersions 117
A.2.2.3. the Electric Double Layer 118
A.2.2.4. Deryaguin-Landau-Verwey-Overbeek Theory 119
A.2.2.4. Theories of Colloid Stability. 125
A.3. References 130
Appendix B: Dispersion Preparation Methodology 131

© University of Pretoria

Nomenclature

d_1:	Diameter of wear scar parallel to the sliding direction	meter
d_2:	Diameter of wear scar perpendicular to the sliding direction	meter
H_R:	Relative humidity	
F_F:	Force required to initiate motion	Newton
F_N:	Normal load	Newton
P_w:	Partial Pressure of water vapour	Pascal
P^*:	Vapour Pressure	Pascal
R:	The initial radius of the ball	meter
R':	The resulting radius of the shape of the wear scar	meter
T:	Temperature	Kelvin
V_{cap}:	The wear volume determined for spherical specimens	meter^3

Greek

η:	Fluid viscosity	kilogram/meter.second
μ:	Coefficient of friction	
ν:	Sliding speed	Oscillations/second

© University of Pretoria

1 Introduction

Background

Due to the continuous improvement of lubricants, simple test specifications became inadequate to differentiate between good and poor lubricants. Test methods on a laboratory scale that are able to determine the friction and wear properties within a reasonable period had to be developed. This is due to operational tests being too expensive with too many variables that could lead to uncertainty (Pugh, 1973: 173).
A number of test methods to determine the friction and wear properties of a lubricant were developed and are described by standard test procedures. The test method for the evaluation of the friction and wear properties of lubricating oils on the SRV test rig is described by ASTM D 6425, DIN 51834 and DIN ISO 9003.

Biodegradable lubricants such as plant oils have also been considered and developed, mainly due to environmental concerns (Bhushan & Nosonovsky, 2012: 8). Furthermore, lubricants must also comply with stricter lubrication requirements, due to metal working machines that have become more advanced. These fluids must be able to withstand higher temperatures and higher loads. This can be provided by the addition of particles (Chang et.al., 2009).

Bartz, 1971, discovered that finer particles have better friction and wear properties than larger particles. He also found that as the load increases, the effect of particle size becomes more pronounced. The particle sizes used in the study by Bartz, 1971 were micro-meter sized particles, but Bhimaraj et.al., 2008 also confirmed improved friction and wear properties for finer particles when nano-meter sized particles were used.

Hexagonal-boron nitride particles have been used as a potential lubricant additive and showed promising results at elevated temperatures (Atnafu et.al., 2009 and Kimura et.al., 1999), due to its high thermal stability (Bernard et.al., 2011). Hexagonal-boron nitride also has a layered structure, similar to graphite and

© University of Pretoria

molybdenum disulfide, both of which are good solid lubricants. It is also considered as a clean lubricant, since it does not contain any sulphur (Kimura et.al., 1999).

Problem Statement

As already mentioned there is a demand for stricter lubrication requirements, due to metal working machines that become more advanced, (Chang et.al., 2009). However, in order to evaluate and compare lubricants a reliable test method that produces repeatable results is required. It has been reported that repeatability is influenced by factors such as the humidity, especially when the amount of wear is considered (Klaffe, 1995). The specification regarding repeatability described in the standard test method (ASTM D 6425), allows for considerable deviation with regard to repeatability. In this investigation it was attempted to investigate test refinements so as to improve repeatability.

At the completion of the running-in period of the standard test method, the load is rapidly increased from 50N to 200N. Since the purpose of the running-in period is to conform the contacting surfaces with each other (Dias et.al., 2002), the possible effect of this sudden load increase on the repeatability of the friction and wear results is uncertain and needed further investigation.

During friction and wear testing of a fluid containing particles, the consistency of the fluid is important in order to produce repeatable results. One of the biggest problems is that particles tend to form clusters when dispersed (Parfitt, 1973: 10). This is especially problematic when particles are dispersed in lubricants, since the particles tend to settle out and an effective dispersing agent is required (Atnafu et.al., 2009).

Objectives

The objectives of this study were to identify what factors affect the repeatability of the friction and wear testing results of lubricants, and if the repeatability can be improved. The effect on the repeatability due to the presence of particles in a lubricant was also determined.

© University of Pretoria

However, since particles were added to test fluid, a dispersion that provided adequate stability for the duration of the test was also required. For this an environmentally friendly dispersing agent had to be identified that prohibits the formation of particle clusters.

Method, Scope and Limitations

The Optimol SRV test rig was used as bench test for the friction and wear tests. The Malvern Zeta sizer was used to determine the particle size distribution over time to verify that the particles do not form clusters.

The test fluid was an environmentally friendly metal working fluid based on rapeseed oil and white mineral oil. It also contained sulphurised esters as extreme pressure additives. Hexagonal-boron nitride nanoparticles were also dispersed in the fluid to form a nanofluid. The nanofluid was also evaluated on the SRV test rig.

The friction and wear test was based on the standard test method as described in ASTM D 6425. Here, however, the SRV block temperature was 100 °C and the load 200 N. The variables that were measured were the coefficient of friction and the wear volume, while wear scar surface was also evaluated.

© University of Pretoria

2 Literature

The literature section includes theory regarding the basics of lubrication and functions of lubricants. The importance of the running-in period is also discussed as well as the role of additives, such as nanoparticle additives. Furthermore, the dispersion of particles is also an important topic and is covered in brief, as well as in Appendix A.

2.1. LUBRICANT EVALUATION

As lubricants improved, simple specification tests became inadequate to differentiate between different products. Tests on a laboratory scale that were able to determine the lubricating properties had to be developed as a tool. These tests had to be done on a laboratory scale, since operational tests are too expensive and there are too many variables involved that leads to uncertainty (Pugh, 1973: 173).

The laboratory tests are used for screening of materials, coatings and surface treatment during development in order to differentiate and rank candidate materials. These tests can be classified into two general categories i.e. physical and chemical examinations and friction and wear tests (Bhushan & Gupta, 1991: 15.1).

Physical and chemical examinations are conducted to ensure that the lubricant, coating or material complies with the specifications. These examinations include thermal stability, oxidative stability, rust and corrosion prevention as well as coating related measurements. It also includes determination of material properties such as hardness and surface properties (Bhushan & Gupta, 1991: 15.1).

Friction and wear testing are used as screening methods in order to rank different materials and products. This will aid in the selection of the material or lubricant for a specific application. These tests are accelerated tests that are inexpensive and should accurately simulate the behaviour of the actual system (Bhushan & Gupta, 1991: 15.59).

© University of Pretoria

Friction and wear tests make use of a contact between two specimens and can be further categorized in three contact classes; point contact (ball-on-disc), line on disc (cylinder-on-disc) and conforming contact (flat-on-flat). However, there are other factors beside the contact type that will influence test and consequently determine whether a simulation is representative. These factors are the type of motion, load, speed and operating environment (Bhushan & Gupta, 1991: 15.59).

The type of motion can be sliding, rolling, spinning or impact and can be unidirectional or oscillating. The load can be applied as a dead mass either as a static load or a dynamic load, depending on the application. Finally the operating environment includes the level of contamination, lubricant, temperature and the humidity of the ambient environment (Bhushan & Gupta, 1991: 15.59).

During friction and wear testing, the coefficient of friction is one of the most important variables to determine, since this is an indication of how the lubricant performs by reducing friction (Mortier and Orszulik, 1997: 181-182). This is measured as the ratio of the friction force to the applied normal force.

The other variable of considerable importance is the measurement of the amount of wear that occurred. This can be measured as the mass loss, volume loss or displacement scar width.

Wear can also be determined by indirect means such as the change of surface finish. Olah et.al., 2005, investigated wear scar surfaces to determine the performance of the lubricant. This was done due to technical failures caused by insufficient lubrication in spite of good results obtained with the HFRR (high frequency reciprocating rig) test rig (point contact configuration).

Even though the wear scar diameters obtained with the HFRR were within the specified limitations, failures still occurred. This led to the inspection of the surface of the wear scars, and it was found that the test comprises of more information of a fluid's lubricating properties than can be obtained from the diameter of the wear scar.

© University of Pretoria

The surface finish of the wear specimens also plays an important role, and a 6-graded visual rating was defined based upon the appearance of the scars. This is also referred to as the complementary rating (CR) and scars obtained from ball-on-disc friction and wear tests are compared to these scars and a CR value assigned. The scars to be used as reference are shown in Figure 2.1.1.

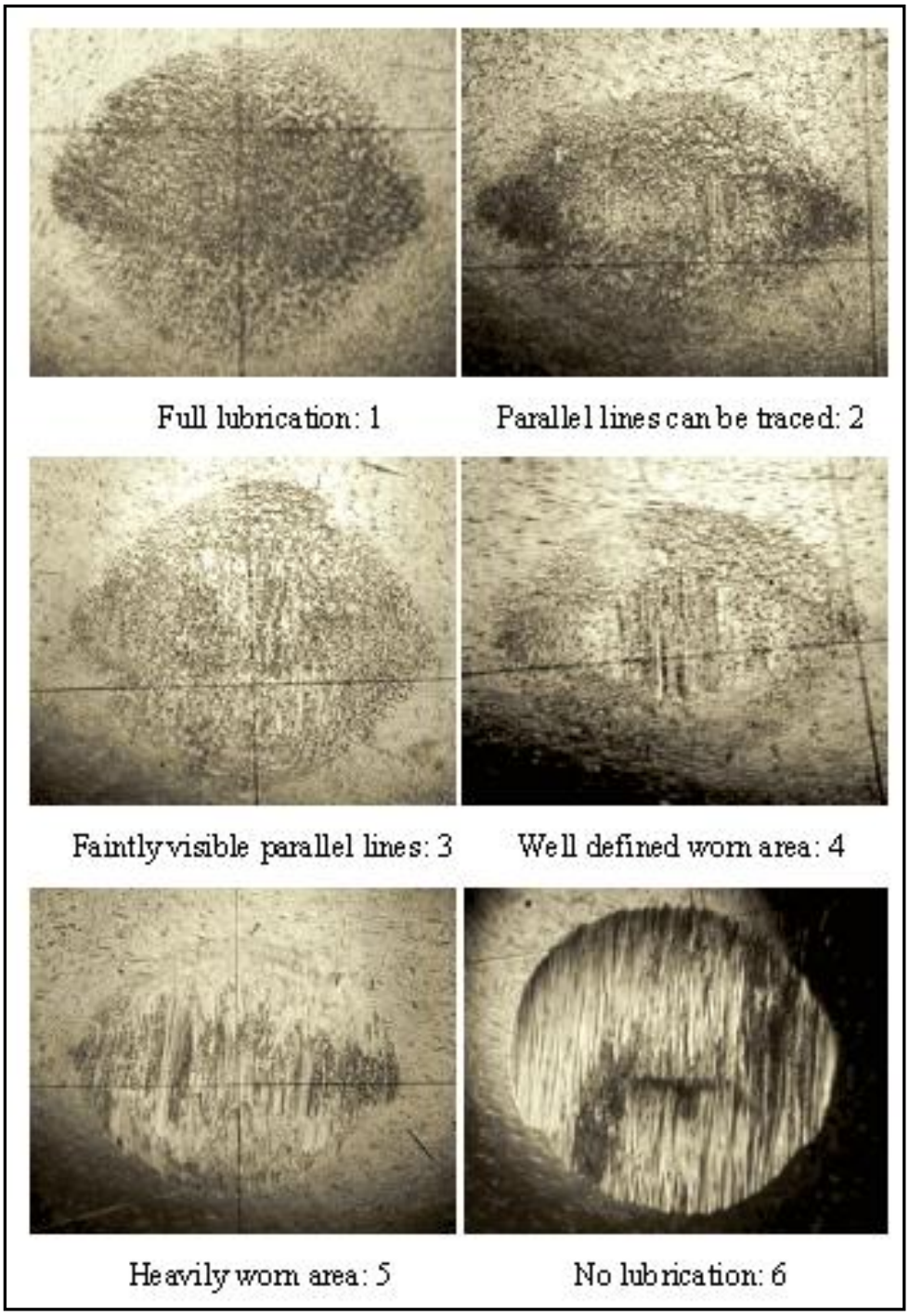

Figure 2.1.1: Wear scars used as reference for the complementary rating as obtained by the HFRR test procedure.

© University of Pretoria

2.2. RUNNING-IN

Running-in, also referred to as break-in, is defined by ASTM D 5707 and D 6425 as "an initial transition process occurring in newly established wearing contacts, often accompanied by transients in coefficient of friction or wear rate, or both, which are uncharacteristic of the given tribological system's long term behaviour".

As the definition suggests, the purpose of the running-in period is to conform two surfaces to each other. This is due to two surfaces not being completely flat, as indicated in Figure 2.2.1. Running-in involves smoothing the heights of the highest asperities and thereby increasing the number of asperities in contact (Dias et.al., 2002).

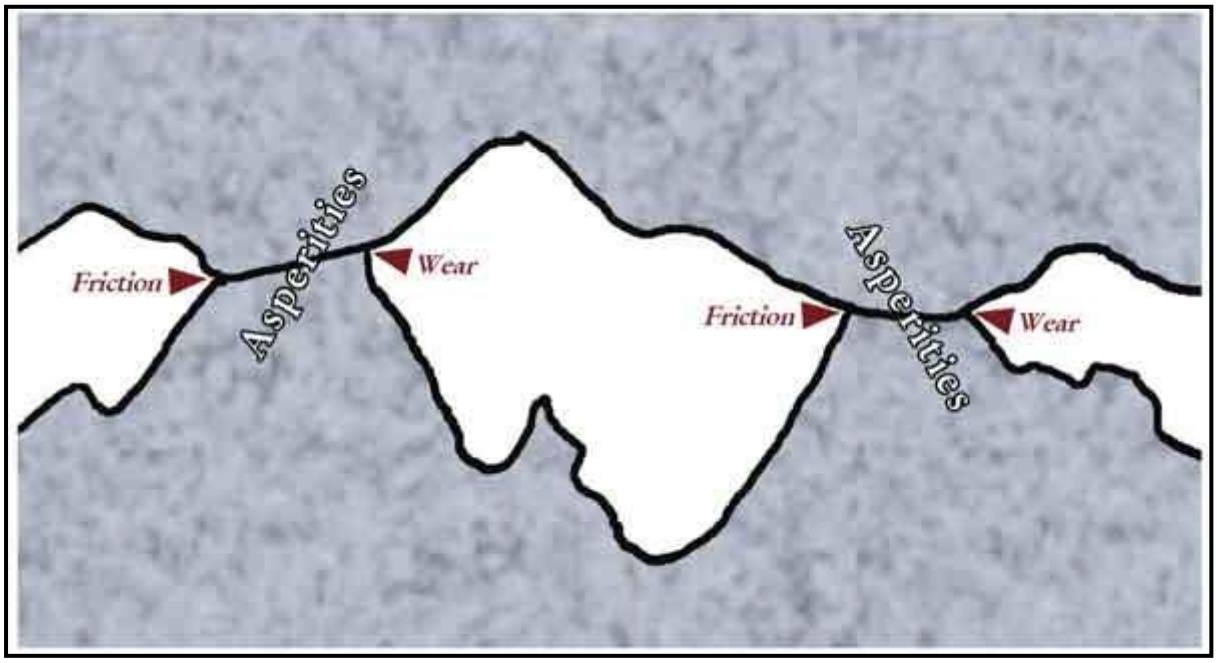

Figure 2.2.1: Diagram of surface asperities in contact (US Synthetic Bearings and US Synthetic Corp, 2014).

For practical applications, the running-in period is important since it affects the effective operation and life time of tribological components (Kumar et.al., 2002). For example, if the initial surface roughness of two rubbing surfaces is correctly chosen, the system will reach a steady state where the surfaces are smoother with a low wear rate that is constant (Dias et.al., 2002).

© University of Pretoria

It is also of importance to be able to determine when the running-in period is completed. The criteria involve stable roughness, stable friction and stable wear. The typical wear behaviour of new components in their life span is given in Figure 2.2.2.

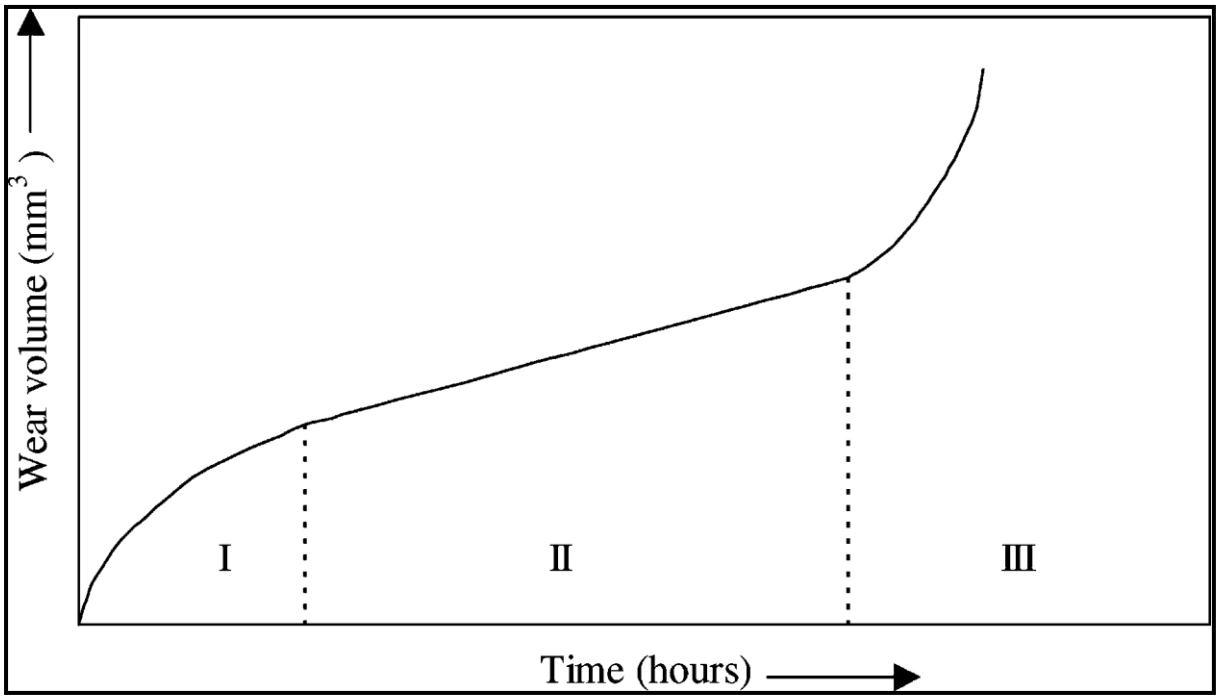

Figure 2.2.2: Wear behaviour of a new component in its life span. (I) Running-in zone; (II) steady-state wear zone; (III) wear out zone (Kumar et.al., 2002).

The running-in period is therefore important, since it affects the lifetime of components. The surface geometry of components (microgeometry) is also important, since this will influence the conformity with which the surfaces adapt to each other. This is an important factor in the reaching of steady state wear and consequently also the lifetime of components.

2.3. LUBRICATING REGIMES

Lubricating regimes can be described by the Stribeck diagram, as shown in Figure 2.3.1, where each regime has its own frictional behaviour. The coefficient of friction is expressed as a function of the lubricant viscosity, sliding velocity and normal force or as a function of the lubricant properties, geometry of the metal surfaces and the operating conditions (Bhushan & Gupta, 1991: 2.30).

© University of Pretoria

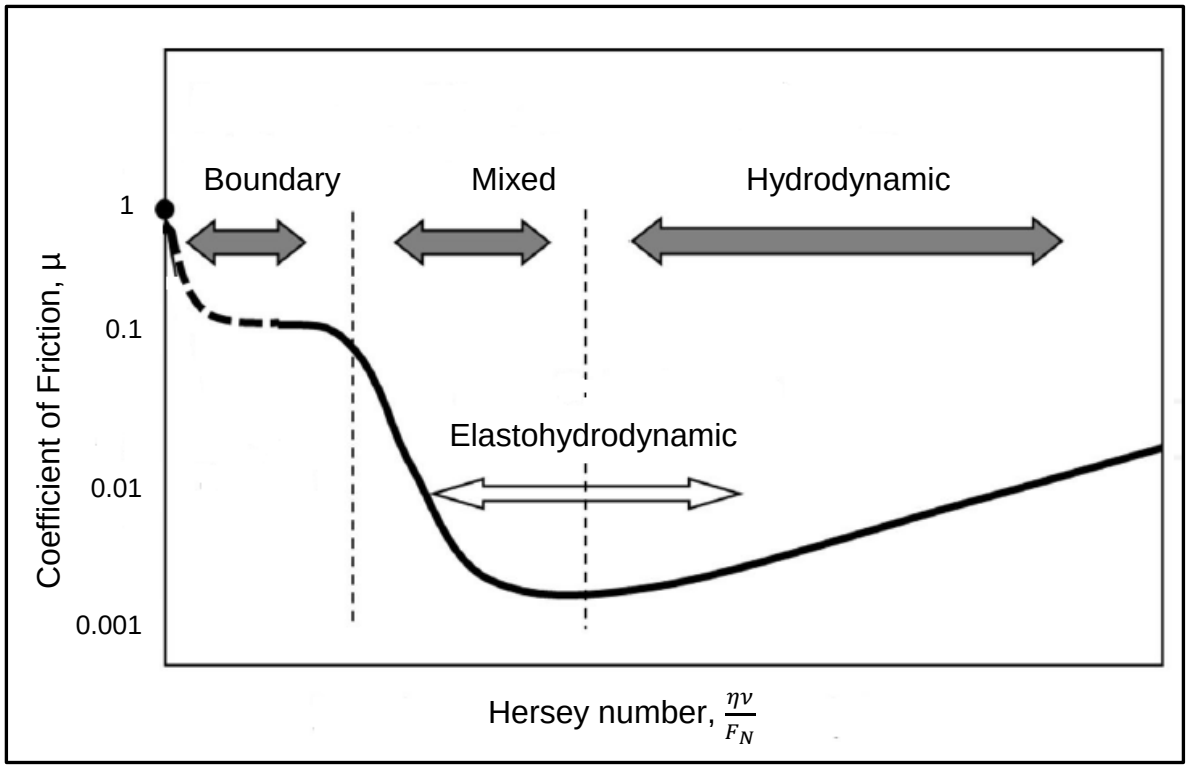

Figure 2.3.1: Stribeck diagram of lubricating regimes, where μ is the coefficient of friction, η is the viscocity, v is the sliding speed and F_N is the normal force (Hamrock et.al., 2004: 20: 18).

The lubrication regimes are:

- Hydrodynamic lubrication
- Elastohydrodynamic lubrication
- Mixed lubrication
- Boundary lubrication

For this investigation, only the boundary lubrication regime is of importance and will be discussed. This is where the contacting solids move so close to each other that there is considerable asperity interaction. This can lead to asperity welding. To inhibit asperity welding, a thin film of lubricant is adsorbed onto the surface of the solid (Bhushan & Gupta, 1991: 2.35). This film is thinner than the surface roughness with the thickness in the order of molecular dimensions (Hamrock et.al., 2004: 8-9). The lubricant properties are then considered to be different when compared to bulk lubrication (Hersey, 1966: 437) and the thickness varies from 5 nm to 100nm (Bhushan & Gupta; 1991: 2.32).

© University of Pretoria

Boundary lubricants must consist of materials that can satisfy the requirements for lubrication with one or two molecular layers. Some of these materials are found in most natural oils and petroleum lubricants. The amount of boundary additives required in an industrial lubricant ranges from 0.1 to 0.5 % (Hamrock et.al., 2004: 9).

Boundary lubricants are in addition classified as either organic or inorganic. This classification depends on the chemical group that provides the lubrication. This means that an organic molecule with an inorganic lubrication group will be classified as an inorganic lubricant (Hamrock et.al., 2004: 10). Organic boundary lubricants are typically fatty acids and esters. Both are long chain molecules with polar ends that bond to the metal surface.

Inorganic boundary lubricants are compounds that contain chlorine, phosphorus, sulphur and iodine. As opposed to organic lubricants that decompose at temperatures above 200 °C, inorganic lubricants can provide effective boundary lubrication up to 700 °C. For example CuCl or $CuCl_2$ will form on copper alloys if chlorine-containing materials are used. This will provide effective lubrication up to 800 °C (Hamrock et.al., 2004: 11-12).

2.4. FUNCTIONS OF LUBRICANTS

2.4.1. CONTROL OF FRICTION

Friction is the resistance to relative motion between two opposing bodies. This is the principal cause of wear and energy dissipation. Energy consumption can be reduced by reducing friction (Batchelor & Stachowiak, 2001: 2), which can be achieved by adding suitable lubricants to unlubricated systems, or to add suitable additives to lubricants to improve lubricant performance.

Friction can be quantified by the coefficient of friction, which is the ratio of the force required to initiate motion tangential to the contacting surfaces divided by the normal load, as can be seen in equation 2.4.1 (Bhushan & Gupta, 1991: 2.1):

© University of Pretoria

$$\mu = \frac{F_F}{F_N} \qquad 2.4.1.$$

Where μ is the coefficient of friction, F_F is the force required to initiate motion (N) and F_N is the normal load (N).

Furthermore, fluid lubricants can operate in any of the regimes listed in section 2.3. In each of these regimes, the mechanism of controlling the friction differs and is related to the distances separating the opposing bodies (Boyd & O'Connor, 1968: 1-2).

In the boundary lubricating regime, the effect of the bulk properties of the fluid is minimal and the friction improvement depends more on the interface properties of the lubricant. The lubricant properties can be improved by the addition of additives. The additives can either adsorb onto the surface or react with the surface (Mortier & Orszulik, 1997: 335) to form a layer that prohibits metal to metal contact. The effect on friction control therefore depends on the reactivity of the rubbing surfaces, the reactivity of the additives and the decomposition temperatures of the end products of these reactions.

2.4.2. CONTROL OF WEAR

Wear is the removal of material from solid surfaces and can occur when two surfaces are in sliding or rolling motion relative to one another (Bhushan & Gupta, 1991: 2.10). The three types of wear mentioned below are the main types of wear that occur in lubricated systems.

Adhesive wear (also galling or scuffing) is adhesion of surfaces due to plastic deformation of asperity contacts (junctions) caused by applied load. This can result in cold welding of the junctions, which are sheared during the sliding motion of the surfaces. In this way new junctions are formed and generation of wear particles take place (Bhushan & Gupta, 1991: 2.13-17).

Abrasive wear (scratching, scoring or gouging) is damage to a surface by a harder material. It can be caused by one of the surfaces being harder than the other or due

© University of Pretoria

to a third body. This is normally a small particle of grit or abrasive that is caught between the surfaces. For this type of wear, asperities of the harder surface press into the softer surface and plastic flow occurs in the softer surface around the asperity. When a tangential motion is imposed, material is removed from the softer surface by microploughing, microcutting and microcracking (Boyd & O'Connor, 1968: 10-3).

Corrosive wear: due to dynamic interaction with the environment. With this type of wear, reaction products are formed at the surface, which are then removed due to abrasion or crack formation. This is followed again by product formation and subsequent removal of the product (Bhushan & Gupta, 1991: 2.20-21). This type of wear is loss of material due to chemical reaction (Mortier & Orszulik, 1997: 324).

The lubricant must therefore be designed to reduce each type of wear. For instance, the flushing action of liquids enables the lubricant to remove potentially harmful particles and to reduce abrasive wear.

In the case of adhesive wear in the boundary lubrication regime, the chemical nature of the lubricant affects its performance. This is determined by the ability of the lubricant to form a film and consequently prevent metal to metal contact (Mortier & Orszulik, 1997: 325-328).

Finally, corrosion can be minimized by proper refinement of the lubricant and with the addition of oxidation inhibitors. However, in some instances, corrosion is desirable. This is in systems where additives are added to react with the surface in order to form a protective film, such as extreme pressure additives (Ludema, 1996: 160-161 and Mortier & Orszulik, 1997: 335).

2.4.3. CONTROL OF TEMPERATURE

In a tribological system, heat is generated due to the work required to overcome friction. This is due to internal friction within the liquid and due to metal to metal

© University of Pretoria

contact. In low-friction fluid systems, the frictional heat is low, while in boundary lubrication the temperature is much higher. This is due to metal to metal contact and the temperatures can approach the melting point of the metal (Boyd & O'Connor, 1968: 10-4).

High temperatures accelerate the rate of oxidation and this can greatly influence corrosive wear. This also causes the lubricant to oxidize and prevent effective lubrication (Hamrock, Jacobson and Schmid, 2004: 105 -106). Furthermore, a rise in temperature will influence metal cutting operations. For example, the dimensional accuracy will be greatly reduced as well as the tool life (Kalpakjian & Schmid, 2006: 609).

In order to control the temperature, a lubricant must be able to control the absorbed heat and to transmit it to the cooler parts of the media. Furthermore, temperature is is reduced due to reduction of friction (Mortier & Orszulik, 1997: 67).

2.5. METAL WORKING FLUIDS

During metal working processes, new surfaces are created when two surfaces, those of the tool and the work piece, are brought into contact. The contact can either be metal flow such as during metal forming processes or controlled removal of excess material, which occurs during metal cutting processes (Mortier & Orszulik, 1997: 251).

These processes involve high friction, high temperatures and tool wear. Consequently, lubricants are added to the process to improve the effectiveness of the metal working operations and the overall efficiency of the manufacturing operation (Mortier & Orszulik, 1997: 251). The main purposes of the fluids are to:

- Cool work piece and tools
- Lubricate tool and chip faces
- Prevent welding of work metal on tools (Boyd & O'Connor, 1968: 23-1).

© University of Pretoria

Metal forming operations allow shape change due the ductility of the metal, while metal cutting involves chip formation and movement of the chip across the face of the tool. Both these processes require lubrication, for example in cold drawing where the fluid must cool dies and work material as well as prevent metal adhesions or welding. In metal cutting operations, the main purpose of the lubricant is to reduce friction and to remove heat as rapidly as possible (Mortier & Orszulik, 1997: 253-254).

For metal forming processes a wide variety of lubricants are used. This is due to the metal compositions that vary and different lubricants or combinations are required. These lubricants include liquid lubricants, pastes, greases, solid lubricants and coatings. Furthermore, the composition of these lubricants includes mineral oils, mineral oils mixed with fatty oils, emulsions, synthetics oils, esters and fatty acids, to name a few (Mortier & Orszulik, 1997: 254).

These lubricants can also be classified into three types which are oils, emulsions and water-based products. Oils are derived from petroleum, vegetable and animal sources and contain various types of additives. Emulsions contain oil that is suspended in water with the aid of an emulsifier and water-based products do not contain oil, but water-soluble chemicals such as glycol, water-soluble polyethers and polyglycols (Mortier & Orszulik, 1997: 257).

Finally, nanometer sized particles can also be added to lubricating fluids in order to improve the fluid's friction and wear properties. Particles are suspended in the fluid with the aid of dispersants. Some of these particles include molybdenum disulfide, tungsten disulfide, graphite and boron nitride (Atnafu et.al., 2009 and Kimura et.al., 1999).

2.5.1. BASE FLUIDS

Base fluids for lubricants can be selected from a range of fluids. These fluids must be able to provide a fluid layer that separates two moving surfaces or removing heat from the contact zone as well as wear particles. One of its most important properties

© University of Pretoria

is also to keep friction at a minimum. Many base fluids consist of crude oil products such as hydrocarbons or organic compounds with ring structures. Vegetable oils can also be used as base fluid (Mortier & Orszulik, 1997: 1).

Vegetable oils (and animal fat) were the main source of lubricants before mineral oil-based products. They were re-introduced as lubricants due to environmental and health and safety issues. Other factors such as changes in economy and supply also played a role (Mortier & Orszulik, 1997: 196).

Vegetable oils are used as additives such as high erucic acid rapeseed oil which is an effective additive in lubricants while jojoba oil is used in high-performance automatic transmission fluids. It can also be used as base fluids for straight cutting oils (Mortier & Orszulik, 1997: 196).

The production of vegetable oils involves the extraction or pressing of the plant tissue. A crude vegetable oil is then obtained where the main component is triglycerides. The triglyceride structure is shown in Figure 2.5.1, which consists of a glycerol with three fatty acids. The fatty acids are usually straight chains with 8 to 22 carbon atoms in the chain. The vegetable oil is then also described in terms of the fatty acid (Mortier & Orszulik, 1997: 196-197).

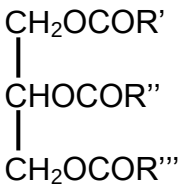

Figure 2.5.1: Triglyceride structure (Mortier & Orszulik, 1997: 197)

Other components such as steroids, pigments and waxes must be removed with purification steps. These purification steps involve free fatty acid removal (refining), colour removal (bleaching), free acid and peroxide removal (deodorization) and wax removal (winterization) (Booser, 1997:103).

© University of Pretoria

Vegetable oils generally have high flashpoints and are viscous with a high viscosity index. Furthermore, their physical and chemical properties depend on the degree of unsaturation of the constituent fatty acids. For instance, a high proportion of saturated fatty acids will result in a solid or semi-solid fat, while double bonds will result in a liquid (Mortier & Orszulik, 1997: 197-199). This is due to the structure of these molecules. Saturated fatty acids have a uniform shape that allows them to pack together efficiently in a crystal lattice. However, the double bonds in unsaturated fatty acids introduce kinks into the hydrocarbon chain, which make crystal formation more difficult (McMurry, 2004: 1030).

Finally, the presence of double bonds has an effect on the oxidative stability, since the methylene groups separating the double bonds are highly reactive. This can be improved with the addition of appropriate additives (Mortier & Orszulik, 1997: 197-199).

White mineral oils can also be used as base fluids. These are oils obtained from additional processing of base oils. White mineral oils are highly refined oils that consist entirely of saturated components. All the aromatic compounds have been removed by treatment with fuming sulphuric acid or by selective hydrogenation. The most highly refined oils are used in medical products and in the food industry (Mortier & Orszulik, 1997: 1).

2.5.2. ADDITIVES

Additives play an important role when the boundary lubrication regime is encountered. In this regime the surface properties become important where the main function of the additives is to control friction and wear. Additives can be selected from a variety of classes. These classes include:

1. *Oxygen containing organic compounds*. These compounds contain polar heads to adsorb at metal surfaces. Examples of these compounds are alcohols, esters and carboxylic acids (Mortier & Orszulik, 1997: 332).

© University of Pretoria

2. *Organic sulphur compounds*. These are molecules that react with the surface in order to form a layer (Mortier & Orszulik, 1997: 332).
3. Organic compounds which contain nitrogen in combination with either oxygen or sulphur (Mortier & Orszulik, 1997: 332).
4. *Organic phosphorus compounds*. These compounds also react with the surface to form a protective layer (Mortier & Orszulik, 1997: 332).
5. *Solid additives*. These are either used in dry powdered form or mixed with oil, synthetic fluids, grease solvents or water (Boyd & O'Connor, 1968: 14-14).

2.6. CORROSION DURING WEAR

In section 2.4.2, one of the properties of a lubricant that was discussed is to prevent the surfaces from reacting with the environment, since this leads to corrosive wear. However, some additives are used in lubricants to specifically react with the surface in order to form a protective layer, such as sulphurised esters (section 2.5.2).

The aim of this section is to cover the products that are possibly formed due to corrosion reactions with metal, but first corrosion will be defined. Corrosion is the undesirable deterioration of a metal or alloy, i.e. an interaction of the metal with its environment that adversely affects those properties of the metal that are to be preserved. This also holds for non-metallic materials and embodies the concept that corrosion is deleterious (Burstein et.al., 1994: 1: 5).

One of the most common metals that is prone to corrosion is steel. The main corrosion reaction of steel is its reaction with oxygen and water in the atmosphere. The overall reaction is shown below.

$$4Fe + 2H_2O + 3O_2 \rightarrow 2Fe_2O_3 \cdot H_2O$$

The products that are formed include Fe (OH)2, Fe3O4, Fe3O4.H2O, Fe2O3.H2O and are loosely adherent and does not form a protective barrier on the metal surface The metal surface is therefore not isolated from the environment and will result in complete consumption of the metal. Iron oxide related corrosion products of metals can be identified by Raman spectroscopy (Bouchard & Smith, 2003).

© University of Pretoria

The corrosive wear that occurs of steel surfaces in a tribological system usually involves the formation of oxide films. For a system with no lubricant, the main products that are formed are mainly magnetite (Fe_3O_4) and hematite (α-Fe_2O_3). It is also possible for these products to form under lubricated conditions, since there is enough oxygen in oil and in water to react with the surface (Quinn, Rowson & Sullivan, 1984). It is also important to remember that the additives in the fluid will also affect the corrosion products. These include organic sulphur and organic nitrogen compounds (Mortier & Orszulik, 1997: 332-335).

Furthermore, it is not only the metal surfaces that are prone to deterioration, but the environment also has an effect on the lubricant and its degradation. The lubricant can either be contaminated or undergo physical and chemical changes due to oxidation (Burstein et.al., 1994: 2: 144-149).

The deterioration of lubricants can be reduced by the use of proper additives. Additives are usually named after their particular function such as anti-oxidants, metal deactivators, corrosion inhibitors, rust inhibitors, water repellants and dispersants (Burstein et.al., 1994: 2: 144-149).

2.7. PROPERTIES OF PARTICLES THAT AFFECT FRICTION AND WEAR

In section 2.5.2, solid additives (also referred to as particle additives) were listed as an additive for liquid lubricants. In this section, the properties of particles that affect the friction and wear behaviour of the liquid lubricant will be discussed.

2.7.1. COMPOSITION AND STRUCTURE OF PARTICLE

Solids such as graphite, boric acid and hexagonal-boron nitride owe their good lubricity to their lamellar structure. Not all solid lubricants, however, have a layered structure. Soft metals such as indium, lead and silver also provide good lubrication, even though they do not have a layered structure. PTFE (polytetrafluoroethylene), a

© University of Pretoria

number of solid oxides and rare earth fluorides also provide good lubrication as well as diamond and diamond-like carbons.

As far as the structure is concerned, Miyake et.al., 1991, compared the tribological properties of cubic, amorphous and hexagonal boron nitride (c-BN, a-BN and h-BN) solid films. Figure 2.7.1 is a comparison of the coefficient of friction of the three different solid films.

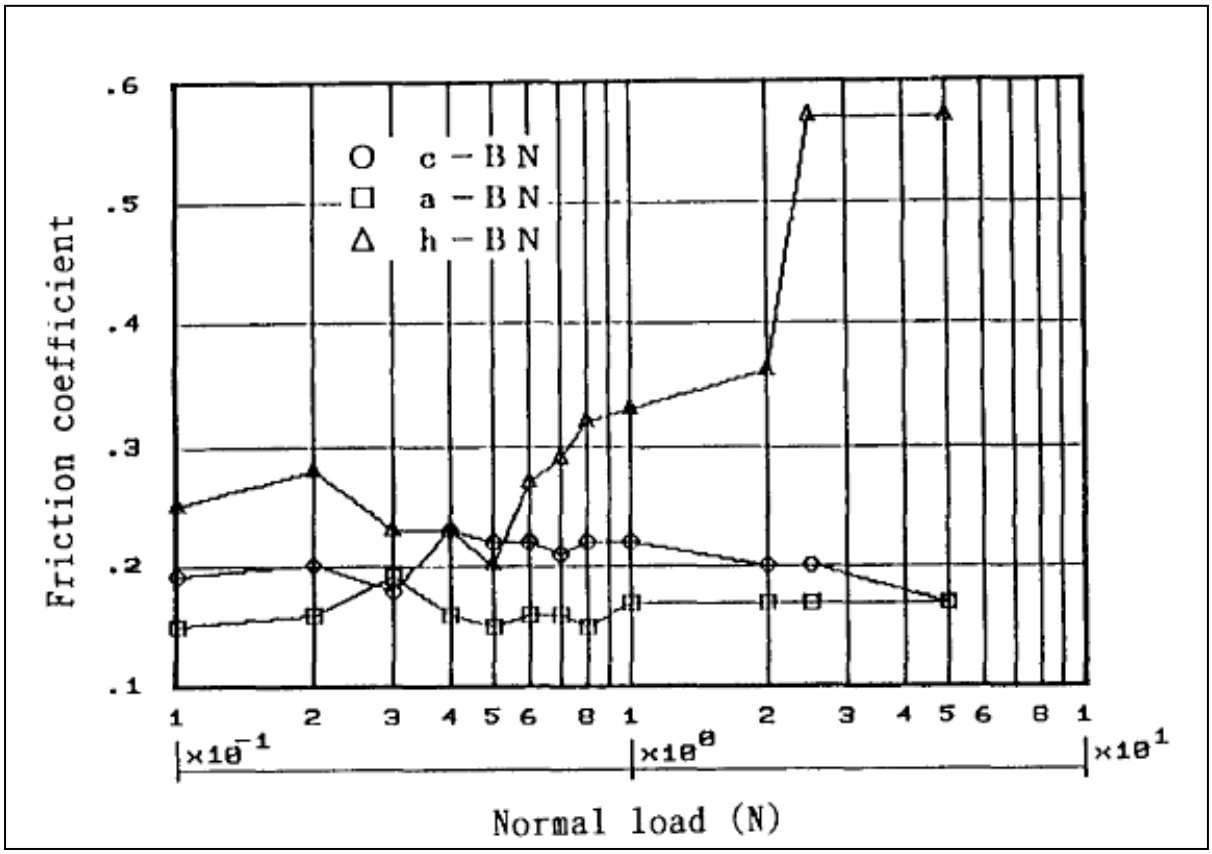

Figure 2.7.1: Comparison of the coefficient of friction obtained for a cubic, amorphous and hexagonal-boron nitride solid film (Miyake et.al., 1991).

From Figure 2.7.1 it can be seen that amorphous and cubic boron nitride resulted in a lower coefficient of friction than hexagonal-boron nitride. Above 0.6 N, the coefficient of friction of h-BN increased, while the coefficient of friction for both c-BN and a-BN decreased slightly or remained constant. This increase for h-BN was due to weaker adhesive properties, causing the protective film to be rubbed away from the contact area.

© University of Pretoria

Chang et.al., 2009, studied the tribological properties of diamond and silicon dioxide nanoparticles added to paraffin. The structure of diamond and SiO_2 are given in Figure 2.7.2.

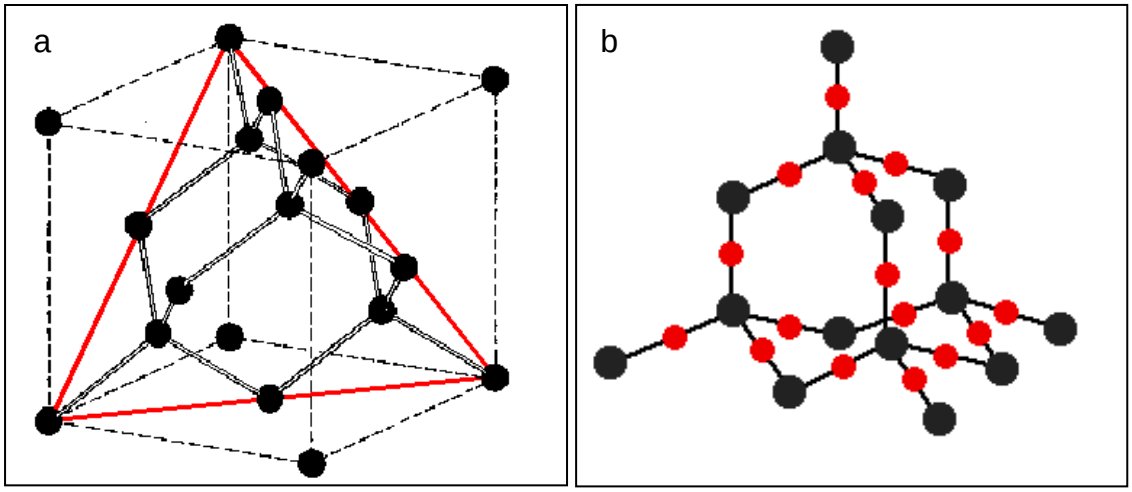

Figure 2.7.2.a: Structure of diamond (Petrovykh, 2008), b: Structure of silicon dioxide (Clark, 2012).

From Figure 2.7.2, it can be seen that both diamond and SiO_2 have structures with an inner hollow sphere. This is known as inorganic fullerene structure. The coefficient of friction obtained from a ball on ring test apparatus (Figure 2.7.3) shows that for both these substances the coefficient of friction was reduced when compared to the coefficient of friction for pure liquid paraffin.

© University of Pretoria

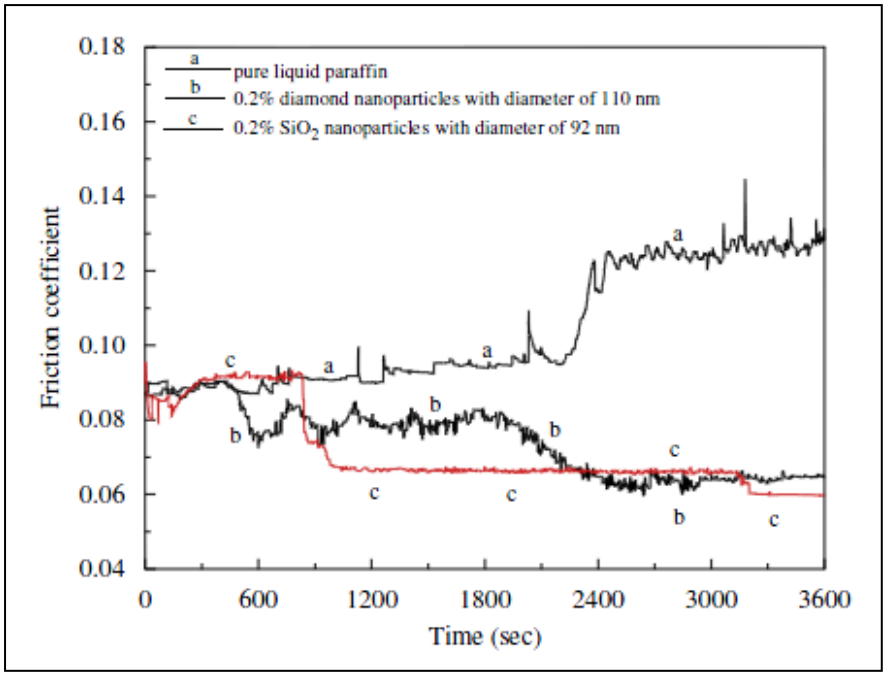

Figure 2.7.3: Coefficient of friction for paraffin, paraffin with diamond fullerene nanoparticles and paraffin with SiO_2 fullerene nanoparticles (Chang et.al., 2009).

In a study on the modification of sheet metal forming fluids with MoS_2, WS_2 and h-BN nanoparticles by Atnafu et.al., 2009, improved friction and wear was also observed. All three these substances have a lamellar structure. The wear plotted as a function of the particle concentration is given in Figure 2.7.4. From this figure it can be seen that the curve for each of the nanoparticles have the same shape, but there are a few differences in the wear behaviour.

© University of Pretoria

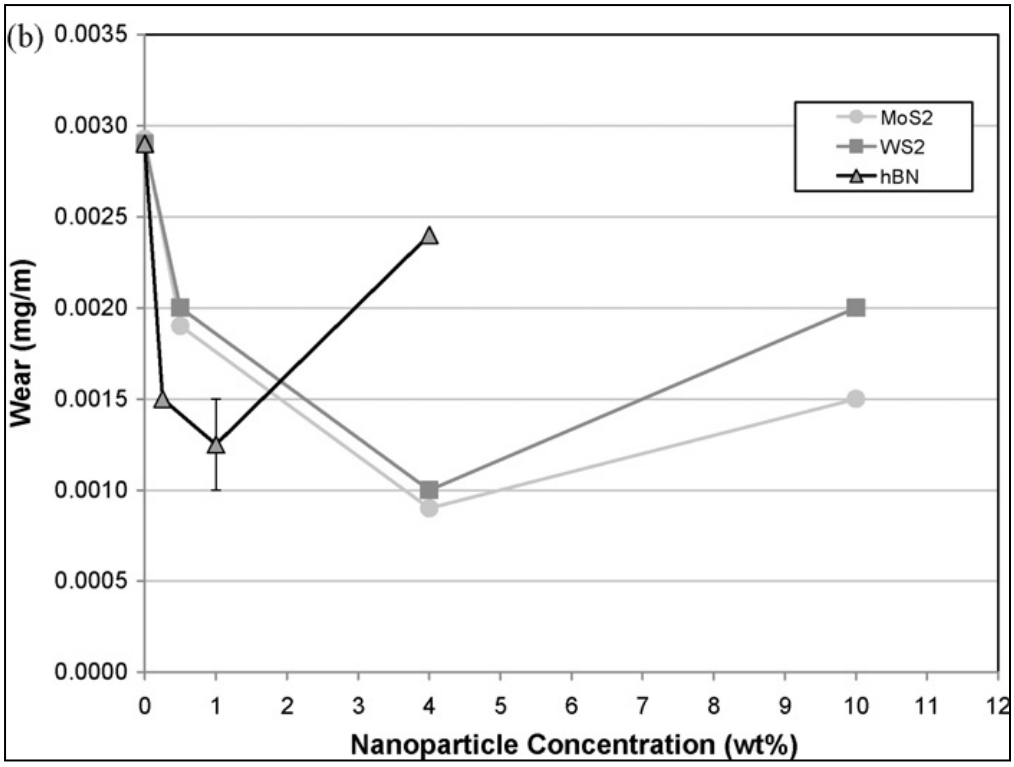

Figure 2.7.4: Wear obtained when sheet metal forming fluids with dispersed MoS_2, WS_2 and h-BN solid particles (Atnafu et.al., 2009).

MoS_2 and WS_2 had similar wear behaviour with a change in particle concentration up to 4 % (mass %). Both had a minimum value at 4 %, after which the wear increased. However, the wear increased at a higher rate for WS_2 than MoS_2. For h-BN, the wear decreased faster, and it reached a minimum value at 1 % (mass). What is also noticeable is that h-BN had poor repeatability at the minimum, which was not observed for MoS_2 and WS_2.

2.7.2. PARTICLE SIZE

Kimura et.al., 1999, examined micron sized boron nitride particles (2.85 µm) as a possible lubricant additive. This was done because boron nitride is considered as a “clean” lubricant, even though graphite and MoS_2 outperforms it as a solid lubricant. From their results, they concluded that boron nitride has lubricating potential for certain applications, which include operations at elevated temperatures. This is due to the high thermal stability of boron nitride.

© University of Pretoria

In the study done by Atnafu et.al., 2009, nanometre size particles, instead of micron sized particles, were used. The size for molybdenum disulphide, tungsten disulphide and hexagonal-boron nitride was 70 to 100 nm, 50 nm and 70 nm respectively. Even though the particles were poorly dispersed (formation of particle agglomerates in dispersion), improvements on the wear of tribological surfaces were also obtained.

The question now arises: What is the effect of particle size? Bartz, 1971, investigated the effect of particle size of MoS_2 with the four-ball test rig. MoS_2 particles were suspended in white oil and four different particle sizes were used: 2, 5, 10 and 15 µm.

It was found in this investigation that the finer particles have better lubricity than the larger particles. It was also found that as the load increases, the effect of particle size becomes more pronounced.

To explain the effect of particle size, it was initially thought that, due to finer powders that have more particles, a continuous film can form on the surface more easily. Surface analysis, however revealed no continuous film and this mechanism fails to explain the effect of particle size.

2.7.3. PARTICLE CONCENTRATION

When particles are dispersed in oils or lubricants (also known as nanofluid), there is usually a concentration at which this dispersion has optimum lubricity. The general trend is that the nanofluid improves the lubricity quite rapidly as the particle concentration in the fluid is increased. This continues until the optimum concentration is reached. When particle concentration is further increased, the wear and coefficient of friction also increase, but at a much slower rate than the initial decrease.

This trend was observed by Chen et.al., 2002. They evaluated the tribological properties of water with acid surface-modified TiO_2 nanoparticles as a lubricant additive. The coefficient of friction decreased rapidly from 0.1 to 0.5 mass % (Figure

© University of Pretoria

2.7.6), after which it seemed to become almost constant. It continued to decrease, but at a much slower rate, until it reached a minimum at 1%.

When the concentration was increased above 1%, the rate at which the coefficient of friction increased was almost the same as the rate between 0.5 and 1%.

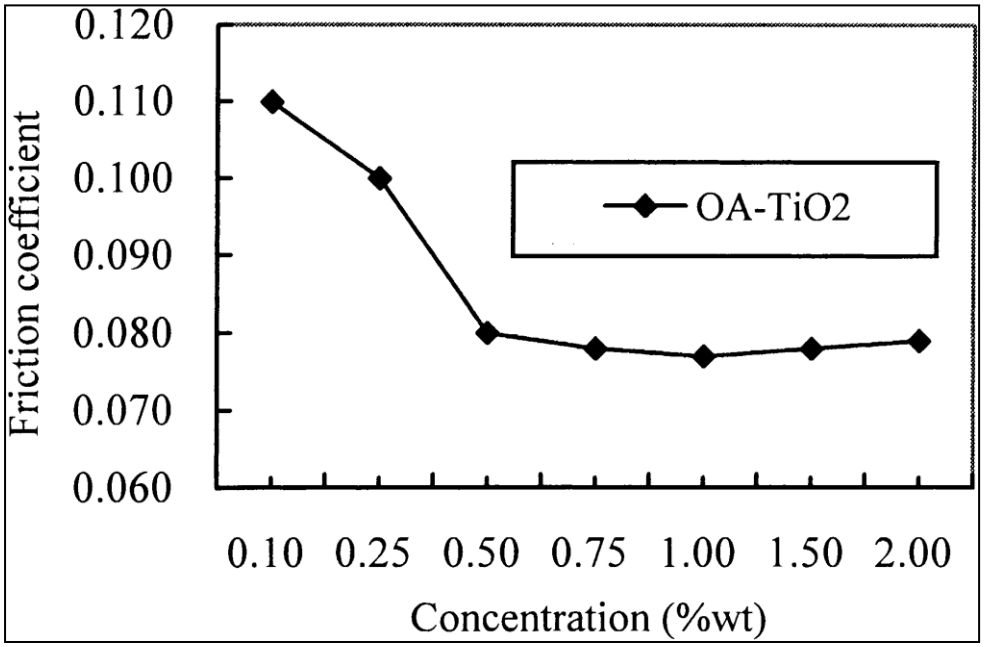

Figure 2.7.6: Change in the coefficient of friction with an increase in the particle concentration (Chen et.al., 2002).

The same trend was observed by Atnafu et.al., 2009 (see Figure 2.7.4). They however found that the presence of nanoparticles only improves the wear, but not the coefficient of friction. (Chen et.al., 2002).

2.8. OPERATING CONDITIONS THAT AFFECT FRICTION AND WEAR

In the previous section, the properties of the nanoparticles that affect friction and wear were discussed. In this section, the influence of the nanoparticles on the load carrying capacity and the influence on the contact point temperature will be discussed. The influence of the composition of the metal surfaces on the tribological properties of a lubricant will also be included.

© University of Pretoria

2.8.1. TEMPERATURE

Temperature is an important variable in manufacturing operations, since it affects the dimensional accuracy during manufacturing of components (Kalpakjian & Schmid, 2006: 610). It also affects the formation of protective films on solid surfaces. For instance, the formation of a film due to physisorption is effective as long as the temperature does not increase much above ambient conditions. However, when the temperature increases, the lubricant cannot form an ordered film on the surface and the lubricant becomes ineffective (Bachelor & Stachowiak, 2001: 362).

He-long et.al., 2008, studied the temperature dependent tribological behaviour of Cu nanoparticles (average particle diameter of 20 nm) dispersed in motor oil. They found that for a certain temperature, the coefficient of friction is lower when nanoparticles are added to lubricating oils. They also found that as the temperature is increased, the coefficient of friction of the pure oil is larger than the coefficient of friction of the nanofluid. This is shown in Figure 2.8.1.

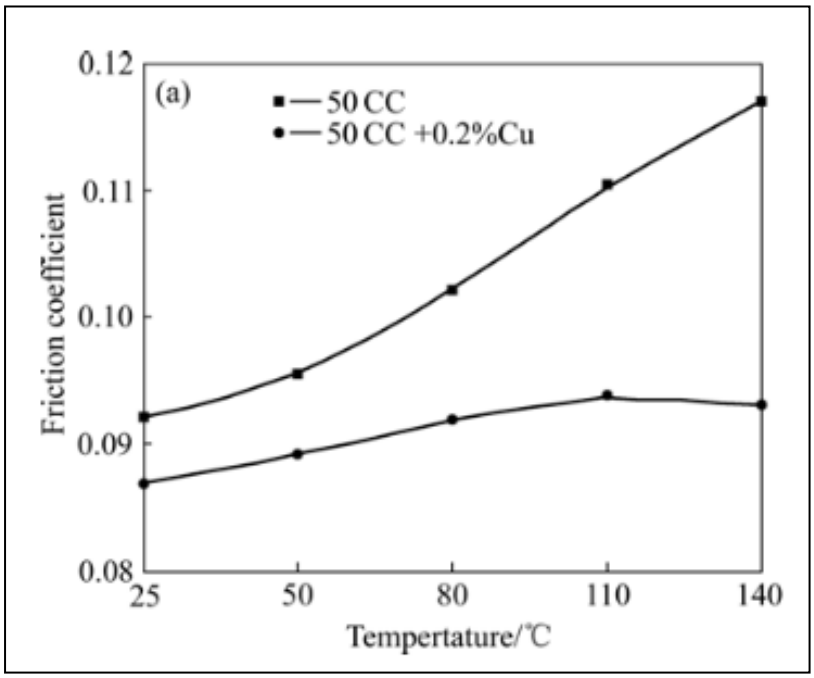

Figure 2.8.1: Coefficient of friction as a function of temperature for pure oil and nanofluids (He-long et.al., 2008).

© University of Pretoria

The temperature axis in the Figure 2.8.1 refers to the oil sump temperature in the experiment and does not refer to the contact point temperature. The contact point temperature will therefore be higher.

This improved coefficient of friction can be explained by a soft copper film that is smeared on the surface as the copper is melted. This is due to the high surface to volume ratio of nanoparticles, which depresses the melting point of the copper particles (Shi et.al., 2004 & Qi & Wang, 2004). Not all nanoparticles, however form a solid film on wear surfaces according to this mechanism. Improved lubrication might also be due to the very high thermal conductivity of nanofluids (Choi et.al., 2002).

Therefore, nanofluids have much better heat management potential, i.e. heat is dissipated much easier, than conventional fluids. This in turn will cause lower temperature gradients as well as lower fluid temperature.

2.8.2. LOAD CARRYING CAPACITY

The influence and effect of nanoparticles suspended in lubricants on the load carrying capacity were studied by various researchers. For the purpose of this study, the work done by Chen et.al., 2002, Hwang et.al., 2006 and Huang et.al., 2006, will be considered.

The study on the tribological properties of TiO_2 nanoparticles in water by Chen et.al., 2002, has already been discussed in section 2.7.3, but was limited to the effect of the particle concentration. Here the effect of solid additives on the load carrying capacity will be discussed here.

The maximum non-seizure load (P_B) and welding load (P_A) value for water, water with dispersant and water with nanoparticles at various concentrations were determined with the 4-ball test and the results are given in Table 2.8.1.

© University of Pretoria

Table 2.8.1: Maximum non-seizure load (P_B) and welding load (P_A) values for water, water with dispersant and water with nanoparticles (Chen et.al., 2002).

Compounds	Concentration (wt%)	P_B(N)	P_A(N)
H_2O	100	<88	1190
Dispersant	0.5	<98	1300
Nano- TiO_2	0.1	696	1800
Nano- TiO_2	0.5	980	2300
Nano- TiO_2	1.0	1000	2400
Nano- TiO_2	2.0	1046	2400

From the table it can be seen that with the addition of nanoparticles the maximum non-seizure load as well as the welding loads improved considerably with a concentration increase of 0.1 to 0.5 % (mass%). When the concentration was increased above 0.5 %, the improvement is small for the maximum non-seizure load (P_B). No improvement was obtained for the welding load (P_A) above 1 %.

Hwang et.al., 2006 studied the influence of nanofluids with C^{60} carbon on the maximum load to maintain an oil film (extreme pressure). They measured the extreme pressure of the fluid with a Falex tester and found that for a concentration of 0.01 and 0.1 mass %, the extreme pressure increased considerably (Figure 2.8.2, green and red graph).

They found that the oil without particles and the oil with 0.3 % (by mass) failed even before aging was completed. For the oil with 0.01 and 0.1 mass %, the extreme pressure however, increased considerably (green and red graph).

The reason for this improvement is possibly due to polymerization of the C60 particle, which in turns form a polymeric tribofilm. This has, however not been verified by experimental methods. It is also noticeable that the amount of particles should not be too high (0.3 mass %), since this seems to have a negative effect on the extreme pressure of the fluid.

© University of Pretoria

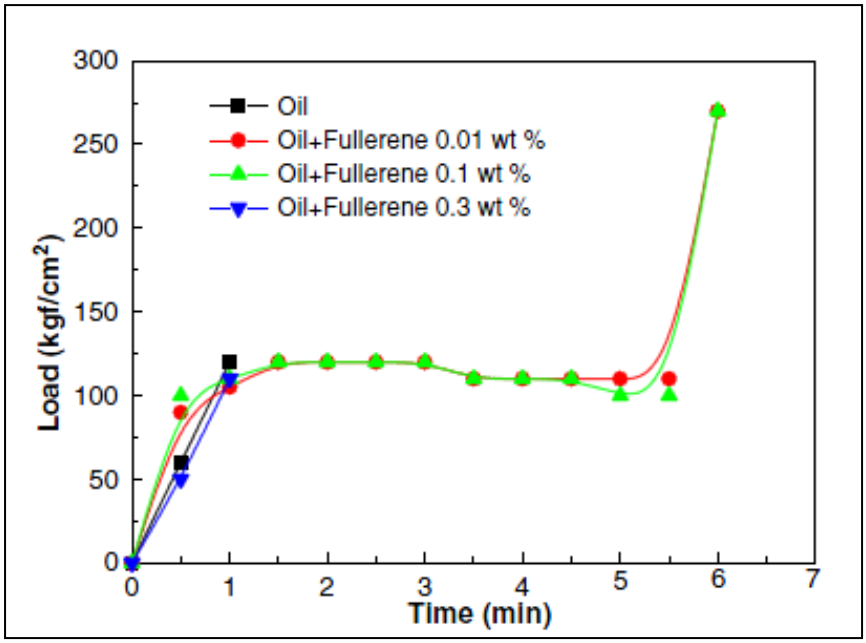

Figure 2.8.2: Extreme Pressure measured with Falex tester for nanofluids containing C_{60} nanoparticles (Hwang et.al., 2006).

Both studies discussed so far had spherical or fullerene structured particles. Huang et.al., 2006, however added graphite nanosheets as well as flake graphite in oil. The effect of these two nanoparticles at various concentrations on the maximum “non seizure” load is given in Figure 2.8.3.

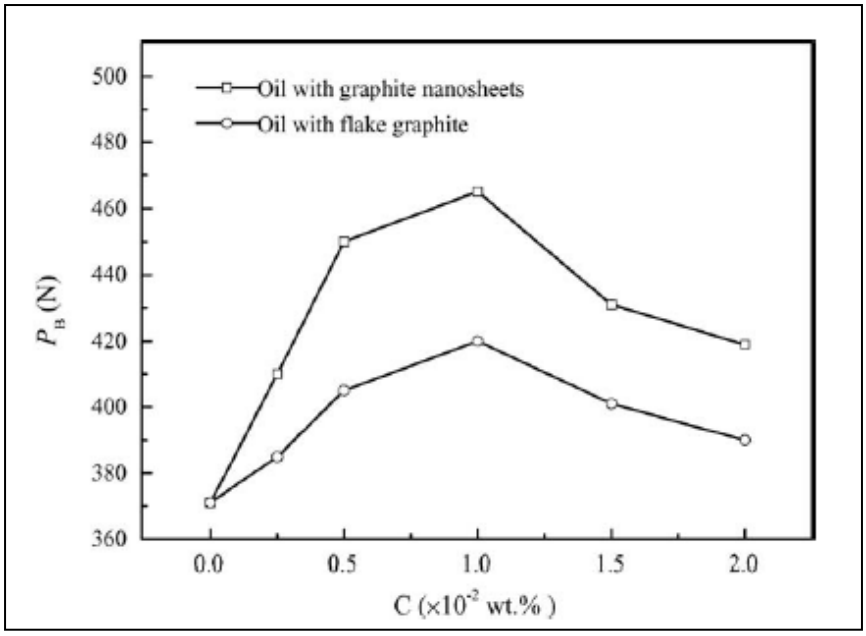

Figure 2.8.3: Effect of graphite nanosheets and flake graphite at various concentrations on the maximum “non seizure” load (Huang et.al., 2006).

© University of Pretoria

Again the maximum non seizure load increased up to 1 % for both particles. When the concentration was further increased, however, the seizure load decreased. This might be due to coagulation of the particles which may affect the stability of the friction or cause vibration and result in a decrease in the non-seizure load.

From these studies, it is quite evident that the load carrying capacity was increased with the addition of nanoparticles to liquid lubricants. This was most probably due to the protective film formed by the solid particles.

2.8.3. COMPOSITION OF OPPOSING BODIES

In the preceding sections, the effect that solid additives have on the load carrying capacity of the lubricant as well as the effect on the temperature has been discussed. In this section, the effect that the composition of the opposing bodies has on the lubricity of the fluid will be considered.

In Figure 2.8.4 the coefficient of friction for a ring-on-roller tribometer is given for two types of ring-on-roller pairs. A paraffinic mineral oil was used as lubricant. The two graphs at the top of the figure are the coefficients of friction for the oil without any solid additives, while the two graphs at the bottom are the coefficients of friction of the oil with micron sized hexagonal-boron nitride particles (Kimura et.al., 1999).

In the two graphs on the left, the coefficient of friction of a JIS SUJ2 bearing steel ring and roller are given. The two graphs on the right are the coefficient of friction for a JIS SUJ2 bearing steel ring and JIS FCD450-10 cast iron roller.

© University of Pretoria

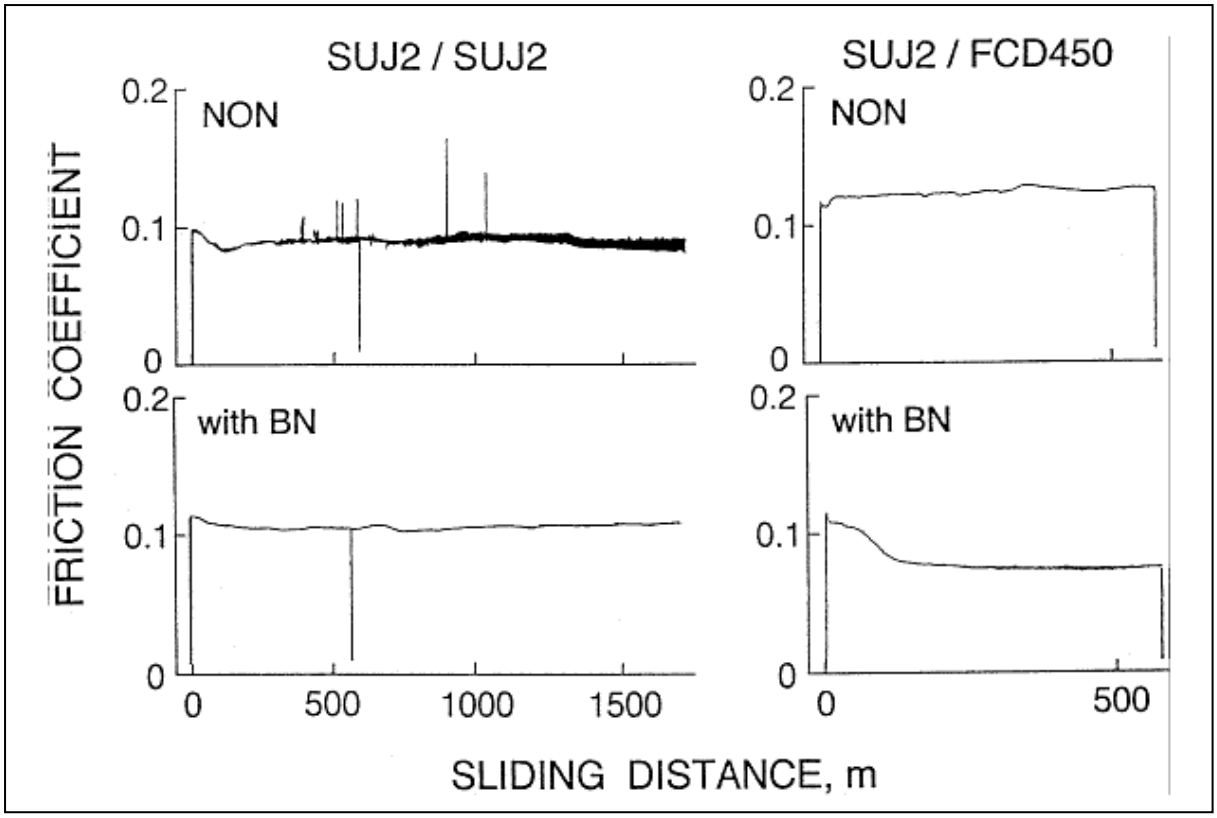

Figure 2.8.4: Effect of composition of ring and roller on the coefficient of friction (Kimura et.al., 1999).

When the graphs on the right are compared to the graphs on the left, it can be seen that the coefficient of friction was more stable for the graphs on the right. This was due to the presence of carbon (in the cast iron) which improved the stability of the coefficient of friction. Furthermore the coefficient of friction was reduced when boron nitride particles were added for the cast iron roller. When boron nitride nanoparticles are added for the steel ring and roller, however, the coefficient of friction was increased.

For the study done by Kimura et.al., 1999, it seems that the presence of graphite plays an important role. The hardness of the material also seems to affect the tribological properties of nanofluids. In the modification of sheet metal forming fluids by Atnafu et.al., 2009, titanium sheets (hardness (RA) 43) and steel sheets (hardness (RA) 39) were used on a pin-on-disc tribometer. A stainless steel ball (hardness (RA) 39) was used in both cases. The result was that the coefficient of friction for the titanium sheet/ stainless steel ball pair was much higher than the steel sheet/ stainless steel ball pair (0.35 compared to 0.13).

© University of Pretoria

It is therefore important to notice that the application of a certain nanofluid can be specialized and only results in improved friction and wear properties for specific contacting surfaces.

2.9. LUBRICATING MECHANISM OF NANOFLUIDS

In order to understand how lubricity is affected by solid lubricants, the lubricating mechanism must also be understood. A number of mechanisms have been proposed by various researchers. These proposed mechanisms include both solid lubricants as well as fluids with solid additives. Furthermore, these mechanisms are closely related to the physical properties of the particles as well as other factors such as the presence of certain chemical species. The electronic state of the atoms in the structure also affects the lubricity as well as the chemical reaction of the solids with the rubbing surfaces (Martin & Ohmac, 2008: 206).

The mechanism for solid lubricant powders that are applied to tribological surfaces as dry lubricants is mainly due to the lamellar or layered structure. For lamellar solids, the atoms are closely packed and strongly bonded to each layer. The layers, however, are far apart with forces that hold them together being of the Van der Waals type. This makes intrafilm sliding of the solid possible since each layer is not as easily deformed as the interlayer structure. Low friction is obtained by the shearing of the solids along the atomic shear planes. The mechanism may also include interface slip. The layered lattice structure of graphite and hexagonal boron nitride are shown in Figure 2.9.1 and the inter layer shear is shown in Figure 2.9.2.

© University of Pretoria

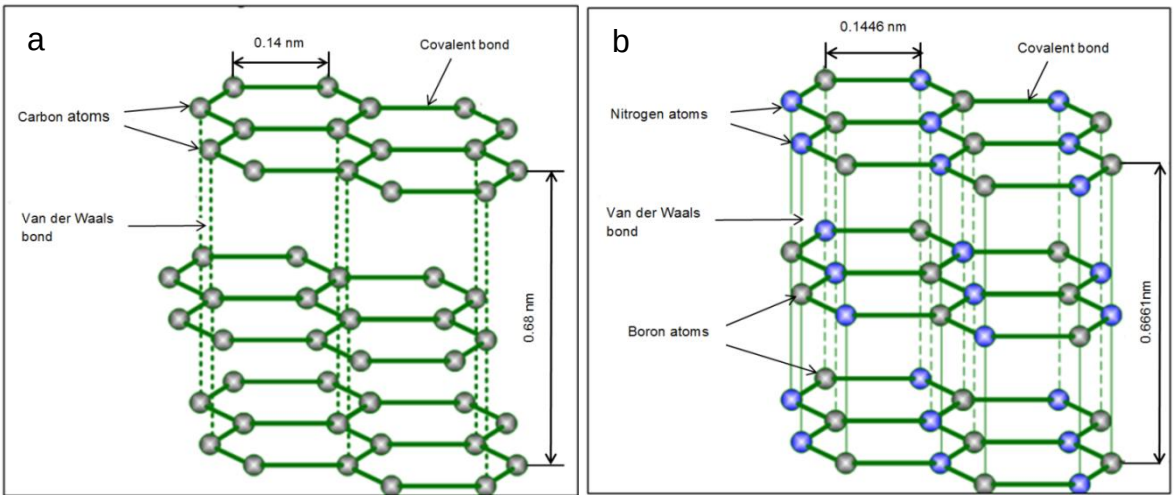

Figure 2.9.1.a: Illustration of layered lattice structure of graphite (Kopeliovic, D, 2012), b: Illustration of layered lattice structure of hexagonal boron nitride (Kopeliovic, D, 2012).

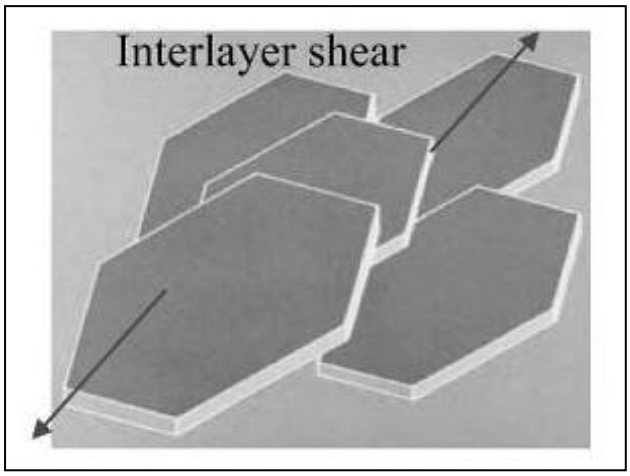

Figure 2.9.2: Interlayer shear mechanism of lamellar solids (Erdemir, 2008: 206).

A layered crystal structure, however, is not the only requirement for effective lubrication. The presence (or absence) of certain chemical species is needed to achieve easy shear. For graphite, Boric acid (H_3BO_3) and h-BN, the presence of moisture weakens of the interlayer bonds and can improve lubricity (Erdemir, 2008: 206).

When MoS_2 and WS_2 are used as a lubricant, however, better lubricity is obtained in the absence of moisture. This is most probably due to the moisture and the solid that react. This can change the interatomic array and consequently poorer lubricity can

© University of Pretoria

be obtained. Better performance is also obtained in non-oxidizing environments (Erdemir, 2008: 206).

The interaction of the solid with the contacting surfaces also has an effect on wear. The solid can adsorb onto the surface to form a bonded transfer layer that protects the layer against wear. Good lubricity, however, is not only limited to lamellar solids, but certain soft metals such as lead and silver, solid oxides, rare earth fluorides, diamond and diamond-like carbons also provide good lubricity.

Furthermore, solid lubricants can also be added to greases and lubricants to improve the tribological properties. Even though promising results have been reported, there is still some uncertainty regarding the mechanism by which the improved friction and wear behaviour was obtained. Several mechanisms have been proposed, and will be discussed below.

A mechanism was proposed by Chang et.al., 2009, where diamond and SiO_2 nanoparticles were dispersed in liquid paraffin. During the friction process, the nanoparticles form a film between the two surfaces. The nanoparticles carry the load and consequently separate the surfaces. This film is then responsible for the reduction in wear and friction. This mechanism is shown in Figure 2.9.3.

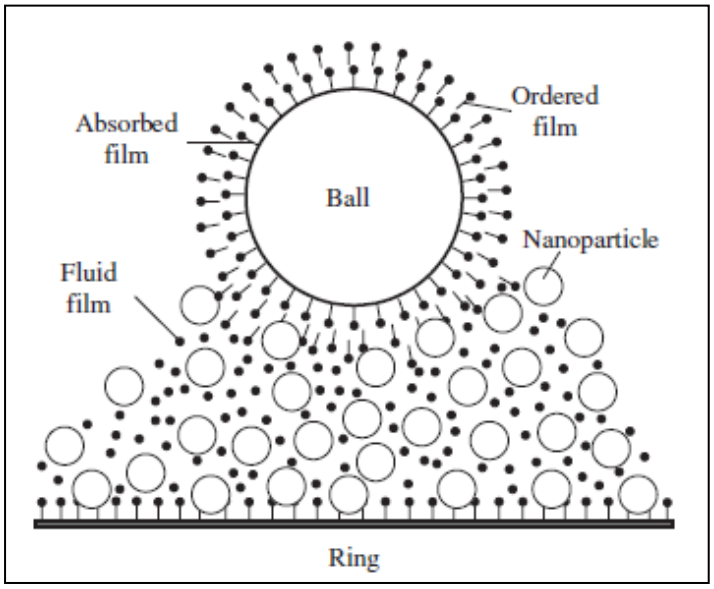

Figure 2.9.3: Physical model of nanoparticles as an additive according to Chang et.al, 2009.

© University of Pretoria

Atnafu et.al, 2009 also proposed a mechanism based on the surface not being flat, but consisting of peaks and valleys. The nanoparticles fill the valleys and consequently prevent metal to metal contact (valley to peak). Trapped particles can also be sheared as shown in Figure 2.9.4 below.

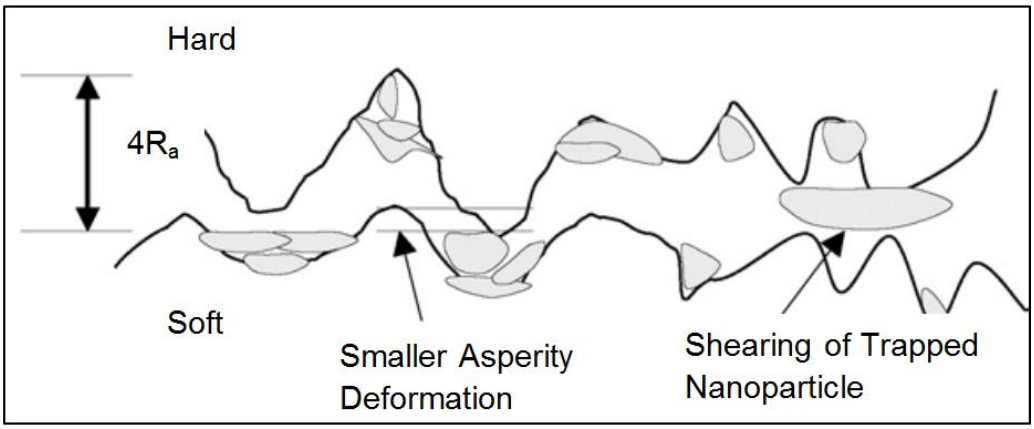

Figure 2.9.4: Nanoparticles filling the valleys as well as trapped particles being sheared Atnafu et.al, 2009.

This model, however predicts lower friction and wear, which was not the case for the results obtained. They found that only the wear decreased, but the coefficient of friction remained unchanged and therefore proposed a different model. In this model, the nanoparticle reduces the size of the entrapped wear particle agglomerate by creating weak shear lines within the agglomerate. This in turn causes the agglomerate to collapse faster and consequently reduces ploughing of the surface (wear), while the coefficient of friction remains the same. This model is shown schematically in Figure 2.9.5.

© University of Pretoria

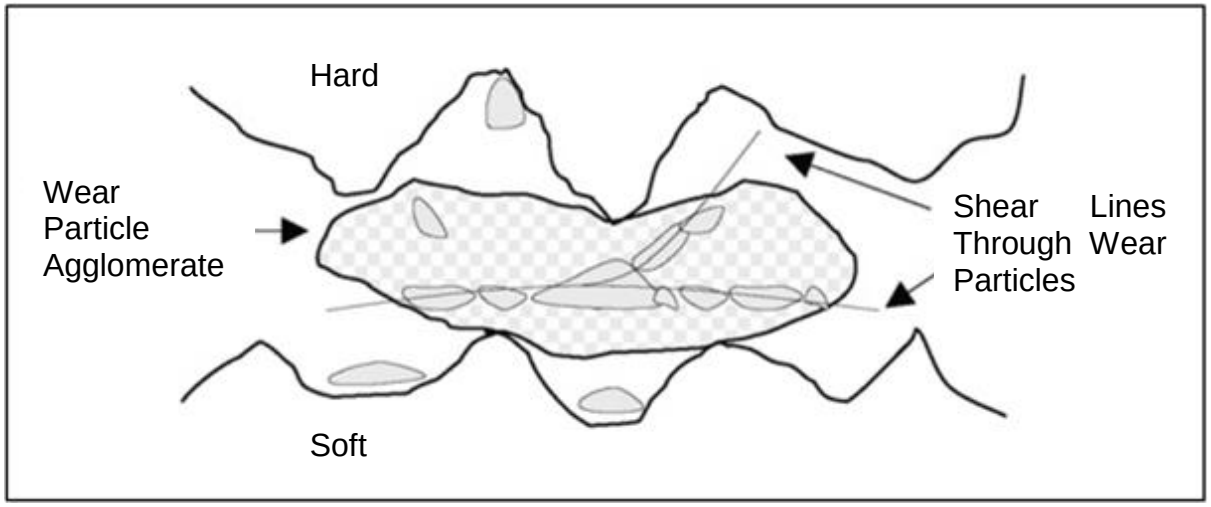

Figure 2.9.5: Nanoparticle breakage of transfer films (Atnafu et.al, 2009).

Finally, in the study of boron nitride additives in bio-based lubricant by Jen et.al., 2013, it was found that the particle size plays an important role. Here it was found that the smaller particles resulted in better friction and wear properties. This is due to the small particles that coalesce in the asperity valleys and consequently a thin transfer film is formed. This can be seen in Figure 2.9.6. The larger particles cannot fill the asperity valleys and consequently, they carry the contact loads (see Figure 2.9.6).

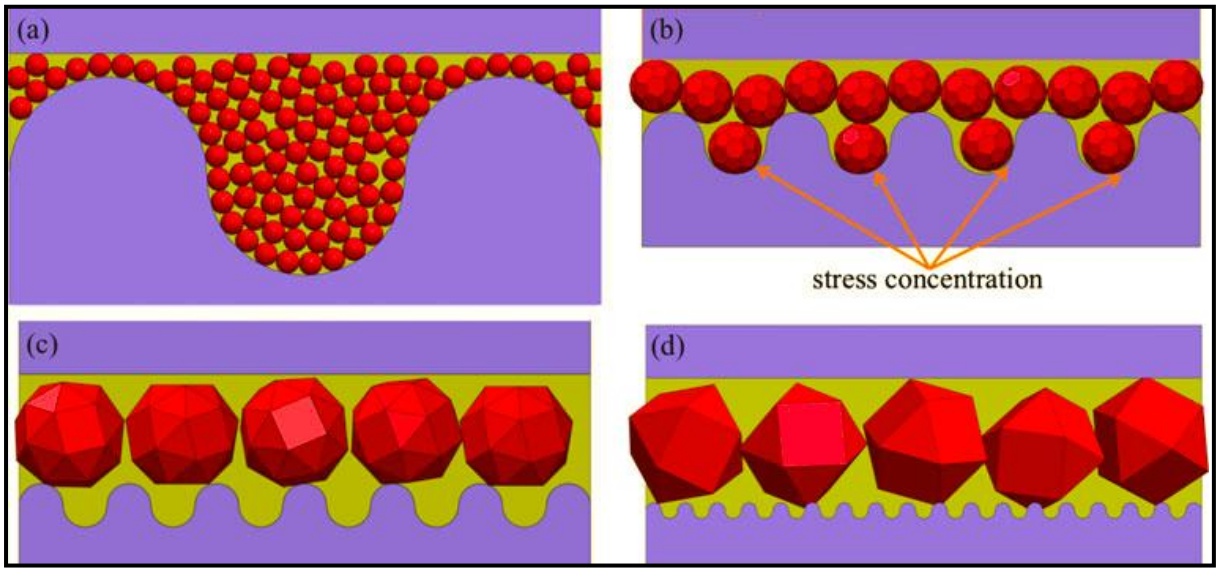

Figure 2.9.6: Schematic diagram of film formation due to particle size (Jen et.al., 2013).

© University of Pretoria

From the models discussed here, it can be concluded that the type of solid (shape, size and composition) plays an important role in the tribological properties of the nanofluid. Also of importance is that in each model proposed, a solid protective layer seems to be formed on the metal surface.

2.10.BORON NITRIDE AS A LUBRICANT ADDITIVE

Boron nitride (BN) is used in a wide variety of applications due to its unique properties. It is not wetted by most molten metals, glasses or salts and therefore has a high resistance to chemical attack (Bernard et.al., 2011). It has a similar structure as graphite and molybdenum disulfide (MoS_2) , both of which are good solid lubricants. It is also considered as a clean lubricant, since it does not contain any sulphur (Kimura et.al., 1999).

Bernard et.al., 2011, studied the thermal stability of boron nitride nanoparticles. It was found that boron nitride nanoparticles remain thermally stable in air below 850 °C. At 850 °C, bulk oxidation occurred whereas below 850 °C, only oxidation of the nanoparticle surface occurred. Furthermore, boron nitride oxidises to form a protective boric acid layer that does not readily volatilise below 1100 °C. The oxidation reaction of boron nitride is given in equation 2.10.1 (Cofer & Economy, 1995).

$$2\,BN + {}^{3}/_{2}\,O_2 \rightarrow B_2O_3 + N_2 \qquad 2.10.1$$

Even though boron nitride is stable with regard to oxidation, hexagonal boron nitride is sensitive to moisture, especially over long periods. This results in the formation of metaboric acid (HBO_2) with traces of orthoboric acid (H_3BO_3). The reactivity of hexagonal boron nitride is also dependent on the layer spacing (Cofer & Economy, 1995). This is due to less densely packed basal planes implying weaker atomic bonding. Boric acid will also react with H_2O to form HBO_2 (Magrave & Randall, 1960).

From the work done on boron nitride Kimura et.al., 1999, and Atnafu et.al., 2009, it was mentioned that boron nitride has potential to be used as a lubricant additive.

© University of Pretoria

Boron nitride showed definite improvements on wear in these studies, if not on the coefficient of friction. Finally, h-BN also has potential as a lubricant additive, especially at elevated temperatures, due to its higher thermal stability.

2.11. NANOPARTICLE DISPERSIONS

Particle dispersions are not as simple and straight forward as one might think. One of the biggest problems with dispersions is to keep the particles from forming clusters. If the particles form clusters, the particle count will decrease and the dispersion is considered as being unstable. One of the effects of unstable dispersions is that the particles settle out of the dispersion (Parfitt, 1973: 10).

It is therefore important to stabilize a dispersion to eliminate uncertainty during lubricity tests. This can be achieved with the addition of a dispersant, which forms a layer on the surface of the particles and thereby prohibits the particles from cluster formation. This is known as steric stabilization, but is only effective if a suitable surfactant is used (Pashley & Karaman, 2004: 86 & Tadros, 2005: 218-219).

2.11.1. DISPERSIONS

A dispersion is the term used to refer to the process where a powder is incorporated into a liquid medium where the final product consists of an even distribution of the particles throughout the medium (Parfit, 1973: 1). They are classified according to the affinity of the powder or particles for the medium. If the particles possess an aversion for the liquid, it is classified as lyophobic, and lyophilic if they possess an affinity for the liquid. If the liquid is water, it is usually referred to as hydrophobic or hydrophilic. Dispersants can also be classified according to their head groups. These two classes are ionic and non-ionic. Ionic dispersants include anionic, cationic and amphoteric surfactants. Non-ionic dispersants have polar head groups which provide the hydrophilic property (Everett, 1994: 155).

Dispersions are used in a wide variety of applications which includes the food industry, pharmaceuticals, cosmetics, agricultural chemicals, paints, oil recovery and

© University of Pretoria

water treatment (Everett, 1994: 11-12). Particles such MoS_2, WS_2, graphite and boron nitride can be dispersed in lubricating fluid to improve the tribological properties. This concept was introduced by Black et.al, back in 1969 and a number of studies followed to date. However, one of the main problems is to keep the particles in dispersion as well as stabilizing the dispersion.

Particle dispersions can be formed through a process known as comminution. This is a milling process during which the solid is broken down to particles of colloidal size range (Williams, 1994: 119), from a few nanometres to tens of micrometers, (Williams, 1994:1). Particulate dispersions can also be formed by condensation which includes nucleation and particle growth. This method works on the principle where molecular complexes of increasing size are formed until colloidal size is reached. Usually the species are formed by chemical reaction to form a molecule that is insoluble in the liquid. The molecules start to aggregate and consequently the particles are formed. This is, however not as simple as described above and the conditions have to be properly controlled (Everett, 1994: 56-57).

In order to stabilize a dispersion, the particle interaction forces must be understood. This is best explained by the Deryaguin-Landau-Verwey-Overbeek (DLVO) theory (discussed in detail in Appendix A) that is based on the forces of attraction and repulsion between the particles. These interacting forces result in an electrical potential that is a function of the distance between the particles. Usually the particles tend to attract one another at small and at large distances, while a repulsive force is experienced at intermediate distances. This repulsive force is referred to as the potential energy barrier (Parfitt, 1973: 13-21).

If the potential energy barrier is not sufficiently high, the particles will be able to collide. The particle number tends to decrease if these collisions are irreversible and the particles aggregate or agglomerate. This is referred to as flocculation and results in precipitation of the particles from the liquid. When the amount of particles in a dispersion decreases over time, the dispersion is considered as being unstable (Parfitt, 1973: 10). This can be remedied with the formation of an electric double layer by dissociation of ionic groups located at the surface of the particles (Williams, 1994: 117). This results in an increase in the repulsion electrical potential that keeps

© University of Pretoria

the particles from colliding. Dispersions can also be stabilized by the presence of an adsorbed layer on the surface. This is known as steric stabilizing where the adsorbed layer prohibits the particles from coming into contact with each other (Parfitt, 1973: 36). This is shown in Figure 2.11.1 below for a particle suspended with a non-ionic dispersant.

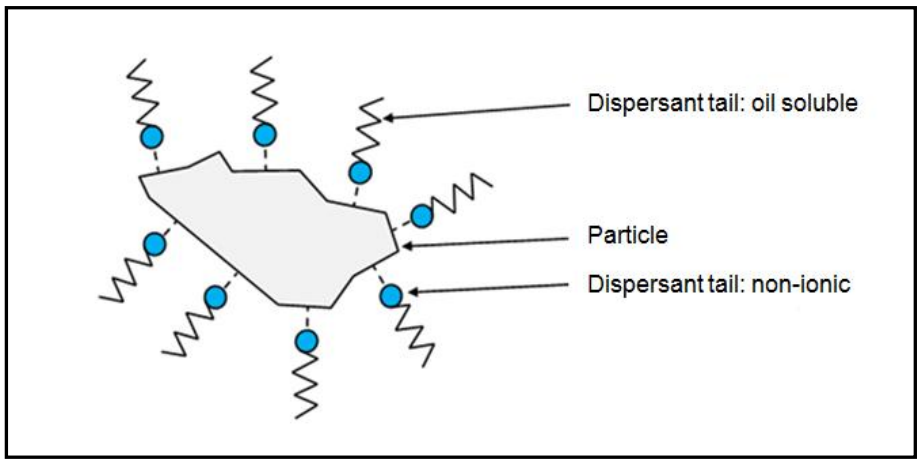

Figure 2.11.1: Mechanism of steric stabilization of a particle with non-ionic dispersant.

2.11.2. DISPERSION OF NANOPARTICLES

In the modification of sheet metal forming fluids with dispersed nanoparticles by Atnafu et.al., 2009, the dispersion characteristics were determined for MoS_2, WS_2 and h-BN nanoparticles (Table 2.11.1).

Table 2.11.1: Dispersion characteristics of modified sheet metal forming fluids.

Materials	Average size (nm)r	Average size (nm) in oil after shaking & stirring	Average size (nm) in oil after sonication
MoS_2 nanoparticles	70-100	1000	600
WS_2 nanoparticles	50	600	450
h-BN nanoparticles	70	800	550

© University of Pretoria

It can be seen in the table that the average particle size increased considerably after the particles were added to the sheet metal forming fluid. This was improved after fluid with particles was subjected to ultrasonic waves (sonication), but the aggregates were not broken down completely. This highlights the importance of improving the dispersion quality and stability, since the effects of aggregation size on lubricity is unknown.

2.11.3. VISCOSITY

One the most essential physical properties of a lubricant is viscosity. This property enables a fluid to separate bodies that are in motion relative to one another. This is due to the restriction of motion between two elements of a fluid caused by inter-molecular interaction (Gohar & Rahnejat, 2012: 83).
If this ability is considered in terms of lubrication, it would appear that as the viscosity of the lubricant is increased, the performance of the lubricant will be enhanced as well. However, this is not always the case, since more viscous oils require more power in order to be sheared. This can result in more heat being generated and consequently the temperature between the contacting surfaces will increase. This could lead to failure of the components that the lubricant should protect. Care must therefore be taken with the lubricant's viscosity to ensure optimum lubricity.

Viscosity is also highly dependent on temperature, and it is important to know what the viscosity is at the temperature of the application (Batchelor & Stachowiak, 2001:11-12). This is to ensure that the lubricant has the correct viscosity characteristics at the intended operating temperature.

Viscosity is also an important element in the selection criteria of a dispersant. The dispersant is evaluated on how the temperature as well as the concentration is affected. Figure 2.11.2 is an example of how viscosity is influenced by temperature. In this figure, the same quantity of dispersant was used, but the type of dispersant was different for each curve and included both ionic and non-ionic types (Williams, 1994: 121).

© University of Pretoria

When samples A to C in Figure 2.11.2 are considered, an increase in viscosity is observed when the temperature is increased. This increase in viscosity is usually due to desolvation of the water-soluble sections of the dispersant, causing the dispersion to destabilize and the particles are no longer dispersed (Williams, 1994: 120-122).

This increase in viscosity can also be due to aggregation of the particles, caused by the breakdown of the electrostatic stabilizing effect. Another possibility is desorption of the dispersant from the particle, if the anchoring effect of the dispersant is insufficiently strong at elevated temperatures. Therefore, when selecting a dispersant for dispersion, the viscosity of the dispersion must decrease as temperature increases. This decrease in viscosity must occur in a temperature range that includes the temperature range of the application of the dispersion (Williams, 1994: 120-122).

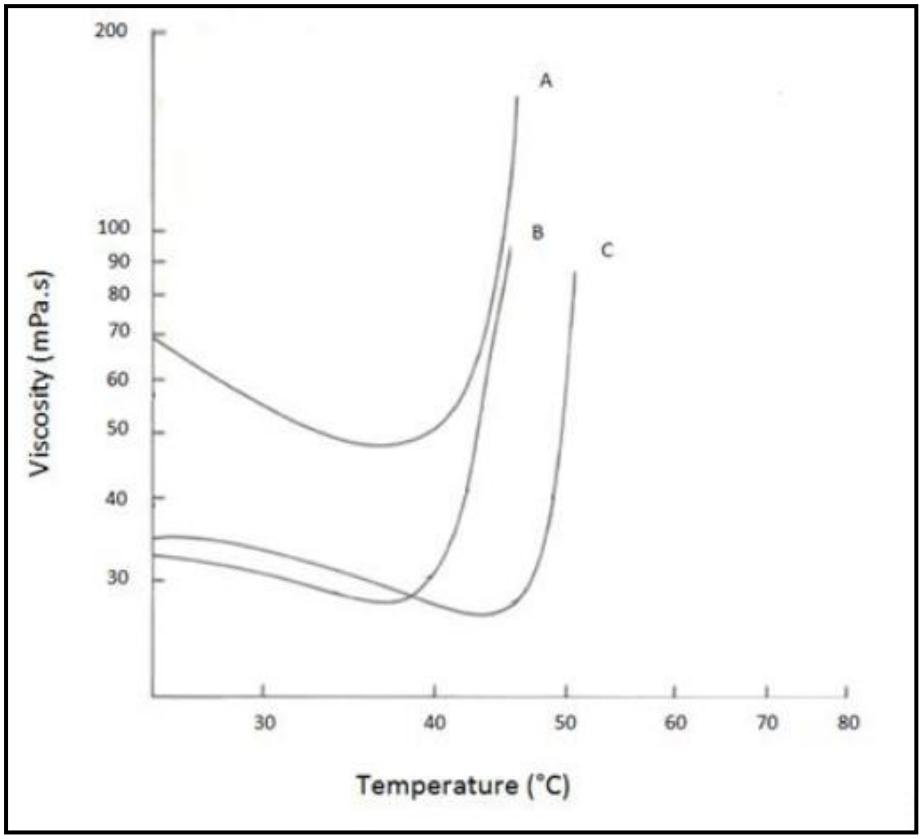

Figure 2.11.2: Viscosity as a function of temperature for hydrophobic particles in an aqueous phase (Williams, 1994: 120).

© University of Pretoria

The amount of dispersant used is also important, since it affects the breakdown of the aggregates. In order to determine the amount of dispersant required, a curve is produced for the change in viscosity as a function of dispersant concentration at a fixed temperature and constant mass fraction particles. This is shown in Figure 2.11.3 (Williams, 1994: 120-122).

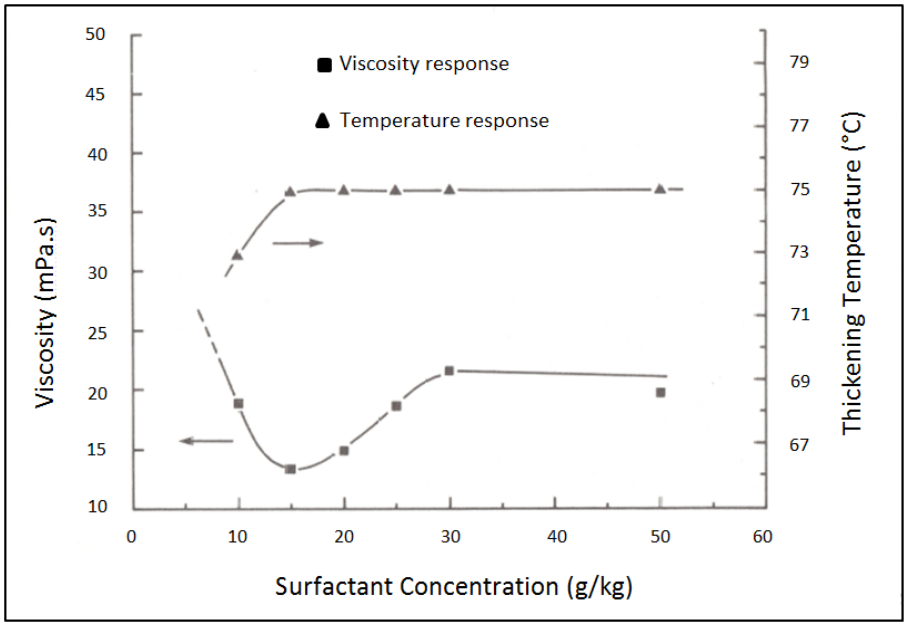

Figure 2.11.3: Viscosity as a function of concentration of hydrophobic particles in an aqueous phase (Williams, 1994: 121).

In this figure it can be seen that viscosity decreases with an increase in surfactant concentration until a minimum is reached. This decrease in viscosity is due to the progressive deflocculation with an increase in the surface coverage of the particle by the dispersant. At the minimum, complete surface coverage is obtained. The increase in viscosity with a further increase in concentration is due to the non-absorbed surfactant. It is preferable to slightly overdose the dispersion with surfactant in the final formulation, to compensate for any change in the surface area of the particles (Williams, 1994: 120-122).

© University of Pretoria

3. EXPERIMENTAL

The experimental section is divided into two parts. The first part covers the dispersion of the particles which also includes the physical properties of the lubricating fluid and the particles. The second part covers the friction and wear testing of the lubricating fluid and the fluid with dispersed nanoparticles (also referred to as nanofluid).

3.1. DISPERSION OF NANOPARTICLES

The aim of this part of the investigation was to produce a dispersion that provided adequate stability for the duration of the friction and wear tests. This was to eliminate the uncertainty that can be caused by the tendency of the particles to form agglomerates and aggregates.

The dispersion was prepared from a metal working fluid that was based on rapeseed oil and white mineral oil. The fluid also contained esters and sulphurised esters. This fluid was chosen, since it is considered as environmentally friendly and is used for general metal working operations.

The boron nitride nanoparticles were obtained from Lower Friction (a division of M K Impex Corp.). Boron nitride nanoparticles were chosen, since it is also considered as a green or environmentally friendly lubricant and are stable at high temperatures. The physical properties of the particles (as supplied by producer) are given in Table 3.1.1.

© University of Pretoria

Table 3.1.1: Physical properties of hexagonal-boron nitride

Property	
Density	2.3 g/cm^3
Melting Point	3000 °C (Dissociates)
Dielectric Constant	4 MHz
Youngs Modulus	20-102 MPa
Thermal Conductivity (at 293 K, directional avg.)	0.08 cal/cm.s.K
Temperature stability	1000 °C in Air 1400 °C in Vacuum 1800 °C in Inert atmosphere

(Lowerfriction, 2014)

3.1.1. APPARATUS: DISPERSION

The apparatus used for the dispersion part of the study included equipment that was essential in the preparation of the dispersion as well optimising the dispersion. Furthermore, some physical properties of the test fluid and particles also had to be measured. The apparatus that was used are summarised in Table 3.1.2.

© University of Pretoria

Table 3.1.2: Apparatus used for preparation of boron nitride in oil dispersion

Function	Apparatus
Physical Properties	
	Viscometer
	Scanning electron microscope
	Thermogravimetric analysis instrument (TGA).
	Zeta Sizer
Dispersion Preparation	
	Scale
	Heating Plate
	Ultrasonic Cleaner
Dispersion Optimization	
	Viscometer
	Zeta Sizer

3.1.1.1. ULTRASONIC CLEANER

The ultrasonic cleaner was used to break down any possible particle clusters that could have formed. Normally these cleaners are used for cleaning of materials and parts. These cleaners transmit sound waves at frequencies beyond the range of human hearing.

The ultrasonic cleaner that was used in this study was a PS-40 model. The specifications for this cleaner are given in Table 3.1.3.

© University of Pretoria

Table 3.1.3: Specifications for PS-40 ultrasonic cleaner (Ultrasonic cleaners made in China, 2014).

Property	
Tank Capacity	10 L
Ultrasonic Power	240 W
Heating Power	400 W
Operating Frequency	40 kHz
Mains Power	240 V
Timer	1-30 min & ∞

3.1.1.2. VISCOMETER

The measurement of the viscosity of the lubricating fluid and nanofluid were done with a Stabinger viscometer (model SVM 3000/G2). This viscometer contains a tube which rotates at a constant speed. In the tube is a measuring rotor with a built-in magnet. This rotor floats in the sample and due to the rotor's low density, is centered by centrifugal forces. Figure 3.1.1 is a diagram of the tube and rotor.

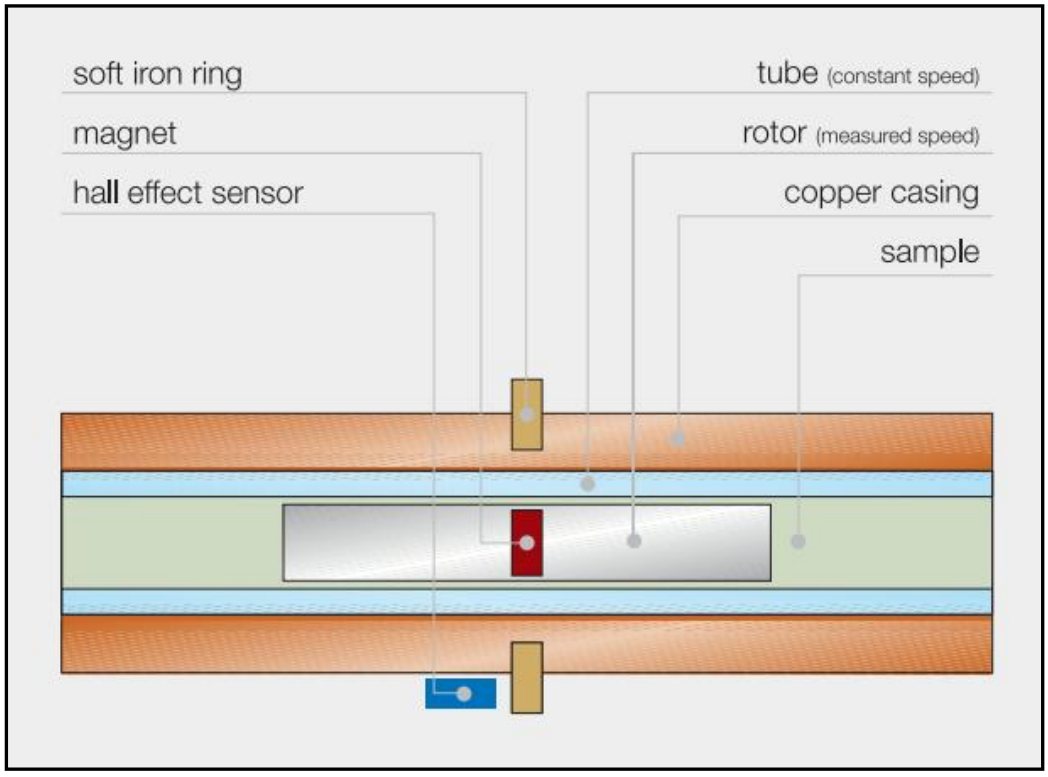

Figure 3.1.1: Diagram of Stabinger viscometer (Kraschitz, 2014).

© University of Pretoria

As can be seen in the figure above, the viscometer measures the rotational speed with a Hall Effect sensor. The fluid measured is inserted in the tube as indicated above. This viscometer is mainly used for oils with a temperature range of – 56 °C to 105 °C (Anton Paar, 2011: 14 & 33).

3.1.1.3. ZETA SIZER

The particle size distribution (PSD) was measured with a Malvern Zeta Sizer (Model: ZEN 3600). This method was also used to confirm that adequate dispersion stability was obtained.

The Zeta Sizer operates on the dynamic light scatter principle, where the analysis is based on the fluctuations in scattered light caused by the Brownian motion of particles. This is then used to determine the particle diameter (Chu & Nose, 2012). This principle is illustrated in Figure 3.1.2.

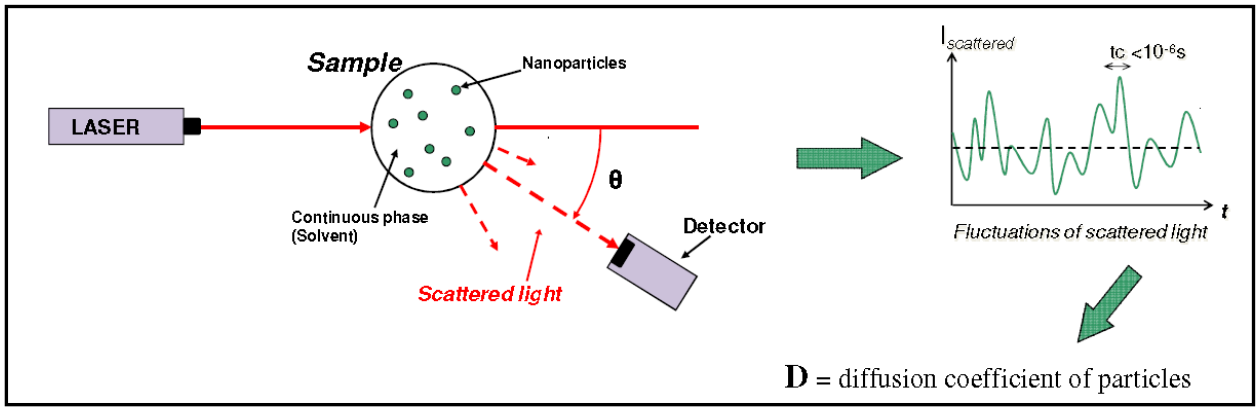

Figure 3.1.2: Illustration of dynamic light scattering principle (Maxit, 2009).

The specifications for the Malvern Zeta Sizer (ZEN 3600) are given in Table 3.1.4 below.

© University of Pretoria

Table 3.1.4: Specifications for Malvern Zeta Sizer (ZEN 3600).

Specification	
Particle size range	0.3 nm – 10 µm
Concentration range	0.1 ppm – 40% particle mass/dispersion volume
Temperature range	Up to 120 °C

3.1.1.4. THERMOGRAVIMETRIC ANALYSIS (TGA)

Thermogravimetric analysis (TGA) is a technique used to determine the thermal stability of a material and the fraction of volatile components it contains. This is done by monitoring the mass change as a specimen of the material is heated until no further mass loss can be observed. A curve is obtained from which the extrapolated onset temperature can be determined (Figure 3.1.3). This is an indication of when the mass loss of the sample commences (PerkinElmer Inc, 2014).

Furthermore, when the first derivative of the mass loss curve is calculated, the point at which the greatest change in mass loss occurs can also be determined (PerkinElmer Inc, 2014). This is shown in Figure 3.1.4, where onset y and x denotes the extrapolated temperature at which mass loss begins. The lubricating fluid in this study was analysed with a model SDT Q 600 TGA.

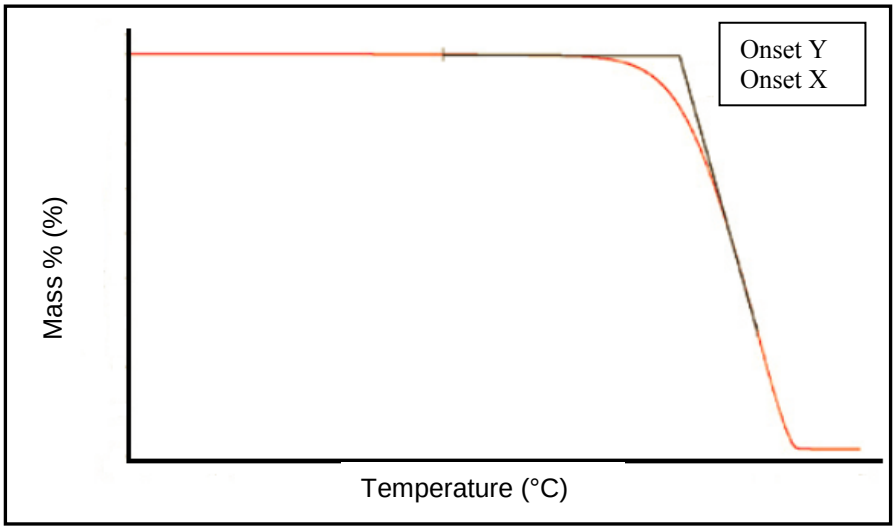

Figure 3.1.3: Mass loss curve obtained with thermogravimetric analysis (PerkinElmer Inc, 2014).

© University of Pretoria

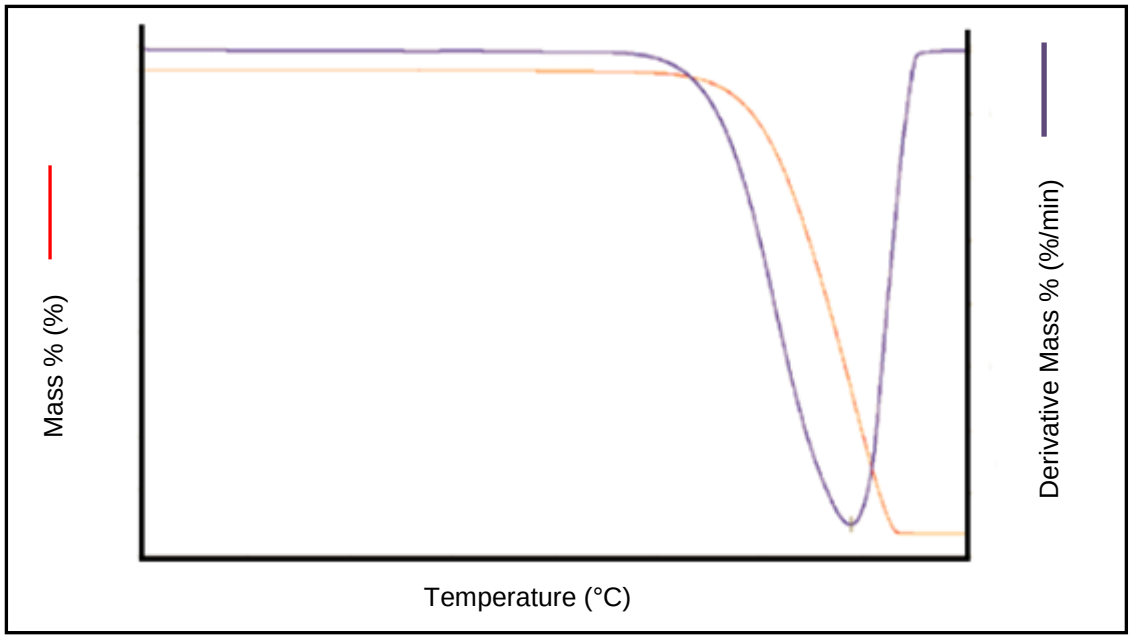

Figure 3.1.4: Mass loss curve and first derivative curve obtained with thermogravimetric analysis (PerkinElmer Inc, 2014).

3.1.2. MEASURED VARIABLES: DISPERSION

All the variables that were measured to determine the physical properties as well as optimizing of the dispersion are summarized in Table 3.1.5.

Table 3.1.5: Variables measured for dispersion of boron nitride particles in lubricating fluid.

	Variable
Physical Properties	
	Viscosity
	Density
	Temperature stability
	Particle Size
Dispersion Optimization	
	Particle size
	Viscosity
	Particle/dispersant ratio (mass)

© University of Pretoria

3.1.3. METHOD: DISPERSION

Before the particles were dispersed in the oil, the size was determined from Scanning Electron Microscopy (SEM) analysis. The lubricating fluid was also characterised by viscosity and density measurements as well as thermogravimetric analysis.

This was followed by a screening process in order to obtain an adequate dispersant. Dispersions with different dispersants were prepared and the effectiveness of the dispersant was monitored by obtaining particle size distributions. This was determined with a Malvern Zeta Sizer.

After a suitable dispersant was obtained, the amount of dispersant required was optimised by plotting viscosity concentration graphs (see section 2.11.3, Figure 2.11.2). This dispersion was then used as a test fluid for the friction and wear test.

It is also important to take note that the method of preparing a dispersion can affect the stability. Therefore, the method is summarized in Appendix B and it is essential to prepare dispersions in the exact order.

3.2. FRICTION AND WEAR TESTING

The objective of the friction and wear testing was to determine what causes the poor repeatability and if any modifications to the test procedure can result in any improvement. Both the lubricating fluid and the nanofluid were subjected to the test.

3.2.1. APPARATUS: FRICTION AND WEAR TESTING

The friction and wear testing was conducted with an SRV tester. Wear scar surfaces were photographed and measured with a metallurgical microscope (Zeiss A x 10) and the composition of layers observed on the scar were analysed with Raman spectroscopy.

© University of Pretoria

3.2.1.1. FRICTION AND WEAR TESTING RIG: SRV

The SRV is a ball-on-disc assembly developed by Optimol-instruments. The abbreviation SRV is for Schwingung, Reibung, Verschleiss, which is the German translation for oscillation, friction and wear. The model of the rig used in this study was the Optimol SRV ®4.

Other assemblies can also be installed such as cylinder on disc and the motion of the upper specimen can also be changed from oscillatory to rotational. For this study, only the oscillation mode was used (Optimol instruments SRV, 2011: 45-102). Figure 3.2.1 is a diagram of how the load is applied on the upper specimen (ball), which is in contact with the lower specimen (disc). The temperature range, the load limit and some other variables are summarized in Table 3.2.1.

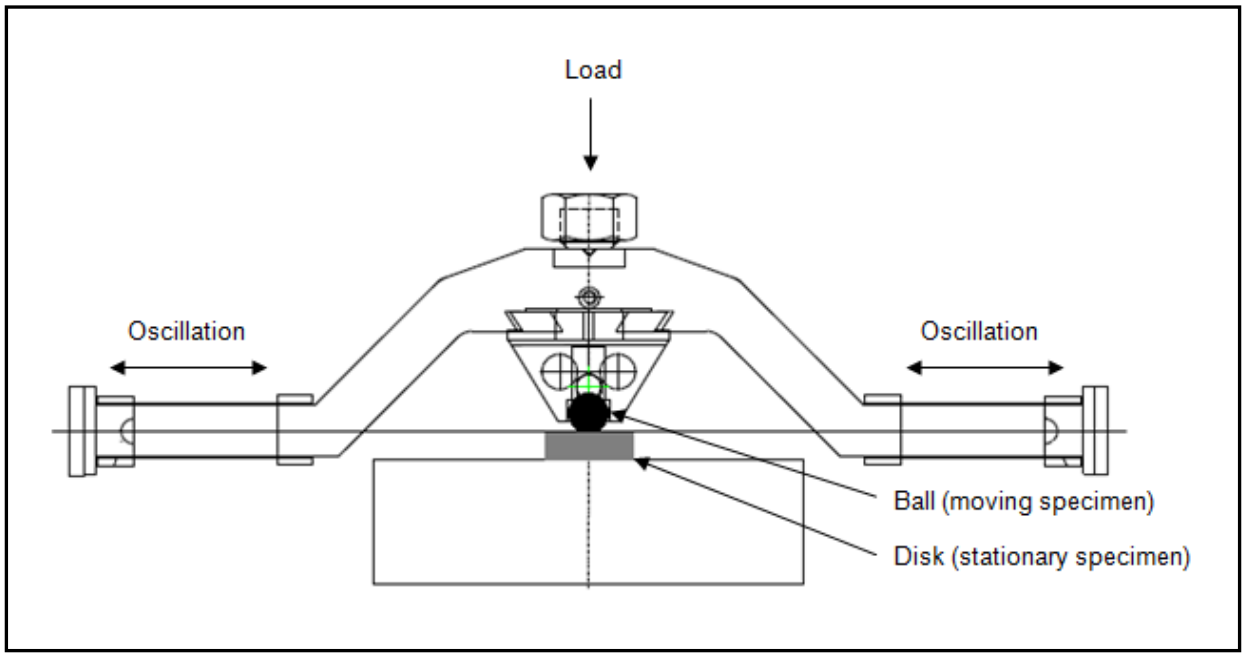

Figure 3.2.1: Illustration of applied load on ball-on-disc assembly with oscillatory motion on Optimol SRV test rig (Optimol-instruments SRV, 2011: 47).

© University of Pretoria

Table 3.2.1: Operating range of the Optimol SRV test rig (Optimol-instruments SRV, 2011: 12-25).

Variable	
Temperature (°C)	- 35 °C to 350 °C
Load (N)	Up to 2000 N
Frequency (Hz)	1-511 Hz
Stroke (mm)	Up to 5 mm

3.2.1.2. SURFACE ANALYSIS: RAMAN SPECTROSCOPY

Raman spectra are acquired by irradiating a sample with a powerful laser source of visible or near infra-red monochromatic radiation. Some of the radiation is scattered by the molecules in the sample. This scattering is measured with a spectrometer. The scattering results in a "shift" in the wavelength and this shift depends on the chemical structure of the molecules. From the shift in wavelength it is therefore possible to determine the composition of a sample (Hollier, Nieman & Skoog, 1998: 429-431). For the analysis done on the wear scar surfaces, a T64000 micro-Raman spectrometer was used.

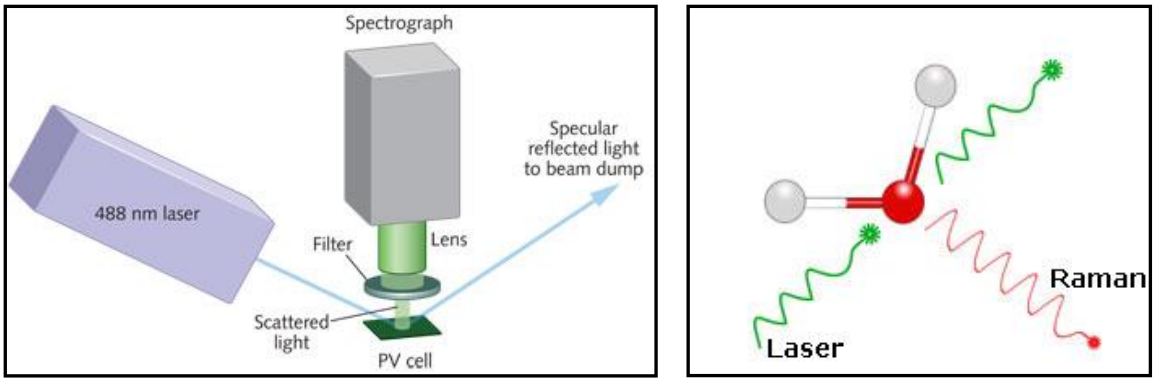

Figure 3.2.2: Diagram of Raman spectroscopy (Siew, 2013 & Horiba Ltd, 2013)

3.2.2. MEASURED VARIABLES: FRICTION AND WEAR TESTING

During the friction and wear test, the coefficient of friction was monitored. After a test, the wear scar surface was measured and photographed with an optical

© University of Pretoria

microscope. A complementary rating was assigned to each scar as described by Olah et.al., 2005 in order to compare the wear scars. The complementary rating (CR) of wear scars is given in Figure 2.1.1.

The wear volume was calculated from the wear scar measurement. The method described in ASTM D 7755. The equation that was used to determine the volume was:

$$V_{cap} = \frac{\pi d_1^2 d_2^2}{64}\left(\frac{1}{R} - \frac{1}{R\prime}\right) \quad 3.2.1$$

- Where V_{cap} is the wear volume
- d_1 is the diameter of the wear scar parallel to the sliding direction
- d_2 is the diameter of the wear scar perpendicular to the sliding direction
- R is the initial radius of the ball
- R' is the resulting radius of the shape of the wear scar

It was assumed that the wear scar shape was almost flat and consequently R' very large. This meant that the $\frac{1}{R\prime}$ term is very small and the equation was simplified to:

$$V_{cap} = \frac{\pi d_1^2 d_2^2}{64}\left(\frac{1}{R}\right) \quad 3.2.2$$

3.2.3. METHOD: FRICTION AND WEAR TESTING

The test procedure for the friction and wear tests was similar to the procedure as described in ASTM D 6425. All the test specifications are summarised in Table 3.2.2 below.

© University of Pretoria

Table 3.2.2: Specifications of friction and wear test procedure

Specification	
Motion	Oscillatory
Running-in duration	5 min
Running-in load	50 N
Test duration	60 min
Test load	200 N
Stroke	1 mm
Frequency	50 Hz
Block Temperature	100 °C
Specimens	
Disc	
Material	AISI E52100 steel
Hardness	C60 +/- 2 Rockwell
Surface finish (R_a[1])	0.025 +/- 0.005 µm
Dimensions	
Diameter	10 mm
Ball	
Material	AISI E52100 steel
Hardness	C62 +/- 2 Rockwell
Surface finish	0.45 to 0.65-µm Rz[2] lapped surface
Dimensions	
Diameter	24 mm
Height	7.85 mm

[1] Arithmetic mean surface roughness

[2] Ten point mean surface roughness

The test fluids were kept at the same temperature. This was to ensure that the lubricating fluid and the nanofluid produced results that could be compared. The set-up is shown in Figure 3.2.4 and Figure 3.2.5. The sample temperature was kept at an elevated temperature with the aid of a heat exchanger, as can be seen in Figure 3.2.4. The flow rate to the sample bath was 1 drop per every 3 to 5 seconds.

© University of Pretoria

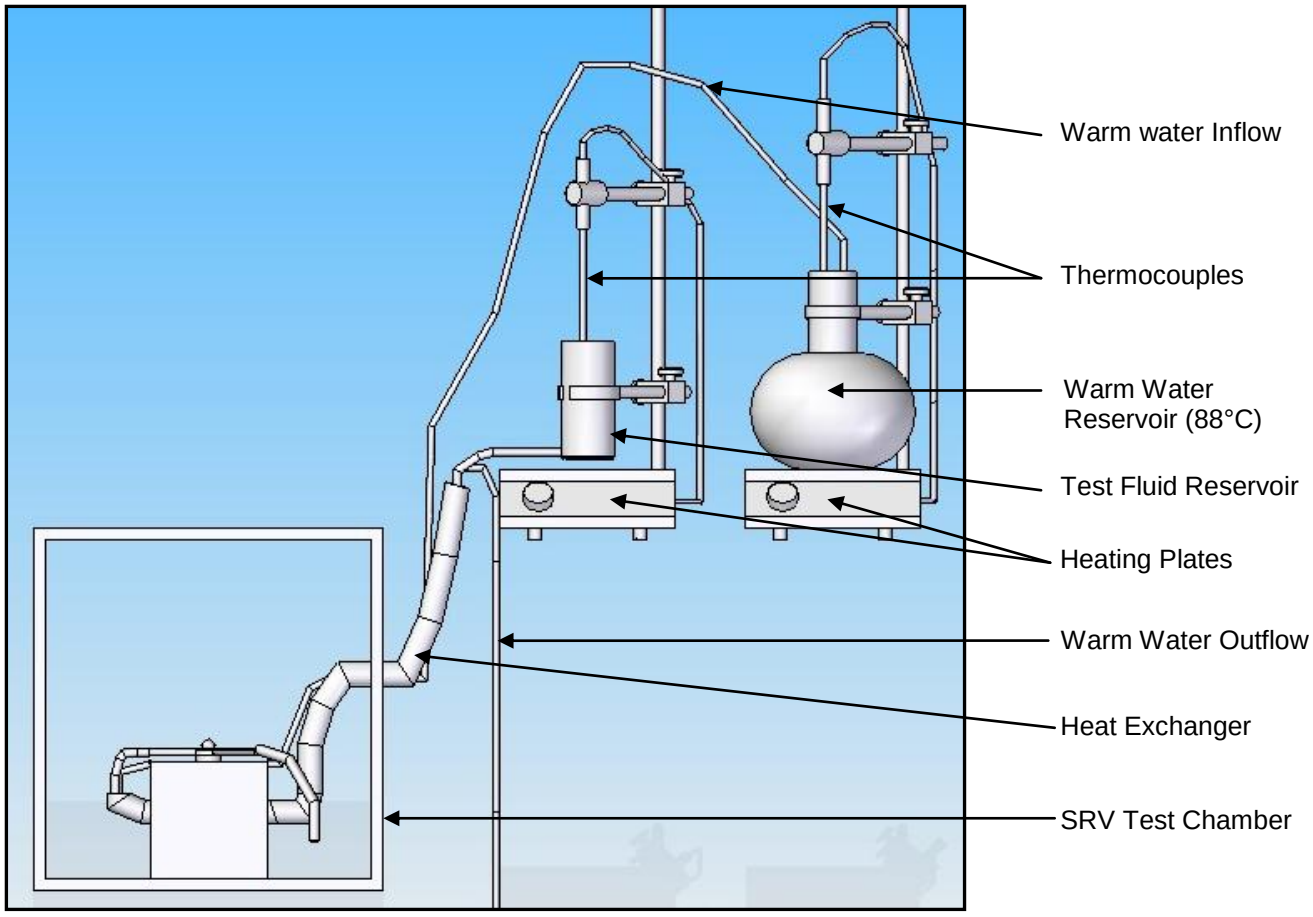

Figure 3.2.4: Experimental setup for friction and wear testing on SRV test rig.

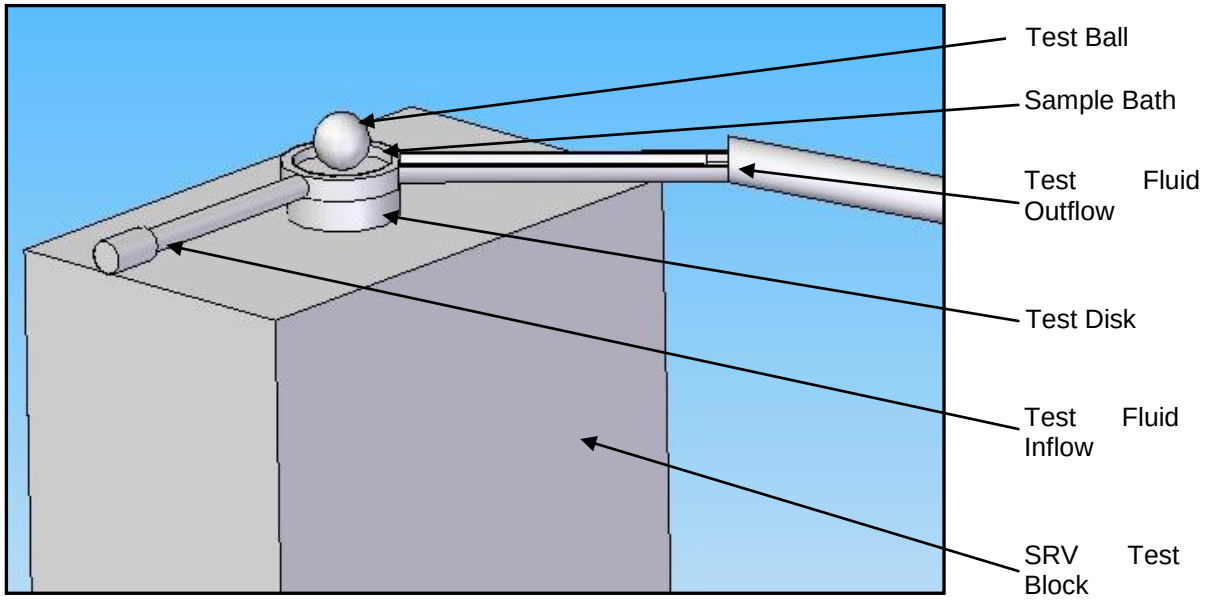

Figure 3.2.5: Ball on disk setup of SRV test rig for friction and wear tests.

The preparation of the specimens is also important. This was to ensure that no contaminants influence the results. The specimens were sonicated in the ultrasonic

© University of Pretoria

bath (see section 3.1.1.1) for ten minutes in toluene. After this sonication period, the specimens were removed from the toluene and left to dry. This was repeated with acetone as cleaning fluid. The specimens were dried again before they were assembled in the experimental setup.

After a test was completed, the wear scar diameter was measured, the wear surface photographed and the coefficient of friction plotted as a function of time. The surface was also analysed with Raman spectroscopy.

© University of Pretoria

4. RESULTS

4.1. PHYSICAL PROPERTIES

In the first part of the results section, the physical properties of the lubricating fluid and particles (as described in the experimental section) will be discussed. It was important to determine these properties in order to be able to design the friction and wear testing experiments that were conducted on the SRV test rig. Some of these properties were also necessary for the preparation of the particle dispersion.

As described in the experimental section, an environmentally friendly metal working fluid as test fluid was used. Hexagonal-boron nitride nanoparticles as solid additives were also dispersed in the fluid and will be referred to as: test fluid with particles. The physical properties that were determined included the viscosity, thermogravimetric analysis and particle size analysis (PSA).

4.1.1. PHYSICAL PROPERTIES: LUBRICATING FLUID

The first property of the fluid that was determined was the viscosity. This is an important property, since it is a measurement of the internal friction of the fluid and its ability to form a film (Mortier & Orszulik, 1997: 7). The viscosity and density of the fluid are given in Figures 4.1.1 to 4.1.3 below as a function of temperature. This was done to confirm that the oil viscosity does not change significantly up to 100 °C, at which friction and wear testing were done.

Note that the measured density value at 60 °C in Figure 4.1.2 is slightly higher than the trend. This was due to experimental error, but had no observable influence on the kinematic viscosity calculation (see Figure 4.1.3). The small effect was due to the small magnitude of the error.

© University of Pretoria

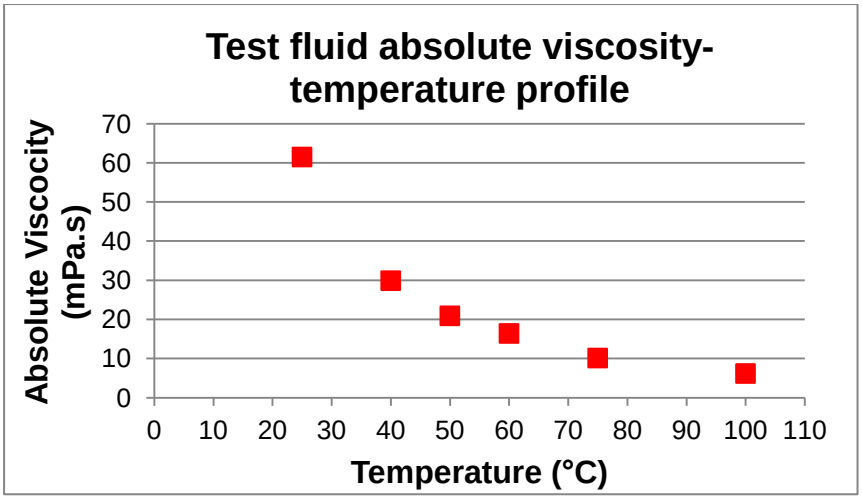

Figure 4.1.1: Absolute viscosity of test fluid at various temperatures

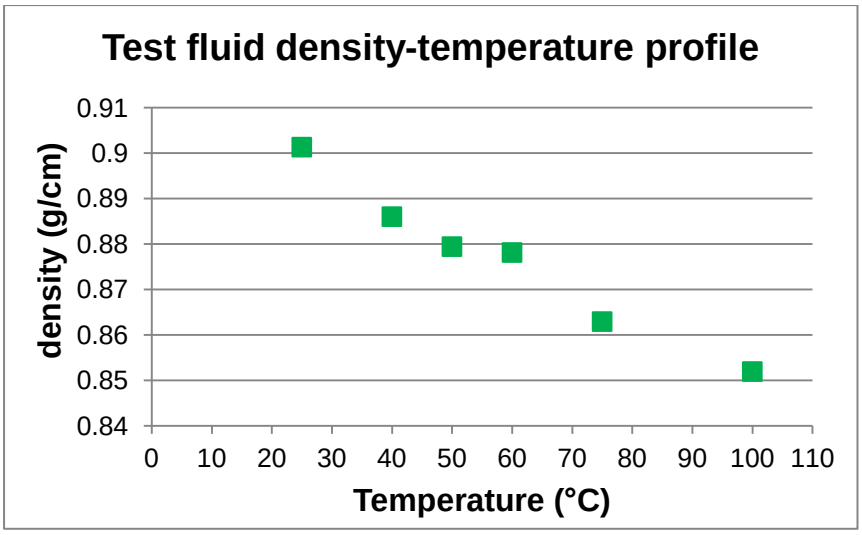

Figure 4.1.2: Density of test fluid at various temperatures

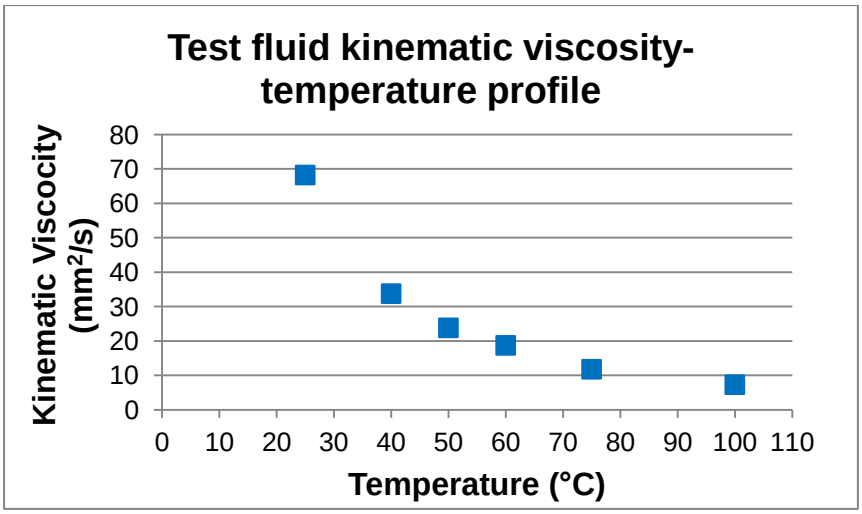

Figure 4.1.3: Kinematic viscosity of test fluid at various temperatures

© University of Pretoria

The kinematic viscosity in Figure 4.1.3 was used to determine the viscosity index, which is an indication of the viscosity temperature relationship. This method is described by ASTM D 2270 for temperatures between 40 and 100 °C. A viscosity index of 100 indicates that the oil is relatively insensitive to temperature while an index of 0 indicates a higher sensitivity (Booser, 1997: 24).

The viscosity index for the test fluid was calculated to be 188. This is well above 100, which indicates that the change with temperature is relatively small. Therefore friction and wear testing at block temperatures of up to 100 °C can be conducted without concern for moderate temperature changes.

It is also important to determine the temperature degradation characteristics of the fluid. This was done with thermogravimetric analysis (TGA). The result for the test fluid is given in Figure 4.1.4.

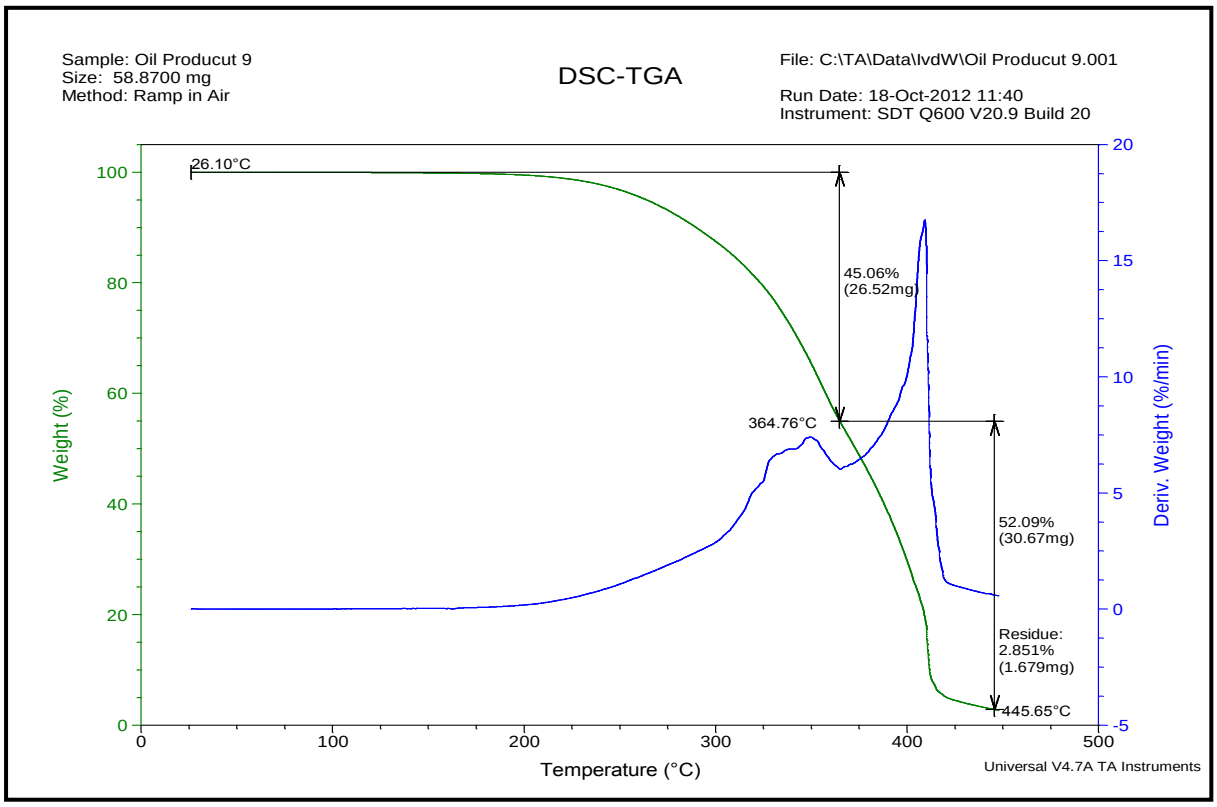

Figure 4.1.4: Thermogravimetric analysis (TGA) of test fluid.

From the green curve (mass loss curve) in Figure 4.1.4, it can be seen that mass loss starts at 175 °C. This mass loss is due to components that change from liquid

© University of Pretoria

phase to gas phase (physical change) as well as components that decompose into gas phase (chemical reactions). The mass loss continued up to 445.65 °C.

The blue curve that was also plotted on this graph represents the first derivative of the mass loss curve (green curve). This curve is the rate of mass loss. The inflection observed at 364 °C, is the point where the greatest change in mass loss occurred.

This curve however, differs from the curves that are normally obtained for single component systems (as shown in Figure 3.1.3 and 3.1.4). The deviation of this curve is most likely due to the fluid consisting of multiple components.

From the results of the physical properties, it can be seen that the fluid properties are consistent for temperature up to 100 °C and that the components do not volatilize below 175 °C.

4.1.2. PARTICLE SIZE ANALYSIS: BORON NITRIDE NANOPARTICLES

The particle size of the boron nitride nanoparticles were verified with scanning electron microscopy (SEM). The SEM images of the boron nitride nanoparticles are given in Figure 4.1.2. From this figure it can be seen that the particles are plate-like, but the shapes are also highly irregular. Furthermore the size distribution of the particles ranges from 50 nm to 700 nm, which is different from the size obtained from the supplier (70 nm). This analysis will be used as reference for particle size distributions (PSD's) of the potential dispersion formulations.

© University of Pretoria

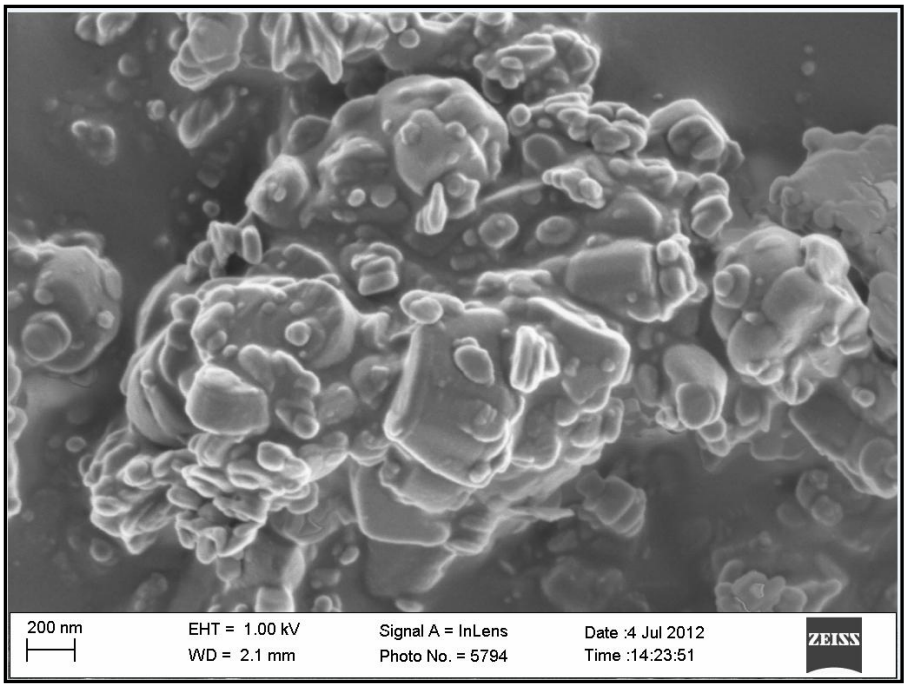

Figure 4.1.5: Scanning electron microscopy image of boron nitride nanoparticles.

4.2. DISPERSION OF PARTICLES

Particles are usually dispersed with the aid of a dispersant as described in section 2.11.1 and Appendix A. A number of dispersants were first screened after which one was chosen. This dispersion was then optimised by determining the amount of dispersant required, and thereby ensuring that the fluid containing particles remained well dispersed throughout the test.

4.2.1. DISPERSANT SCREENING

A number of different dispersants were screened. The dispersants were all non-ionic surfactants with a negative net charge. This is to enable the dispersant to adsorb onto the particle surface, which has a positive net charge. These dispersants include: sorbitan oleate, sorbitan laurate, polyoxyethylene sorbitan monolaurate, Poly(oxyethylene)(4) lauryl ether and glycerol monostearate (GMS).

The effectiveness of the dispersant in preventing poor stability (formation of aggregates and agglomerates) was verified by obtaining a particle size distribution of the dispersion with the Malvern Zeta Sizer. It was found that when glycerol mono-

© University of Pretoria

stearate was used, the PSD with the Zetasizer (Figure 4.2.1) compared well with the particle size estimation of the dry boron nitride powder in section 4.1.2. Other dispersants such as sorbitan oleate showed larger PSD's, an indication of particle aggregation or agglomeration (Figure 4.2.2).

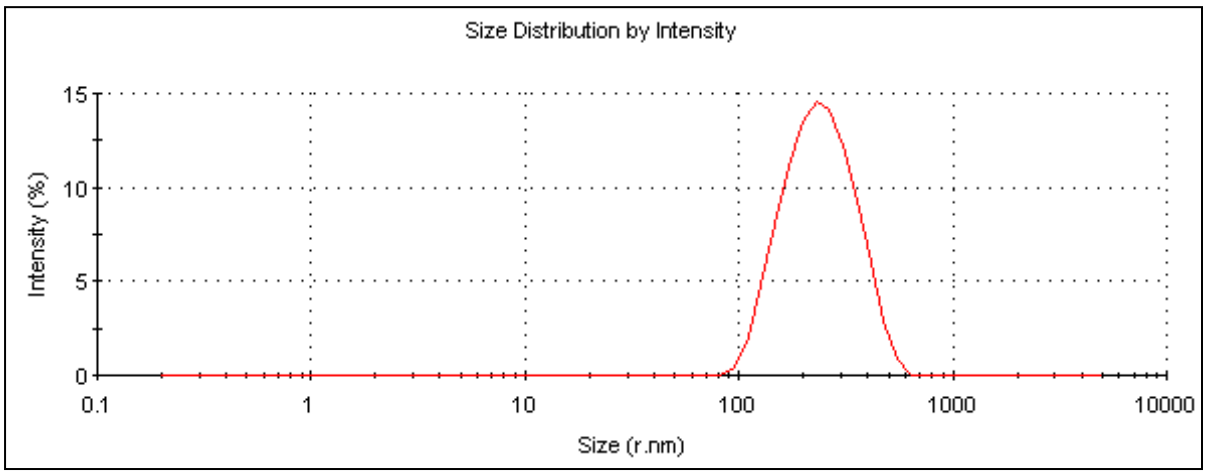

Figure 4.2.1: Particle size distribution of boron nitride dispersed with glycerol mono-stearate (GMS) in the test fluid.

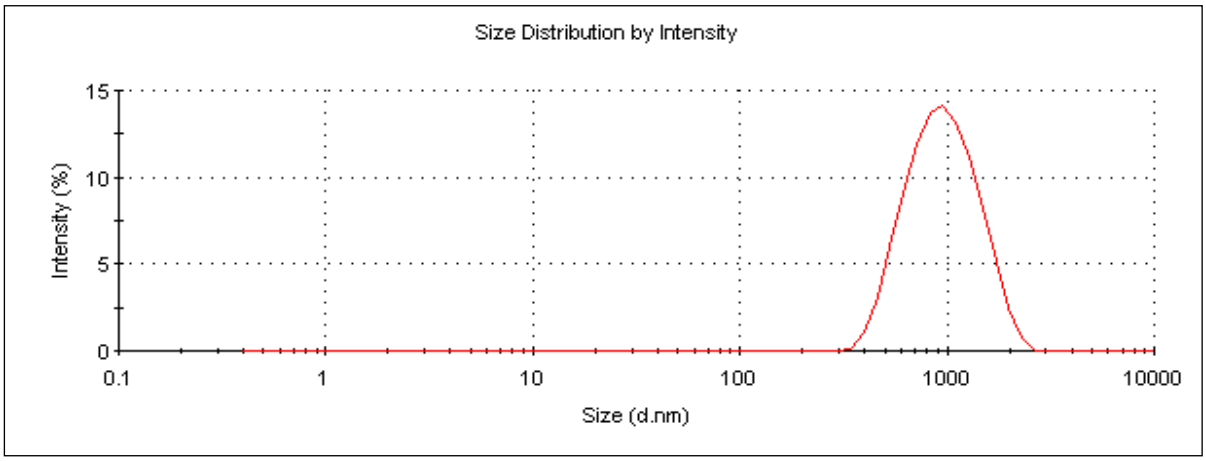

Figure 4.2.2: Particle size distribution of boron nitride suspended with sorbitan oleate in the test fluid.

Glycerol mono-stearate ($CH_3(CH_2)_{16}COOCH_2CHOHCH_2OH$) was therefore effective in the breakdown of particle clusters and was used as dispersant. There are, however, certain limitations such as the dispersant being only soluble in the oil (lubricant) above 65°C. Consequently the dispersion loses its stability when the temperature of the fluid decreases below 65 °C.

© University of Pretoria

4.2.2. DISPERSANT OPTIMIZATION

The dispersion was optimized by determining the amount of dispersant required. This was done by generating the viscosity profiles as described in section 2.11.3. These profiles are given in Figure 4.2.3 for a dispersion with 1% (mass) boron nitride. This was the amount of particles that were used in the friction and wear testing.

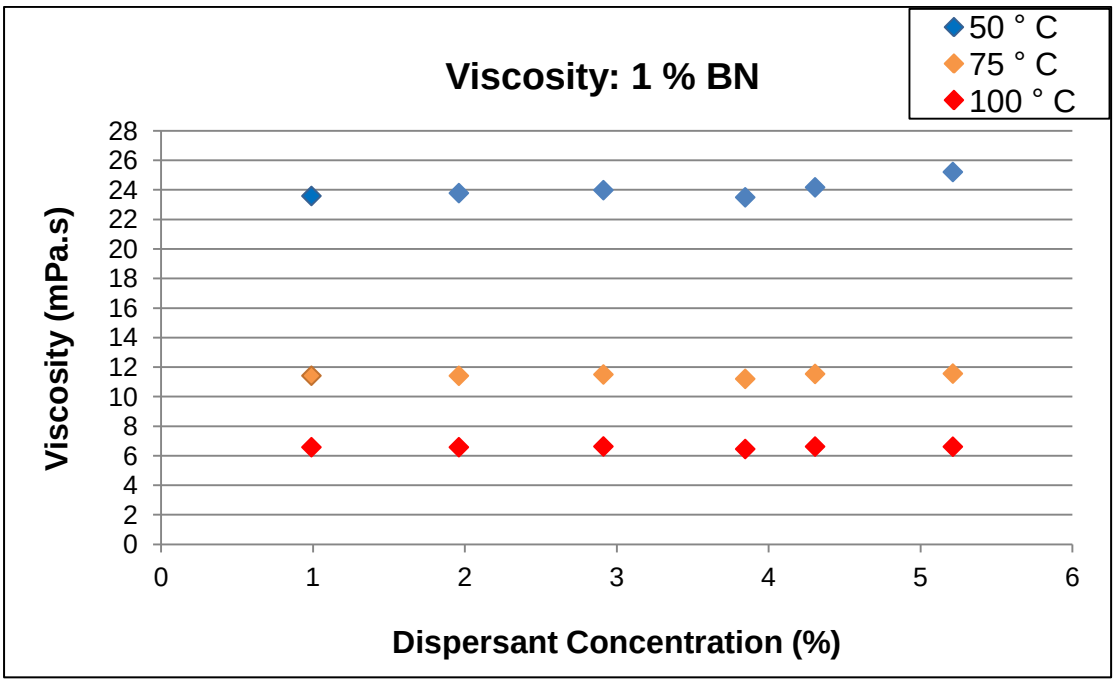

Figure 4.2.3: Viscosity profiles for 1 % (wt %) boron nitride nanoparticle dispersions in test fluid at 50 °C, 75 °C and 100 °C.

In these graphs, the viscosity was measured at higher temperatures (50 °C, 75 °C and 100 °C). This was due to the friction and wear testing that was to be done at higher temperatures as well as poor stability of dispersion at low temperatures. However, the effect of the amount of dispersant on the viscosity was very small and the viscosity profile as described in section 2.11.3 (Figure 2.11.3) could not be observed. This small effect on the viscosity was most likely due the amount of dispersant which was too small to have any significant effect on the viscosity.

Another problem was that at room temperature, the dispersion solidified. It was therefore important to keep the temperature of the dispersion above 65 °C to ensure that a liquid phase is maintained.

© University of Pretoria

It is also important to notice that the viscosity of the dispersion decreased as the temperature increased. This means that the dispersant does not desorb from the particles at elevated temperatures (Figure 2.11.2 in section 2.11.3) and the dispersant can be used over a temperature range of 65 to 100 °C.

4.2.3. VERIFICATION: ZETA SIZING

The viscosity profiles in the previous section were insufficient for determining the amount of dispersant required. Therefore, in order to verify that the particle clusters were completely broken down by the dispersant, particle size distribution (PSD) of the dispersion was done with the Zetasizer.

The PSD for 1% BN are given in Figure 4.2.4. The ratio of BN to GMS was 1 to 10. The PSD's compared well with the particle size estimation obtained from the SEM analysis and therefore it can be assumed that the aggregates were broken down and the particles remained in suspension. This ratio can then be used to prepare dispersions for lubricity tests.

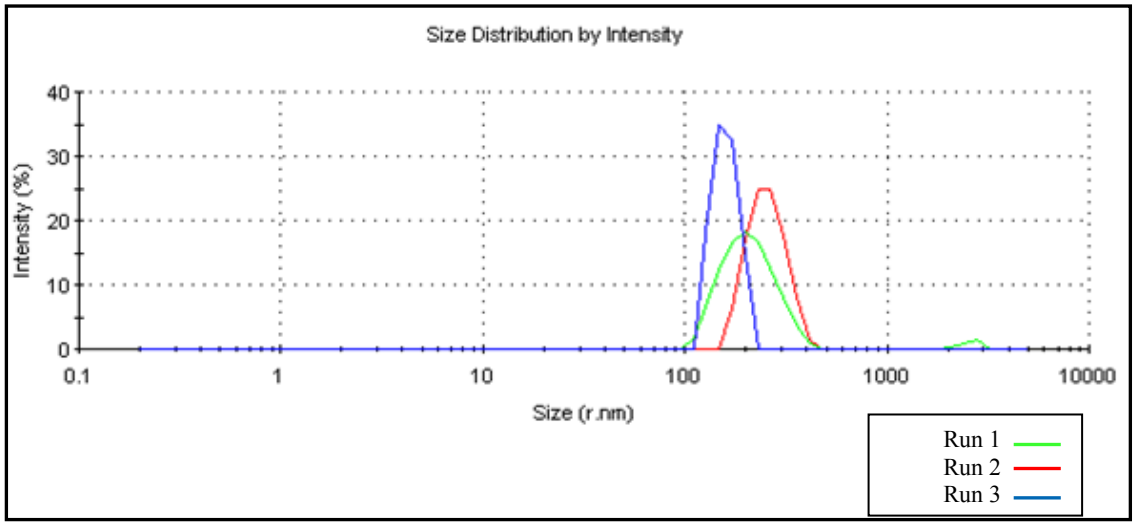

Figure 4.2.4: PSD with Zetasizer with a BN to GMS ratio of 1:10 after 1 hour in the ultrasonic bath. The BN concentration was 1% (wt %).

© University of Pretoria

4.3. DISPERSION STABILITY

As mentioned earlier, the main objective of this part of the study was to obtain a dispersion that provided adequate stability for the duration of friction and wear tests. Furthermore, due to the limitations of the dispersant which requires the temperature to be kept above 65 °C, the experimental setup had to be adjusted accordingly.

These adjustments included maintaining the dispersion at an elevated temperature of 75 °C on a heating plate while being continously stirred. Since the duration of each test was 65 minutes, the stability of the dispersion had to be verified after one hour in the ultrasonic bath and after 65 minutes on a heating plate.

A verification of the stability also had to be done after an additional 10 minutes when the sample was removed from the heating plate. This was done, since this included the period for the sample to flow from the test fluid reservoir to the contact point (see Figure 3.2.4).

The stability was verified by measuring the PSD's obtained with the Malvern Zeta Sizer. Figures 4.3.1 and 4.3.2 below contain the PSD's after 65 minutes and 65 minutes plus an additional 10 minutes. The PSD's contains three repeats where a new sample was prepared for every repeat.

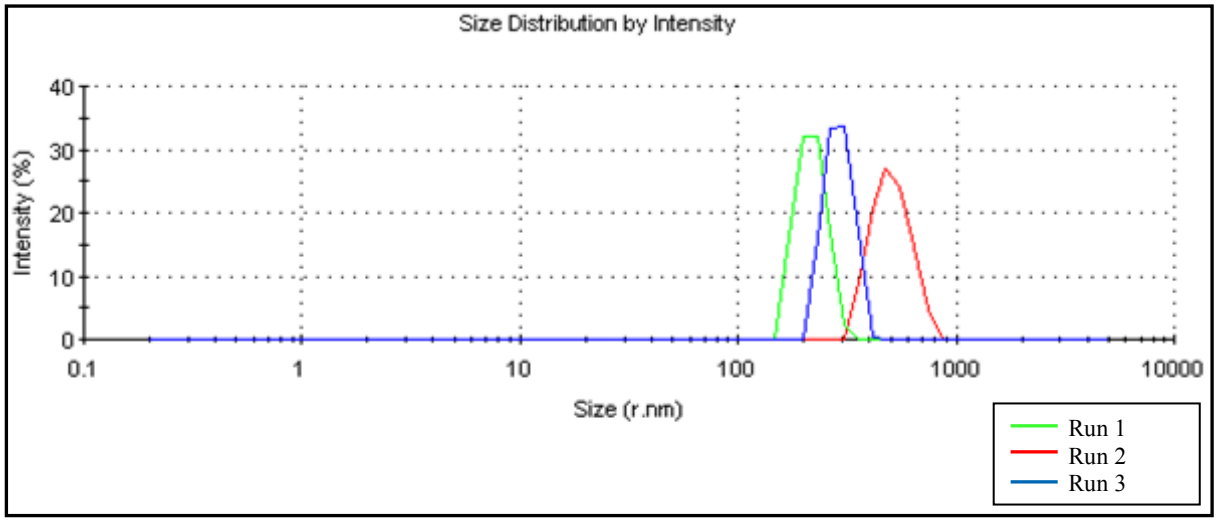

Figure 4.3.1: PSD with a BN to glycerol mono-stearate (GMS) ratio of 1:10 after 65 minutes on a heating plate at 75 °C. The BN concentration was 1%.

© University of Pretoria

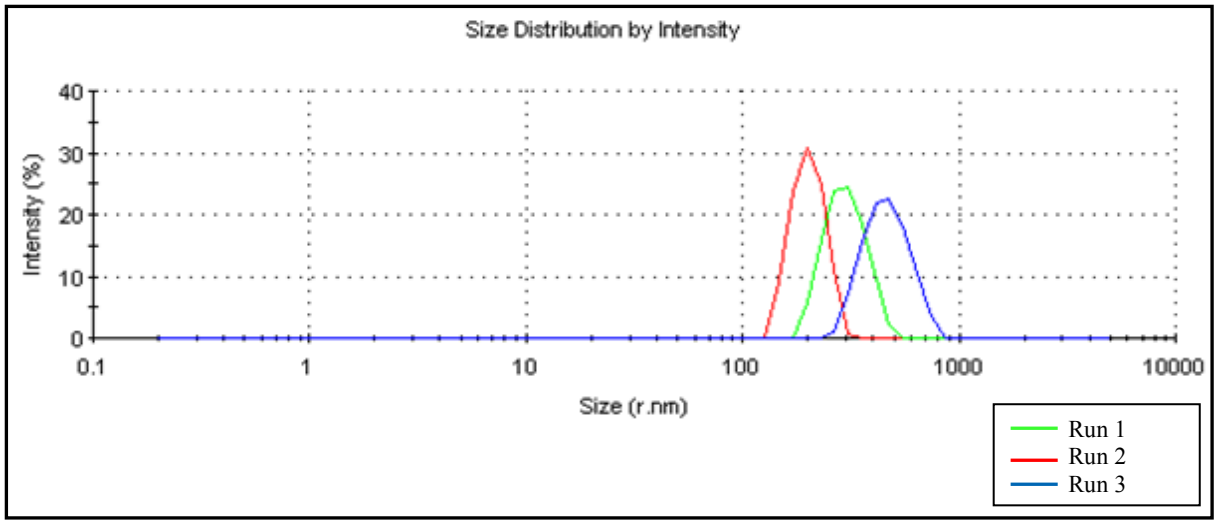

Figure 4.3.2: PSD with a BN to GMS ratio of 1:10 after 65 minutes and an additional 10 minutes on a heating plate at 75 °C. The BN concentration was 1%.

From these graphs, it can be seen that the PSD's compared well with the particle size estimation obtained with the SEM analysis. The dispersant therefore provided adequate stability for the duration of the friction and wear test.

4.4. REPEATABILITY OF FRICTION AND WEAR TESTING WITH TEST FLUID WITHOUT PARTICLES.

In this section the repeatability of the friction and wear testing of test fluid without any particle additives was investigated. The method was based on ASTM D 6425, and each test was repeated three times. This method was then adjusted accordingly and the procedure was repeated.

4.4.1. STANDARD TEST METHOD.

The lubricant was first evaluated with the standard friction and wear test on the SRV test rig at 100 °C. Three runs were done and the coefficient of friction (COF) is plotted in Figure 4.4.1. From these graphs, it can be seen that the coefficient of friction converged after 50 to 55 minutes to an average value of 0.128.

© University of Pretoria

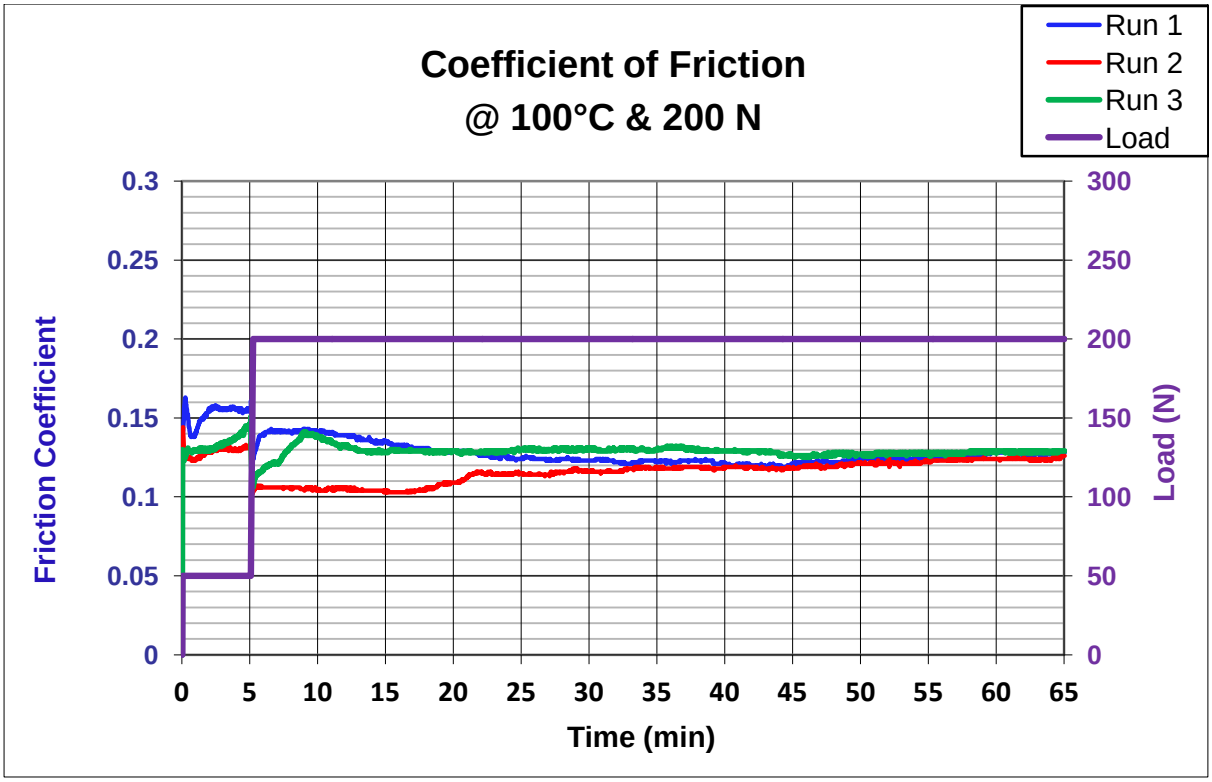

Figure 4.4.1: Coefficient of friction for test fluid with no particles (standard test method: ASTM D 6425).

When the repeatability is considered, the difference of the coefficient of friction at specified intervals as well as the minimum and maximum values between successive tests must not exceed 0.02. This is a requirement of the standard test method as described by ASTM D 6425.

According to this criterion, good repeatability was obtained for the minimum and maximum coefficient of friction values (Table 4.4.1). This was also true for the coefficient of friction after 30 minutes and the end value. The difference between the coefficient of friction obtained after fifteen minutes (COF_{15}) between run 1 and 2 and between run 2 and 3, however exceeded 0.02 (highlighted in red in Table 4.4.1).

© University of Pretoria

Table 4.4.1: Coefficient of friction values for test fluid with no particles (standard test method: ASTM D 6425).

Repeat	COF_{min}	COF_{max}	COF_{15}	COF_{30}	COF_{end}
1	0.119	0.163	*0.136**	0.123	0.128
2	0.102	0.144	*0.104**	0.116	0.126
3	0.106	0.151	*0.128**	0.13	0.129
AVG	**0.110**	**0.153**	**0.123**	**0.123**	**0.128**
STDEV	**0.009**	**0.010**	**0.017**	**0.007**	**0.002**

*Values emphasized in *italic* indicate that the difference from the previous value exceeds the criterion of 0.02, as described in ASTM D 6425.

Furthermore, the behaviour of the COF for the repeats after the running-in period was different for all the repeats, and stayed that way up to 30 minutes. It was also noticed that after the running-in period (first 5 minutes), a sudden drop in the COF was observed. This was probably due to the sudden load increase, which caused an increase in the amount of metal being worn away. The increase in the wear rate in turn resulted in a larger contact area as more material was removed and consequently a lower COF value was obtained. This caused uncertainty and is possibly the reason for the poor repeatability.

The next variable which was measured was the wear volume, as plotted in Figure 4.4.2. This was calculated from the wear scar diameters, which are given in Table 4.4.2. In Figure 4.4.2, it can be seen that the wear volumes varied considerably. The largest volume was obtained in run 1 with a value of 79×10^{-4} mm^3, and the volume decreased to a minimum of 55×10^{-4} mm^3 in run 3. This resulted in poor repeatability, since the amount of material lost was about 1.4 times more in run 1.

The differences in the wear scar diameters between successive runs were, however still within the repeatability limit of 100 µm, as described in ASTM D 6425. It should be mentioned that since the wear volumes were calculated from measured values, the wear values were subjected to small measurement errors. This error is amplified to the fourth power, due to the $d_1^2 d_2^2$ term in the wear volume calculation (equation 3.2.2).

© University of Pretoria

The standard deviation as obtained in Table 4.4.2 was also subjected to the fourth power as above. This caused the deviation from the average to be amplified for the wear scar volume, when compared to the wear scar diameter (wear scar diameter average of: 514 µm with standard deviation of 25 µm, compared to wear scar volume average of 69 $\times 10^{-4}$ mm^3 with standard deviation of 13 $\times 10^{-4}$ mm^3).

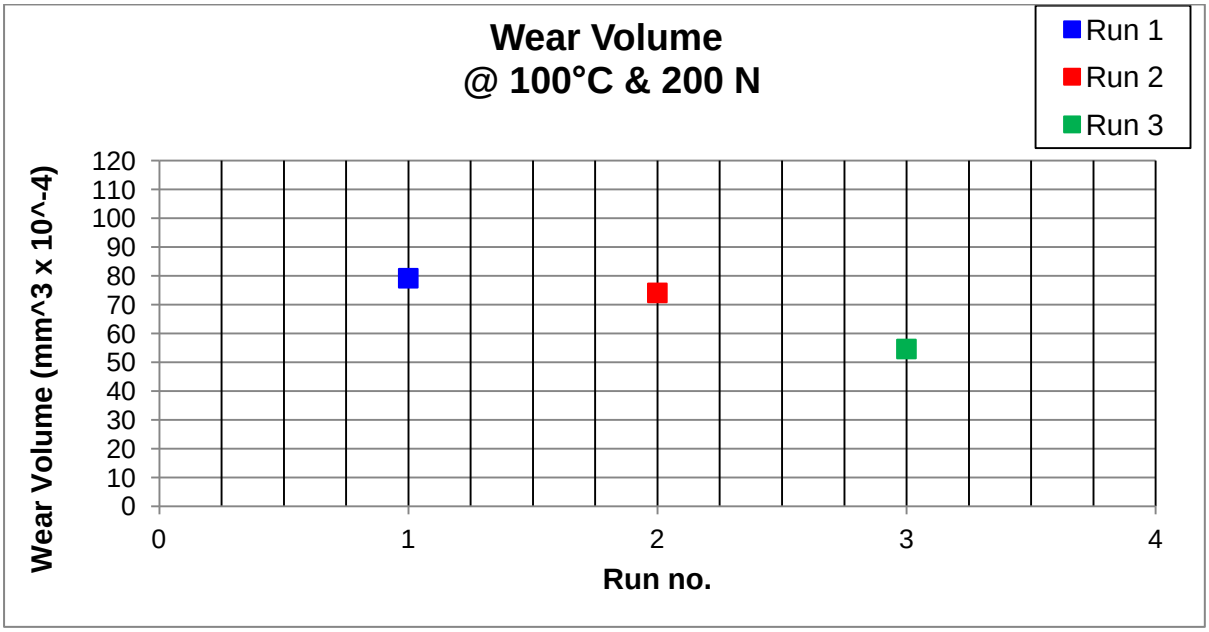

Figure 4.4.2: Wear volume for test fluid with no particles (standard test method: ASTM D 6425).

Table 4.4.2: Wear scar diameters measured and wear scar volumes calculated for test fluid with no particles (standard test method: ASTM D 6425).

Run	Wear Scar Diameter: d_1 (µm)	Wear Scar Diameter: d_2 (µm)	Average Wear Scar Diameter: $\frac{d_1+d_2}{2}$ (µm)	Wear Scar Volume ($\times 10^{-4}$ mm^3)
1	524	543	533	79
2	518	531	524	74
3	464	509	486	55
AVG	**502**	**528**	**514**	**69**
STDEV	**33**	**17**	**25**	**13**

© University of Pretoria

The third variable that was evaluated was the wear scar surface, which is shown in Figure 4.4.3. According to the complementary wear scar rating (Olah et al., 2005) all the surfaces were heavily worn and were classified as CR 5. This was a poor result in terms of wear performance (no lubrication is classified as CR6). It was also observed that the surfaces for all 3 runs are unevenly distributed with light and dark grooves that differed from each other.

Wear Scar Surface		
Run 1	**Run 2**	**Run 3**
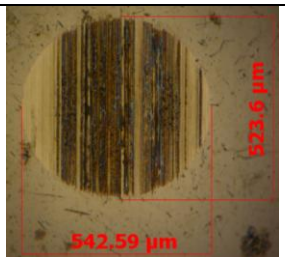	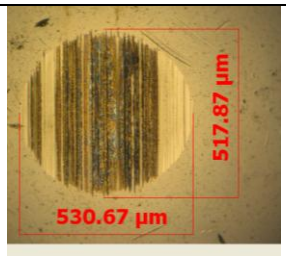	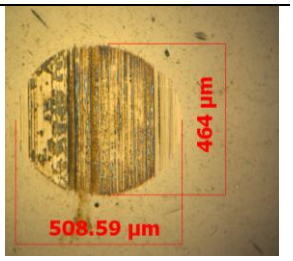

Figure 4.4.3: Wear scar surfaces obtained for test fluid with no particles (standard test method: ASTM D 6425).

Therefore, from these results obtained with the standard test method, it can be seen that the repeatability was poor. It was also observed that the sudden load increase after the running-in period had a marked influence on the COF. This might contribute to the poor repeatability obtained.

4.4.2. MODIFIED TEST METHOD.

As mentioned in the previous section, it was suggested that the sudden load increase from 50 to 200 N after the running-in period possibly caused uncertainty and poor repeatability. In this section, the test method was modified by replacing the running-in period and the sudden load increase with a more gradual load increase over a period of 5 minutes (30 N/min), as indicated in Figure 4.4.4.

From this figure, it is immediately evident that the more gradual load application rate had a smaller effect on the COF. The sudden change in the coefficient of friction was not observed and the graphs all had the same trend. However, the COF measured in run 2 was higher than the COF obtained for the other 2 runs.

© University of Pretoria

The values of the coefficient of friction at various intervals as well as maximum and minimum values are also given in Table 4.4.3. From this table it can be seen that all the differences in the values are within the repeatability limit as specified by ASTM D 6425 (0.02), except the value measured after 15 minutes between run 1 and 2 and between run 2 and 3. The standard deviation was also similar to the standard deviation obtained for the standard test method and no improvement in the repeatability was observed as far as the coefficient of friction is concerned.

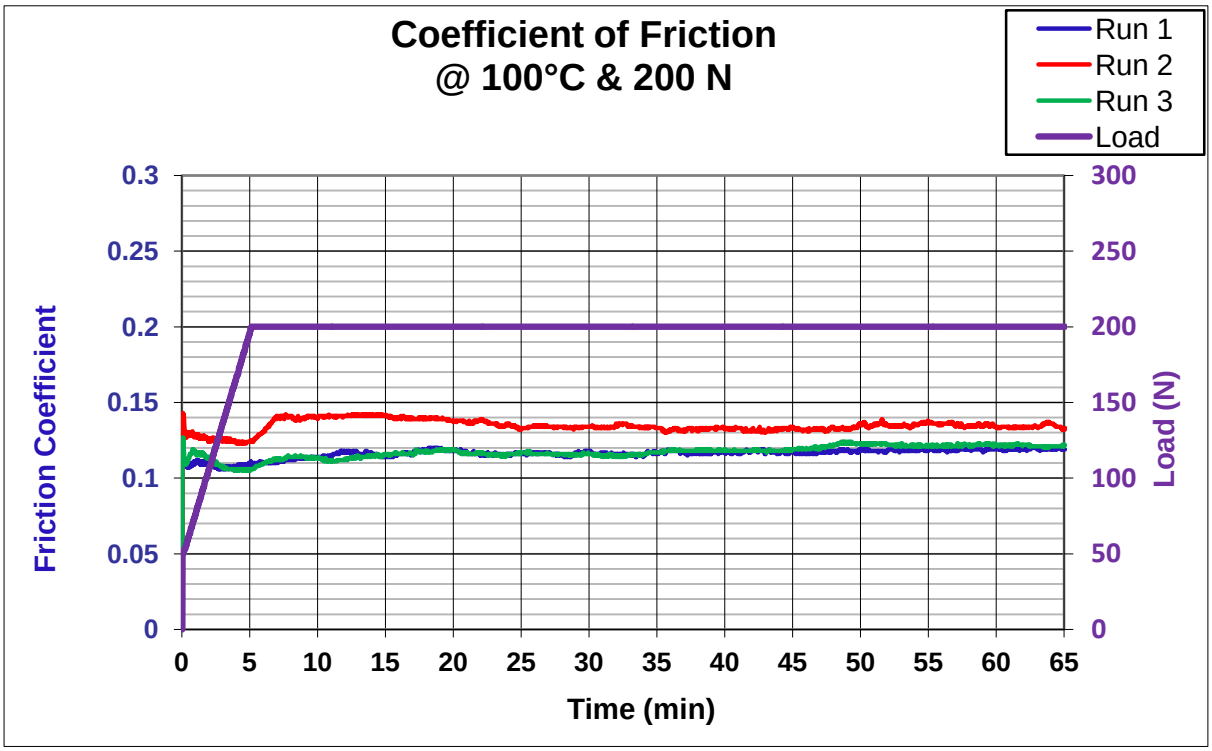

Figure 4.4.4: Coefficient of friction for test fluid with no particles (modified test method).

© University of Pretoria

Table 4.4.3: Coefficient of friction for test fluid with no particles (modified test method).

Repeat	COF_{min}	COF_{max}	COF_{15}	COF_{30}	COF_{end}
1	0.106	0.128	*0.114**	0.117	0.119
2	0.123	0.143	*0.141**	0.134	0.133
3	0.105	0.127	*0.116**	0.116	0.122
AVG	**0.111**	**0.133**	**0.124**	**0.122**	**0.125**
STDEV	**0.010**	**0.009**	**0.015**	**0.010**	**0.007**

*Values emphasized in *italic* font indicate that the difference from the previous value exceeds the criterion of 0.02, as described in ASTM D 6425.

The wear volumes calculated from the wear scar diameters are plotted in Figure 4.4.5. When these values are compared to the values obtained with the standard test method in section 4.4.1, it can be seen that the repeatability improved. Here the standard deviation calculated was 10 $\times 10^{-4}$ mm^3 (Table 4.4.4), which is smaller when compared to 13 $\times 10^{-4}$ mm^3 in Table 4.4.2. Furthermore, the differences in the successive wear scar diameters were all smaller than the repeatability limit of 100 µm as specified by ASTM D 6425.

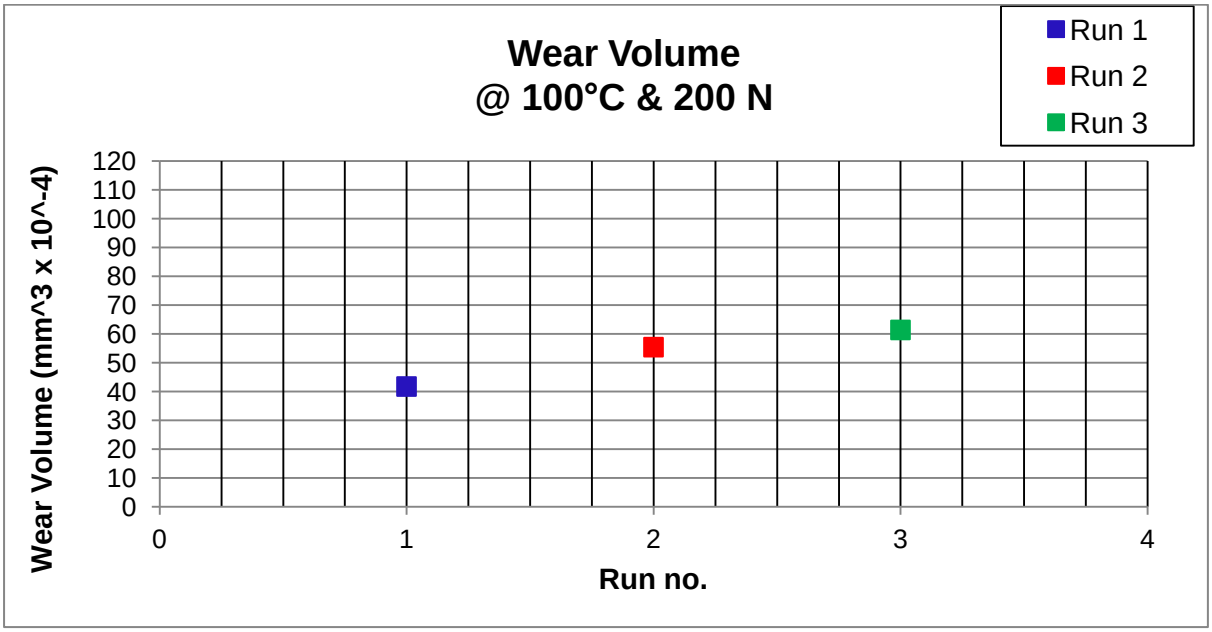

Figure 4.4.5: Wear volume obtained for test fluid with no particles (modified test method).

© University of Pretoria

Table 4.4.4: Wear scar diameters measured and wear scar volumes calculated for test fluid with no particles (modified test method).

Run	Wear Scar Diameter: d_1 (µm)	Wear Scar Diameter: d_2 (µm)	Average Wear Scar Diameter: $\frac{d_1+d_2}{2}$ (µm)	Wear Scar Volume ($\times 10^{-4}$ mm^3)
1	448	460	454	42
2	466	502	488	55
3	470	505	500	61
AVG	**461**	**489**	**481**	**53**
STDEV	**12**	**25**	**24**	**10**

The wear surfaces however, also did not indicate that any improvement was obtained (Figure 4.4.5) and was also classified as CR 5 (Olah et al., 2005). The scars also had an uneven distribution of light and dark grooves as observed in Figure 4.4.3. These dark grooves are possibly corrosion layers that are formed during the wear process. It is possible that if the conditions under which these layers are formed are not kept constant, the repeatability might be affected. This must be confirmed by first determining the composition of the dark areas and to confirm if it is indeed corrosion layers.

Wear Scar Surface		
Run 1	**Run 2**	**Run 3**
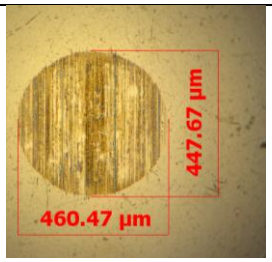	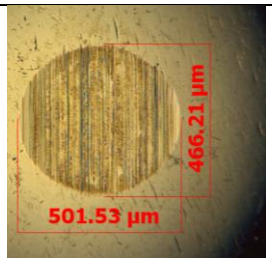	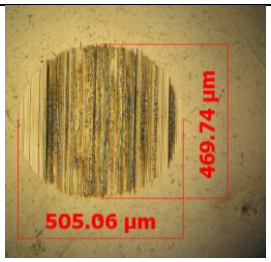

Figure 4.4.5: Wear scar surfaces obtained for test fluid with no particles (modified test method). The photographs were taken at 10 × magnification.

© University of Pretoria

4.4.3. SURFACE ANALYSIS.

In Figure 4.4.3 and Figure 4.4.5, dark grooves were observed on the wear scars. These grooves were analysed with Raman spectroscopy in order to determine the composition and to confirm that it is indeed corrosion layers that were formed. Two peaks were found at wavenumbers 340 and 374 cm^{-1} respectively, as can be seen in Figure 4.4.6. The peak at 340 cm^{-1} is an indication of greigite , Fe_3S_4, (Bourdoiseau et.al., 2010) and the peak at 374 cm^{-1} is an indication that goethite, α-FeOOH, (Bouchard and Smith, 2003) was formed on the wear surface.

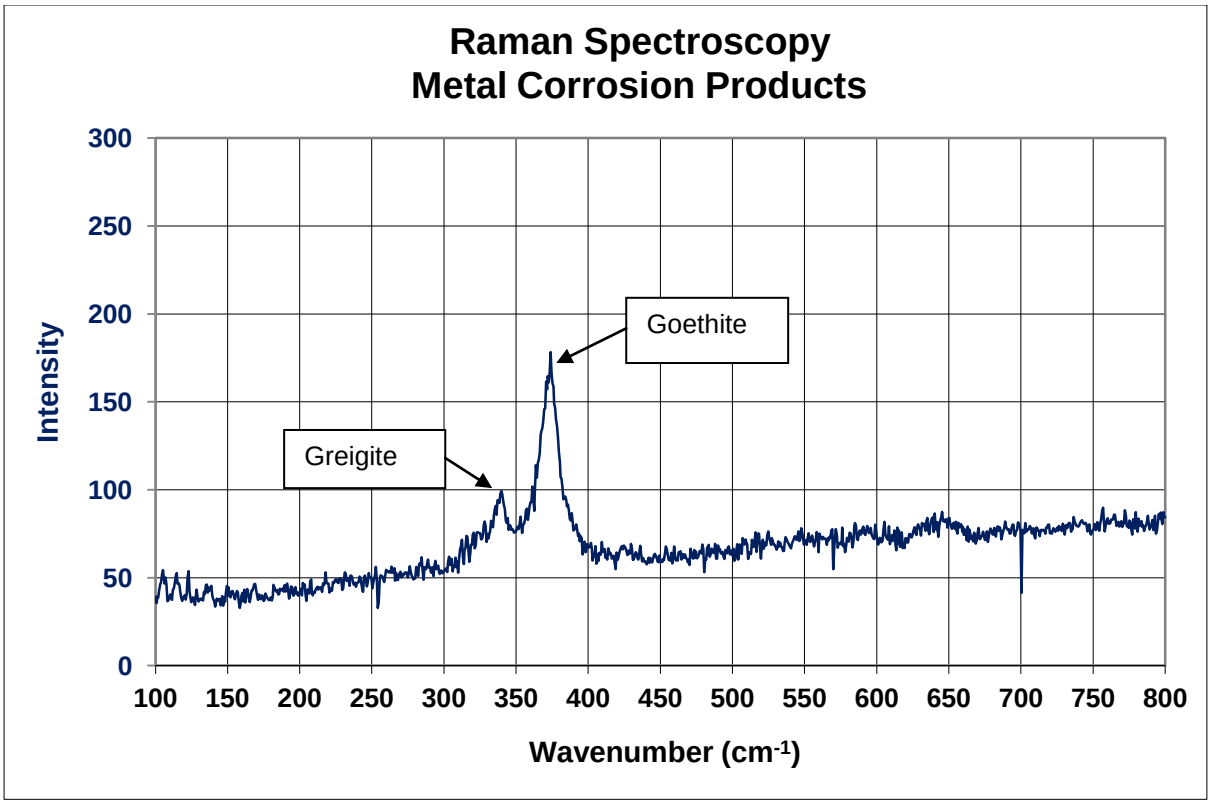

Figure 4.4.6: Raman spectra of dark areas of wear scars.

The presence of these products can be explained by the pathways by which greigite and goethite can be formed due to the transformation of mackinawite (FeS) when it reacts with oxygen and water. Mackinawite in turn can be formed due to the reaction of sulphur-containing compounds with iron. In this study, the sulphur containing compound was a sulphurised ester, which is an extreme pressure additive in the metal working fluid. These additives react with surfaces in order to form a protective

© University of Pretoria

layer (Mortier and Orszulik; 1997, 335). The iron was supplied by the test specimens, which were manufactured from AISI 52100 steel.

The sulphurised ester is thought to adsorb onto the surface of the specimens where-after the ester is decomposed due to an increase in the load, sliding speed or temperature. The sulphur atoms remain on the surface and react with iron of the worn metal. This mechanism is shown in Figure 4.4.7 below (Batchelor & Stachowiak, 2001: 398).

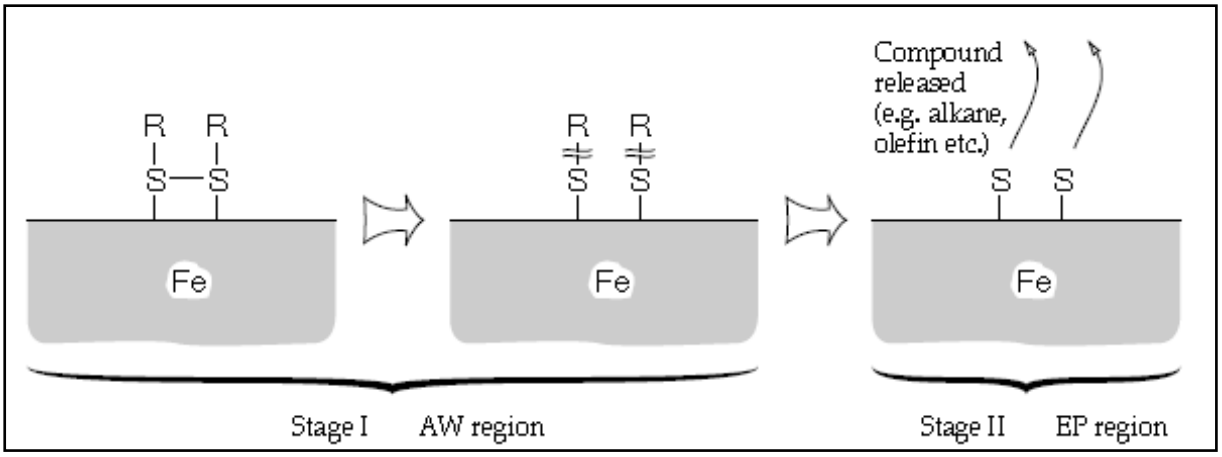

Figure 4.4.7: Mechanism of sulphur layer formation on metal surface. In this mechanism the additive adsorbs onto the surface and the wear is reduced or an anti wear effect is obtained (AW). This is followed by decomposition of the additive and the formation of sulphide layers in the extreme pressure region (Batchelor & Stachoviak, 2001: 398).

After decomposition of the sulphurised ester molecules, organic residue molecules are released. These molecules include alkanes and olefins, but are difficult to detect due the extreme dilution (Batchelor & Stachowiak, 2001: 398). The sulphide layers that are formed include FeS and $FeSO_4$ (Mortier & Orszulik; 1997, 335) and it is suggested that these layers are formed where the temperatures are the highest, i.e. in the wearing contact.

However, mackinawite (FeS) was not observed (peak at 315 cm^{-1}), but could have been hidden by the greigite peak. Also $FeSO_4$ were not observed, which is usually

© University of Pretoria

found between 900 and 1100 cm^{-1} (Chio et.al., 2006). This would suggest that there is a sequence for the formation of greigite and goethite from mackinawite.

Bourdoiseau et.al., 2010, studied the transformation of mackinawite (FeS) into greigite (Fe_3S_4) and can explain the presence of greigite and goethite (α-FeOOH). This mainly occurs due to oxidation of mackinawite, which is sensitive to the oxidizing action of oxygen and can occur in the solid state. This is a 4 stage process that is summarized below:

1. The first stage is the oxidation of Fe^{II} to Fe^{III} and can be described by the following equation:

$$Fe^{II}S + \frac{x}{2}\,O_2 + x\,H_2O \;\rightarrow\; Fe^{II}_{1-3x}\,Fe^{III}_{2x}\,S + x\,Fe^{2+} + 2x\,OH^-$$

   This oxidation stage is more likely restricted to small x values ($x \leq 0.09$, (Abdemoula, 2002)), and consequently Fe^{2+} and OH^- species are not easily detected by analysis.

2. In the second stage the oxidation continues with the formation of FeOOH phases and elemental sulphur:

$$Fe^{II}{}_{1-3x}\,Fe^{III}{}_{2x}\,S + \frac{3-3x}{4}O_2 + \frac{1-x}{2}H_2O \rightarrow (1-x)Fe^{III}OOH + S(0)$$

3. The remaining Fe (III) containing mackinawite reacts with elemental sulphur to form greigite:

$$3FeS + S(0) \rightarrow Fe_3S_4$$

4. And finally, greigite is oxidised into FeOOH compounds and elemental sulphur.

© University of Pretoria

This transformation of mackinawite into greigite and subsequent oxidation to goethite explains their presence on the wear scar surfaces and were most likely formed by this mechanism.

One factor that has also to be taken into consideration is that the presence of water and oxygen has an influence on the formation of the corrosion products (step 1 and 2). These layers that are formed as well as the extent to which these layers are formed can have an influence on the results obtained.

Therefore, it is possible that the humidity can influence the results and if this is not kept constant, poor repeatability can be obtained. This means that the atmosphere must also be controlled in order to confirm that the presence of water influences the repeatability.

Finally, when the hardness is compared, the greigite and goethite is softer than the specimens. The Vickers hardness of greigite is (VHN_{50}) 401 to 423 kg/mm^2 (Ralph, 2014) and for goetite the Vickers hardness is (VHN_{100}) is 667 kg/mm^2 (Ralph, 2014), which is smaller than the hardness of the specimens, which have a Vickers hardness of 848 kg/mm^2 (Matweb LCC, 1996). These products will then not have a negative influence on the wear behaviour.

4.4.4. MODIFIED TEST METHOD WITH CONSTANT HUMIDITY

In section 4.4.2, it was seen that there was some improvement in the repeatability of the WSV when the load application rate was reduced. It was also found that the dark grooves on the wear scar surface are corrosion layers that were formed due to reactions between sulphurised ester in the metal working fluid, the metal surface, oxygen and water.

Since this layer formation can influence the friction and wear properties, it is important to ensure that the corrosion layers that are formed are consistent. Due to the lubricating fluid composition that is fixed, standard specimens that are used as well as the consistency of oxygen in the atmosphere, the differences in the amount of water vapour (moisture content) can possibly have an effect.

© University of Pretoria

This section investigates the effect on the repeatability if the relative humidity is controlled. The modified version of the test method was still used while the relative humidity was kept at 10%. The humidity was controlled at 10 % to minimize the influence of the water vapour on the friction and wear results. The results for COF measurements are plotted in Figure 4.4.8.

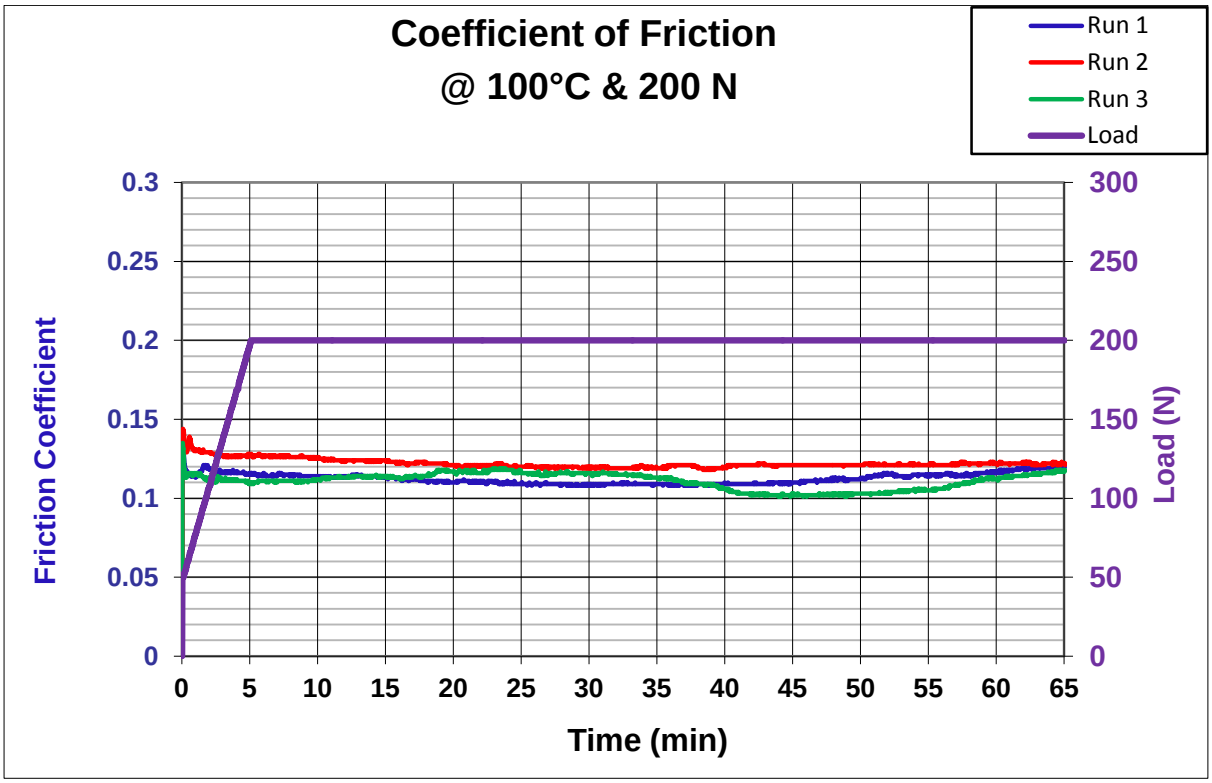

Figure 4.4.8: Coefficient of friction for test fluid with no particles (modified test method with constant humidity).

In Figure 4.4.8 it can be seen that the COF values converged at the end of the test to a value of 0.119. What is also noticeable is that the behaviour for each run differed slightly and except for the converging values at the end, no trend can be observed. The minimum and maximum values for the COF as well as the values at specified intervals are also given in Table 4.4.3.

© University of Pretoria

Table 4.4.3: Coefficient of friction values for test fluid with no particles (modified test method with constant humidity).

Repeat	COF_{min}	COF_{max}	COF_{15}	COF_{30}	COF_{end}
1	0.108	0.140	0.114	0.108	0.119
2	0.097	0.134	0.106	0.099	0.116
3	0.088	0.144	0.124	0.119	0.122
AVG	**0.098**	**0.139**	**0.115**	**0.109**	**0.119**
STDEV	**0.010**	**0.005**	**0.009**	**0.010**	**0.003**

From Table 4.4.3 it can be seen that the COF values was within the repeatability limit of a difference smaller than 0.02 between successive runs and the standard deviation was overall smaller than the standard deviations obtained in Table 4.4.1 and 4.4.3. The wear scar volumes were also determined and are plotted in Figure 4.4.9 below.

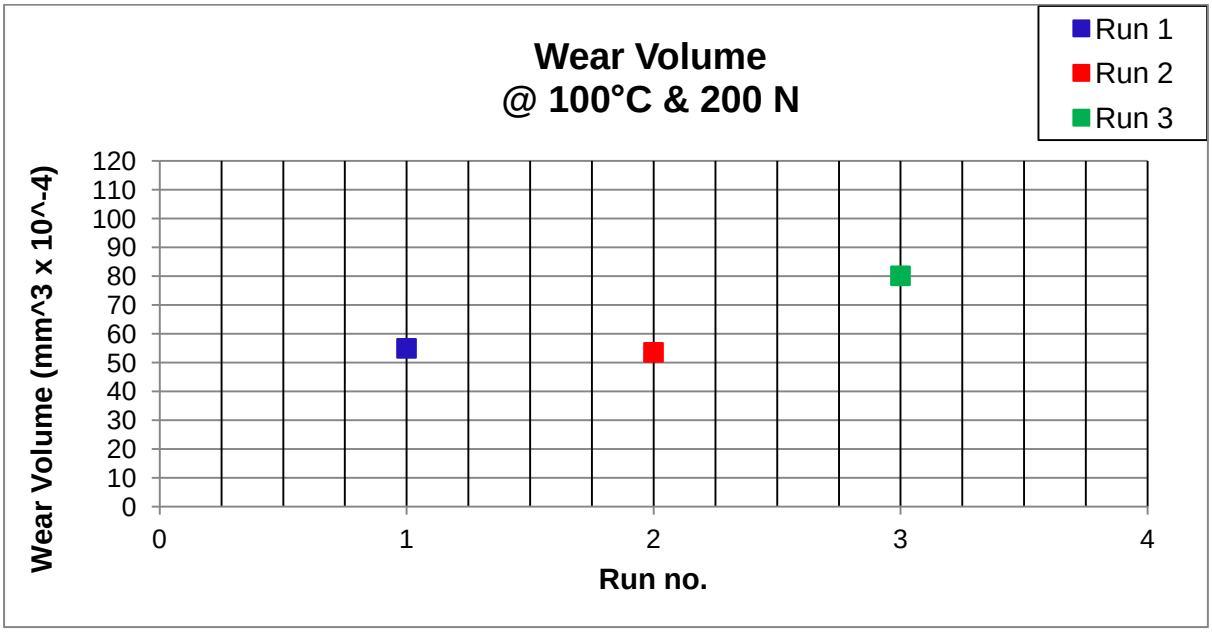

Figure 4.4.9: Wear volume obtained for test fluid with no particles (modified test method with constant humidity).

According to this figure, the wear volumes for run 1 and 2 were quite similar, with the wear volume obtained in run 3 being higher. Furthermore, as can be seen from Table 4.4.6 below and Table 4.4.6 in section 4.4.2, the standard deviation was slightly larger (12 $\times 10^{-4}$ mm^3 compared to 10 $\times 10^{-4}$ mm^3 in Table 4.4.4). Therefore,

© University of Pretoria

when only the wear volume is considered, no improvement was obtained in the repeatability.

It should also be noted that the amount of wear was higher. This could be due to differences in the atmospheric conditions or humidity, where the humidity was higher for the repeats in section 4.4.2. This can possibly influence the corrosion layer formation, which in fact forms a protective layer (section 4.4.3). Since this layer formation requires water (steps 1 and 2 in section 4.4.3), the low humidity could have caused the formation of the layer to occur at a slower rate and consequently more wear occurred.

Table 4.4.6: Wear scar diameters measured and wear scar volumes calculated for test fluid with no particles (modified test method with constant humidity).

Run	Wear Scar Diameter: d_1 (µm)	Wear Scar Diameter: d_2 (µm)	Average Wear Scar Diameter: $\frac{d_1+d_2}{2}$ (µm)	Wear Scar Volume ($\times 10^{-4}$ mm^3)
1	477	496	487	55
2	466	501	484	54
3	524	546	535	80
AVG	**489**	**514**	**502**	**63**
STDEV	**31**	**28**	**29**	**15**

The wear scar surfaces, as shown in Figure 4.4.10, were similar in appearance, except for the scar obtained in run 3. This difference in appearance conforms to the higher amount of wear that occurred during this run (Figure 4.4.9).

© University of Pretoria

Wear Scar Surface		
Run 1	**Run 2**	**Run 3**
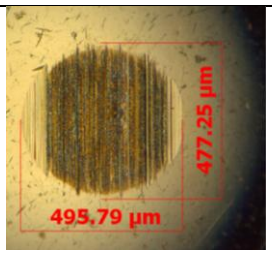	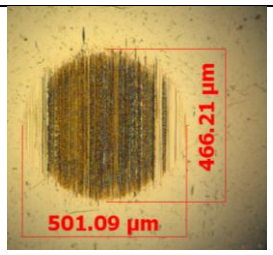	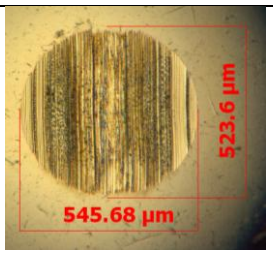

Figure 4.4.10: Wear scar surfaces for test fluid with no particles (modified test method with constant humidity). The photographs were taken at 10 × magnification.

We have seen an improvement in the repeatability of the results, but there is still uncertainty. This is mainly due to the unpredictability of the repeatability of the results, such as obtained in run 3.

Since the fluid contains a significant amount of plant oil, the handling of the fluid prior to the test and during the test is also important. This is due to plant oils being prone to hydrolysis. This means that if the oil samples are in contact with the atmosphere for longer or shorter periods for repeat runs, the properties of the fluid might not be the same at the start of a test run and can result in poor repeatability.

Furthermore, it is important to notice that the temperature in the chamber does not remain constant (Figure 4.4.11). This would mean that the vapour pressure will not remain constant as can be seen in equation 4.4.1 (Perry & Green, 1997: 2-49).

$$P^* = f(T) \qquad 4.4.1$$

Where P^* is the vapour pressure of the water and T is the atmospheric temperature. Since the relative humidity is a function of the vapour pressure, the relative humidity will also vary with the temperature. This can be seen in equation 4.4.2 (Perry & Green, 1997: 12-3).

$$H_R = \frac{P_w}{P^*} \qquad 4.4.2$$

© University of Pretoria

Where H_R is the relative humidity and P_w is the partial pressure of the water vapour.

This variation in the temperature is illustrated in Figure 4.4.11 for the test duration. The variation of the pressure of the water vapour is illustrated in Figures 4.4.12 by the red curve.

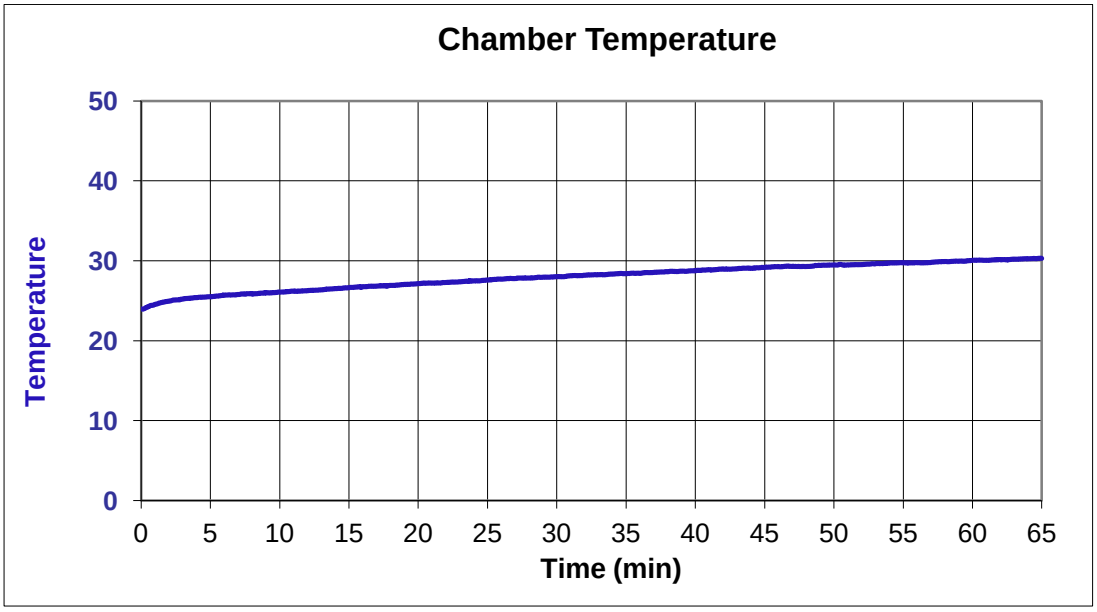

Figure 4.4.11: Increase in the atmospheric temperature in the test chamber for duration of the friction and wear test.

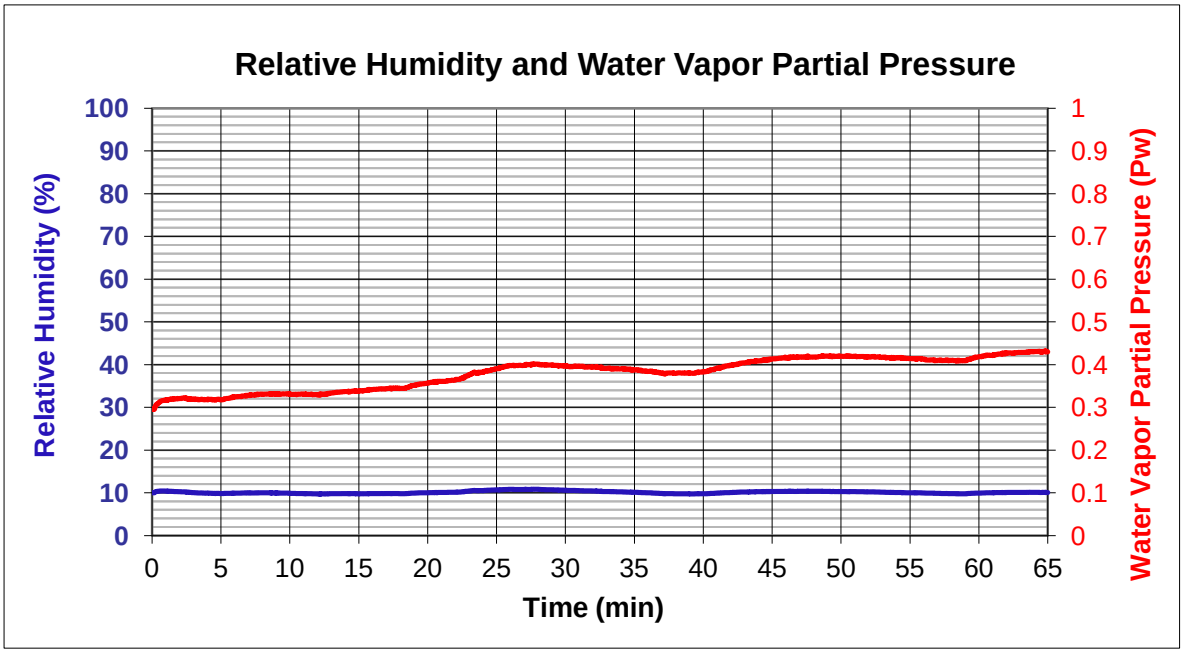

Figure 4.4.12: Influence on the partial pressure of water vapour due to humidity control for duration of the friction and wear test.

© University of Pretoria

This temperature dependency would also mean that the partial pressures of the water vapour were different at the start of the tests since the atmospheric temperatures were not the same at the start. This is shown in Table 4.4.7.

Table 4.4.7: Initial temperature, relative humidity and partial pressure of water vapour.

Run	Initial Temperature	Relative Humidity	Water Vapour Partial Pressure
1	24.90	10.02	0.31
2	27.50	10.01	0.36
3	23.24	10.45	0.29

Therefore, in order to reduce uncertainty and improve repeatability, the exposure of the fluid to the atmosphere must be consistent for all the repeats. Also the partial pressure and not the relative humidity must be kept constant for the duration of these tests.

4.5. REPEATABILITY OF FRICTION AND WEAR TESTING OF TEST FLUID WITH PARTICLES

In this section the repeatability of the friction and wear test of test fluid with added boron nitride nanoparticles was investigated. This included the standard test method with no humidity control (see section 4.4.1) and since it was already found that the moisture (humidity) also influences the results, the test modification step was skipped (see section 4.4.2). Instead, the repeatability of the modified test method with atmospheric control (see section 4.4.4) was determined.

4.5.1. STANDARD TEST METHOD

The standard test method with the boron nitride nanofluid was also repeated three times. The result of the COF was plotted in Figure 4.5.1. From these plots, it can be seen that the repeatability for the three repeats was poor and did not converge at the

© University of Pretoria

end of the test. The sudden load increase also had a marked influence on the COF behaviour, which decreased considerably after the load was rapidly increased to 200 N. This was due to the contact area that increased, which was caused by material which was rapidly removed from the ball specimen (increase in wear scar diameter) with the sudden increase in load (see section 4.4.1).

The coefficient of friction values after 15 and 30 minutes as well as the maximum, minimum and end values are given in Table 4.4.1. From this table, however it can be seen that the difference between the values of the successive runs was not larger than 0.02, as specified in ASTM D 6425. Therefore, despite the uncertainty and differences in the final value, the repeatability is considered to be adequate according to ASTM D 6425.

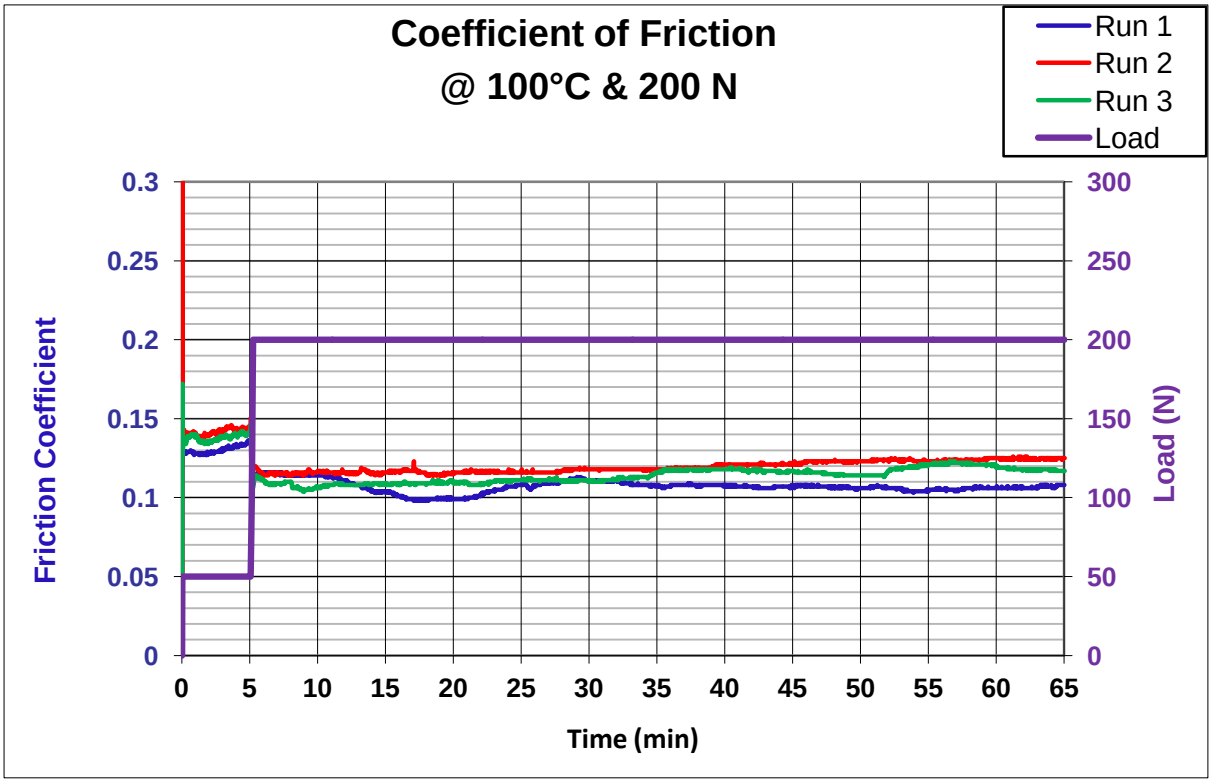

Figure 4.4.1: Coefficient of friction for test fluid with particles (standard test method: ASTM D6425).

© University of Pretoria

Table 4.4.1: Coefficient of friction values obtained for test fluid with particles (standard test method: ASTM D6425).

Repeat	COF_{min}	COF_{max}	COF_{15}	COF_{30}	COF_{end}
1	0.098	0.137	0.104	0.111	0.108
2	0.114	0.151	0.116	0.118	0.125
3	0.104	0.147	0.109	0.11	0.117
AVG	**0.105**	**0.145**	**0.110**	**0.113**	**0.117**
STDEV	**0.008**	**0.007**	**0.006**	**0.004**	**0.009**

However, the wear volumes that were calculated (Figure 4.5.2 and Table 4.5.2) varied considerably. Furthermore, the wear scars were also dissimilar in appearance, with more severe damage caused during repeat 2 and 3 (Figure 4.5.3). In the wear scar obtained from repeat 1, dark grooves can also be observed and to a lesser extent in repeats 2 and 3. In section 4.4.3, the grooves for the test fluid without any particle additives were analysed with Raman spectroscopy. This revealed that the dark grooves consisted of greigite (Fe_3S_4) and goethite (α-FeOOH). Due to the presence of the particles, this must also be confirmed for this part of the investigation.

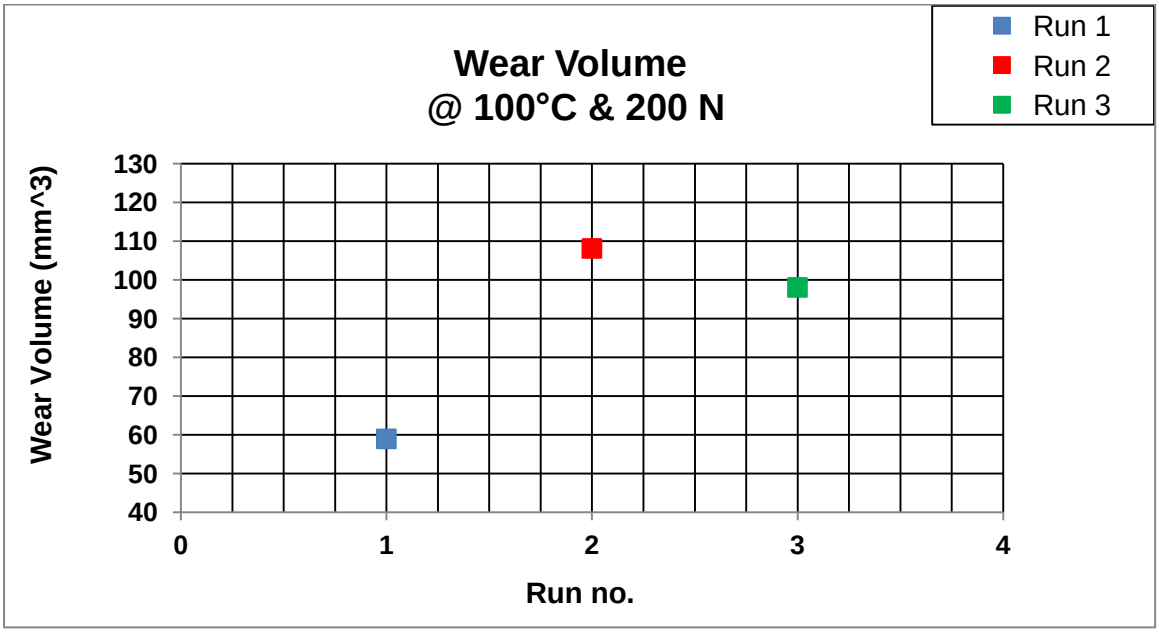

Figure 4.5.2: Wear volume determined for test fluid with particles (standard test method: ASTM D6425).

© University of Pretoria

Table 4.5.2: Wear scar diameters measured for test fluid with particles (standard test method: ASTM D6425).

Run	Wear Scar Diameter: d_1 (µm)	Wear Scar Diameter: d_2 (µm)	Average Wear Scar Diameter: $\frac{d_1+d_2}{2}$ (µm)	Wear Scar Volume ($\times 10^{-4}$ mm^3)
1	496	494	495	59
2	558	593	576	108
3	547	577	562	98
AVG	**534**	**555**	**544**	**88**
STDEV	**33**	**53**	**43**	**26**

Wear Scar Surface		
Run 1	**Run 2**	**Run 3**
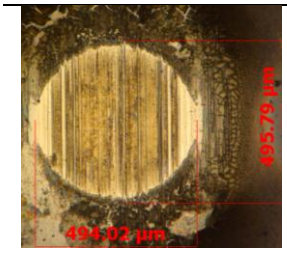	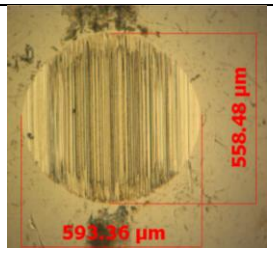	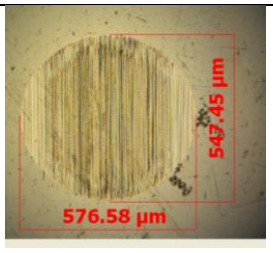

Figure 4.5.3: Wear scar surfaces for test fluid with particles (standard test method: ASTM D6425).

4.5.2. SURFACE ANALYSIS

As mentioned in the previous section Raman spectroscopic analyses had to be done on the dark grooves on the wear scar surfaces in order to determine the composition. The spectrum for metal oxides is plotted in Figure 4.5.4. This plot confirms the presence of greigite (340 cm^{-1}) (Bourdoiseau et.al., 2010) and goethite (374 cm^{-1}) (Bouchard and Smith, 2003), which was also observed in Figure 4.4.6. The possible formation of these two compounds was explained in detail in section 4.4.3.

Two peaks at wave numbers 785 and 965 cm^{-1} were also found (Figure 4.5.5). These two peaks indicate that melanterite ($FeSO_4.7H_2O$) and rozenite ($FeSO_4.4H_2O$)

© University of Pretoria

(Chio et.al., 2006) were also present on the wear scar surface. These compounds can be formed from the oxidation of mackinawite (FeS) with pyrite (FeS_2) and greigite (Fe_3S_4) as intermediate compounds (Benning & Hunger, 2007 and Vaughan & Rimstidt, 2003).

The pathway by which melanterite and rozenite can possibly form is represented by steps 1 and 2 below. It is also important to note that the oxidation reaction in step 1 occurs at temperatures of 125 to 200 °C, which is close to the block temperature of the SRV test rig. This also makes this pathway feasible, since the contact temperature between the ball and disc will be higher than the block temperature.

1. Oxidation of mackinawite (FeS) to first greigite (Fe_3S_4) and then to pyrite (FeS_2).

$$4FeS \xrightarrow[-Fe^{2+}]{-2\bar{e}} Fe_3S_4$$

$$Fe_3S_4 \xrightarrow{-4\bar{e}} 2FeS_2$$

2. Formation of Iron (II) sulphate in the presence of oxygen and water.

$$FeS_2 + 3.5\,O_2 + H_2O \rightarrow Fe^{2+} + 2\,H^+ + 2\,SO_4^{2-}$$

Finally, amorphous carbon was also observed (Figure 4.5.6), but with a peak super imposed at wave number 1364 cm^{-1} (Chu and Li, 2006). The carbon was most likely observed due to the composition of the alloy that contains carbon.

The superimposed peak is most likely boron nitride particles that remained on the surface (Bando et.al., 2006). Furthermore, no borates or boric acid (Luther et.al., 2003) were found and it can be assumed that the boron nitride did not react with oxygen or water. This would mean that the contact temperature is below 800 °C, since boron nitride only experiences minimal oxidation up to this temperature (Cofer and Economy, 1995).

© University of Pretoria

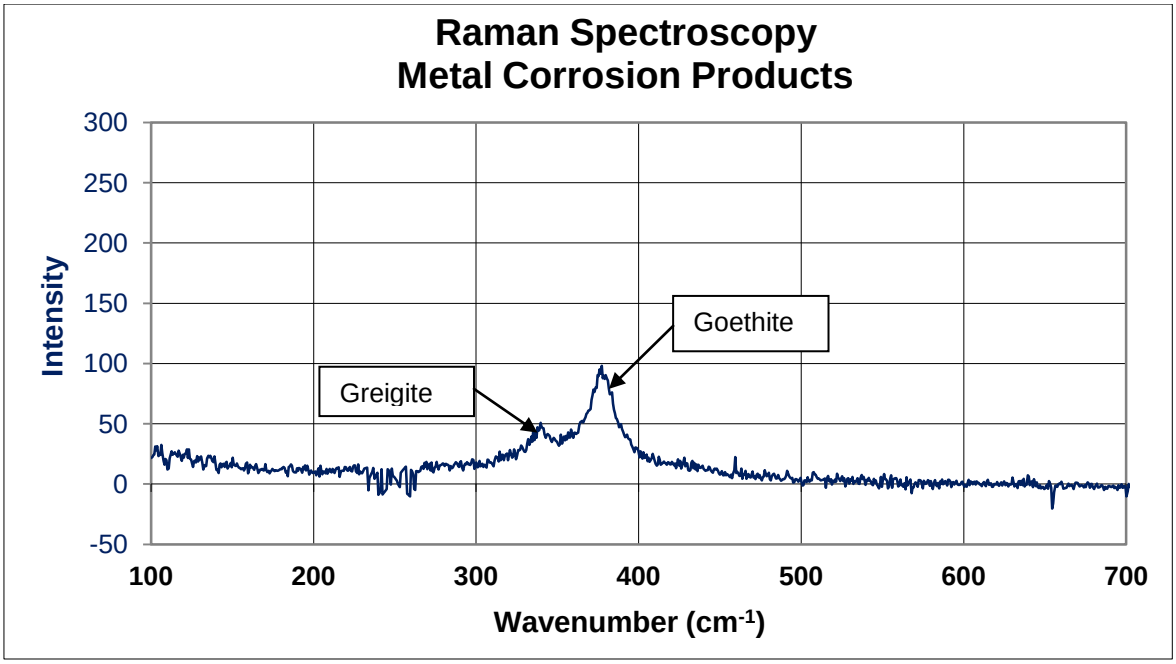

Figure 4.5.4: Raman spectra for scars formed during friction and wear tests with boron nitride nanoparticles dispersed in lubricating fluid as test lubricant (Bourdoiseau et.al., 2010 and Bouchard and Smith, 2003).

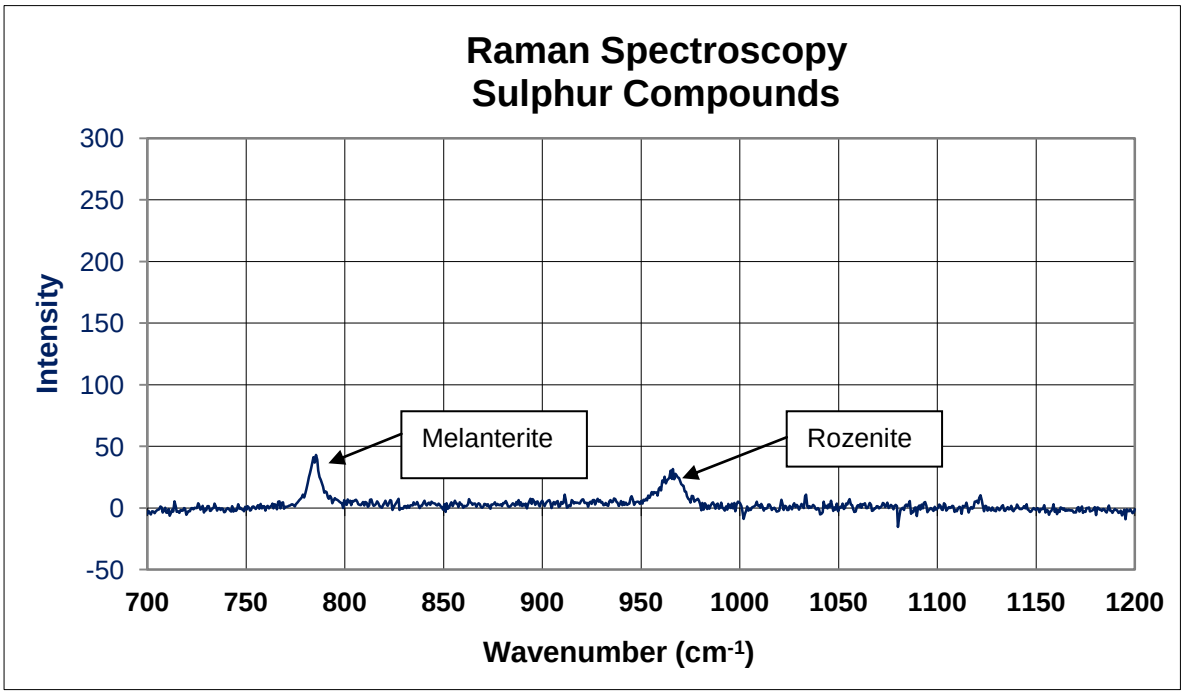

Figure 4.5.5: Raman spectra for scars formed during friction and wear tests with boron nitride nanoparticles dispersed in lubricating fluid as test lubricant (Chio et.al., 2006).

© University of Pretoria

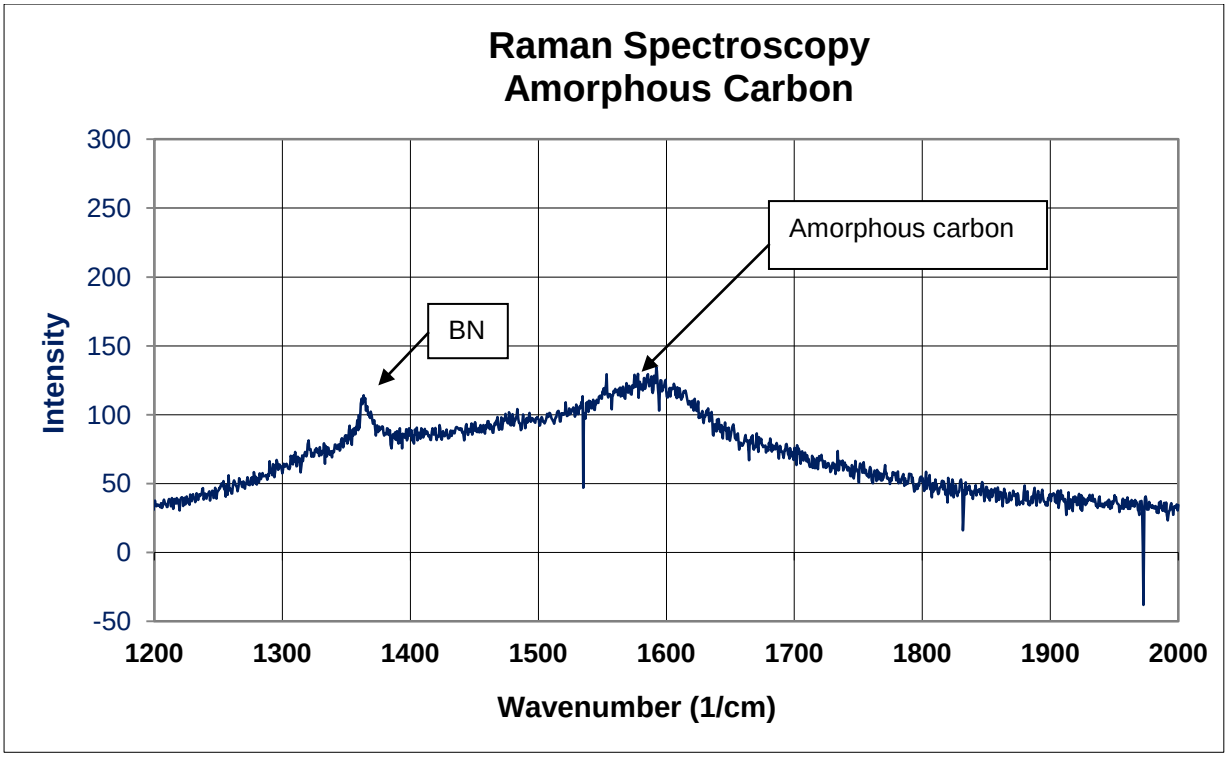

Figure 4.5.6: Raman spectra for scars formed during friction and wear tests with boron nitride nanoparticles dispersed in lubricating fluid as test lubricant (Chu and Li, 2006 and Bando et.al., 2006).

4.5.3. MODIFIED TEST METHOD WITH CONSTANT HUMIDITY

It was already observed that the rapid load increase of the standard test method as well as the atmospheric conditions (relative humidity) influences the repeatability (sections 4.4.1, 4.4.2 and 4.4.4) of the coefficient of friction, wear scar volume and wear scar surface. The repeatability of the modified test method with humidity control was also investigated for the test fluid with h-BN nanoparticles. The same load application rate of 30 N/min was used and the relative humidity was also regulated at 10%, as was done in section 4.4.4. The results for the coefficient of friction are plotted in Figure 4.5.7.

It can be seen that repeatability improved when the modified test method was used and the relative humidity controlled, except for the two peaks obtained during run 2 and 3. After the peak in the second repeat (red graph), there was also a decrease in the COF due to the wear that increased. This increase in the wear in turn increased the surface area which resulted in a decrease in the COF. This then caused the

© University of Pretoria

second repeat to deviate from the first and third run. The second and third run had good repeatability for the duration of the test.

It should also be noticed that the COF at various stages during the test in Table 4.5.3 were within the repeatability limit as described in ASTM D 6425.

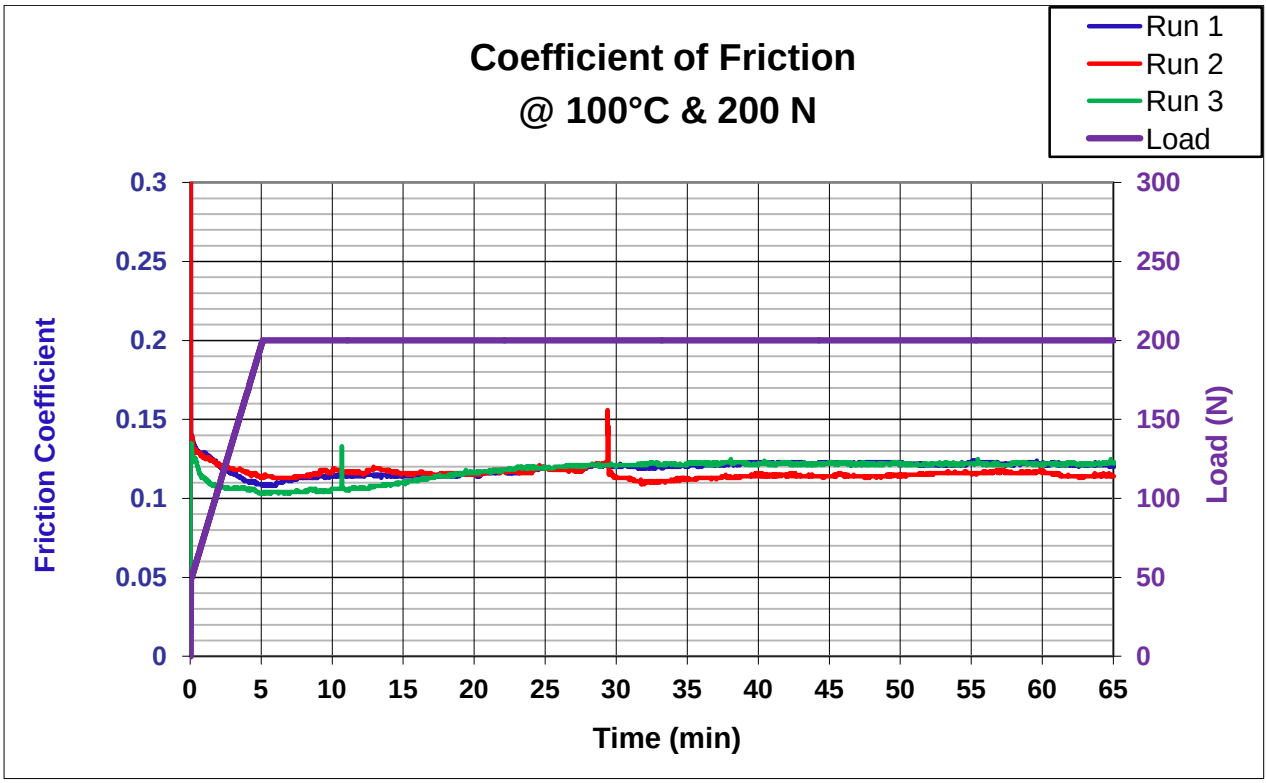

Figure 4.5.7: Coefficient of friction for test fluid with particles (modified test method with constant humidity).

Table 4.5.3: Coefficient of friction values for test fluid with particles (modified test method with constant humidity).

Repeat	COF_{min}	COF_{max}	COF_{15}	COF_{30}	COF_{end}
1	0.108	0.140	0.114	0.120	0.120
2	0.110	0.156	0.116	0.114	0.114
3	0.103	0.136	0.110	0.120	0.123
AVG	**0.107**	**0.144**	**0.113**	**0.118**	**0.119**
STDEV	**0.004**	**0.011**	**0.003**	**0.003**	**0.005**

© University of Pretoria

The repeatability of the amount of wear also improved, as can be seen from Figure 4.5.8 and Table 4.5.4 since the deviation decreased from 26 $\times 10^{-4}$ mm^3 to 8 $\times 10^{-4}$ mm^3. There also seemed to be an improvement in the similarity in the appearance of the wear scar surfaces (Figure 4.5.9).

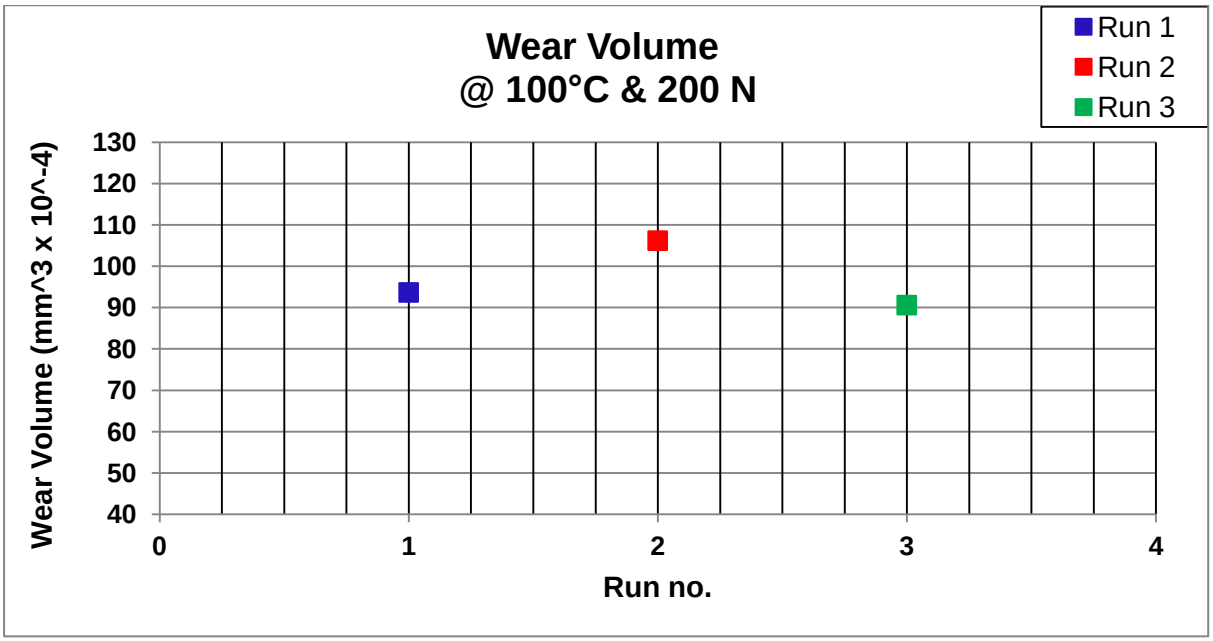

Figure 4.5.8: Wear volume for test fluid with particles (modified test method with constant humidity).

Table 4.5.4: Wear scar diameters measured and wear scar volumes calculated for test fluid with particles (modified test method with constant humidity).

Run	Wear Scar Diameter: d_1 (µm)	Wear Scar Diameter: d_2 (µm)	Average Wear Scar Diameter: $\frac{d_1+d_2}{2}$ (µm)	Wear Scar Volume ($\times 10^{-4}$ mm^3)
1	540	571	556	106
2	549	597	573	90
3	538	564	551	93
AVG	**542**	**577**	**560**	**96**
STDEV	**6**	**17**	**12**	**8**

© University of Pretoria

Wear Scar Surface		
Run 1	**Run 2**	**Run 3**
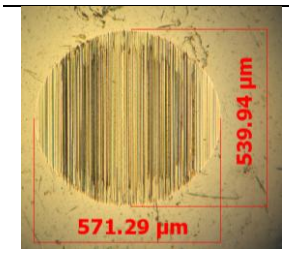	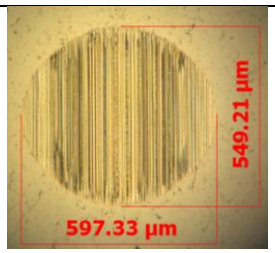	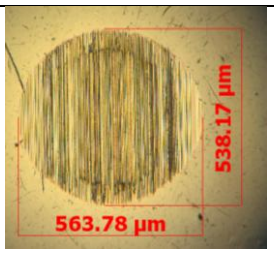

Figure 4.5.9: Wear scar surfaces for test fluid with particles (modified test method with constant humidity).

The repeatability therefore improved when the test method was modified and the humidity kept constant. This was most likely due to the corrosion layer formation that will be more consistent. It is also important to note that, as discussed in section 4.4.4, the partial pressure must be kept constant instead of the relative humidity. This is due to the relative humidity being a function of the atmospheric temperature and the amount of water vapour that varies with temperature (Figures 4.4.11 and 4.4.12).

4.6. INFLUENCE ON REPEATABILITY WITH ADDITION OF PARTICLES

In this section, the repeatability of the friction and wear results will only include the results obtained with the modified test method where the relative humidity was controlled. Here the effect of the presence of the particles on the repeatability of the coefficient of friction, the wear volume and the wear surface will be investigated

The coefficients of friction (COF) for the test fluid with out and with particle additives are given in Figure 4.6.1. Here it can be seen that except for the peaks obtained in the second graph (fluid with particles), the behaviour of the COF was similar.

The average values of the COF as specified by ASTM D 6425 are also given in Table 4.6.1. Here it can be seen that the standard deviation for both test fluids compared well with each other, and the particles did not seem to influence the repeatability of the coefficient of friction.

© University of Pretoria

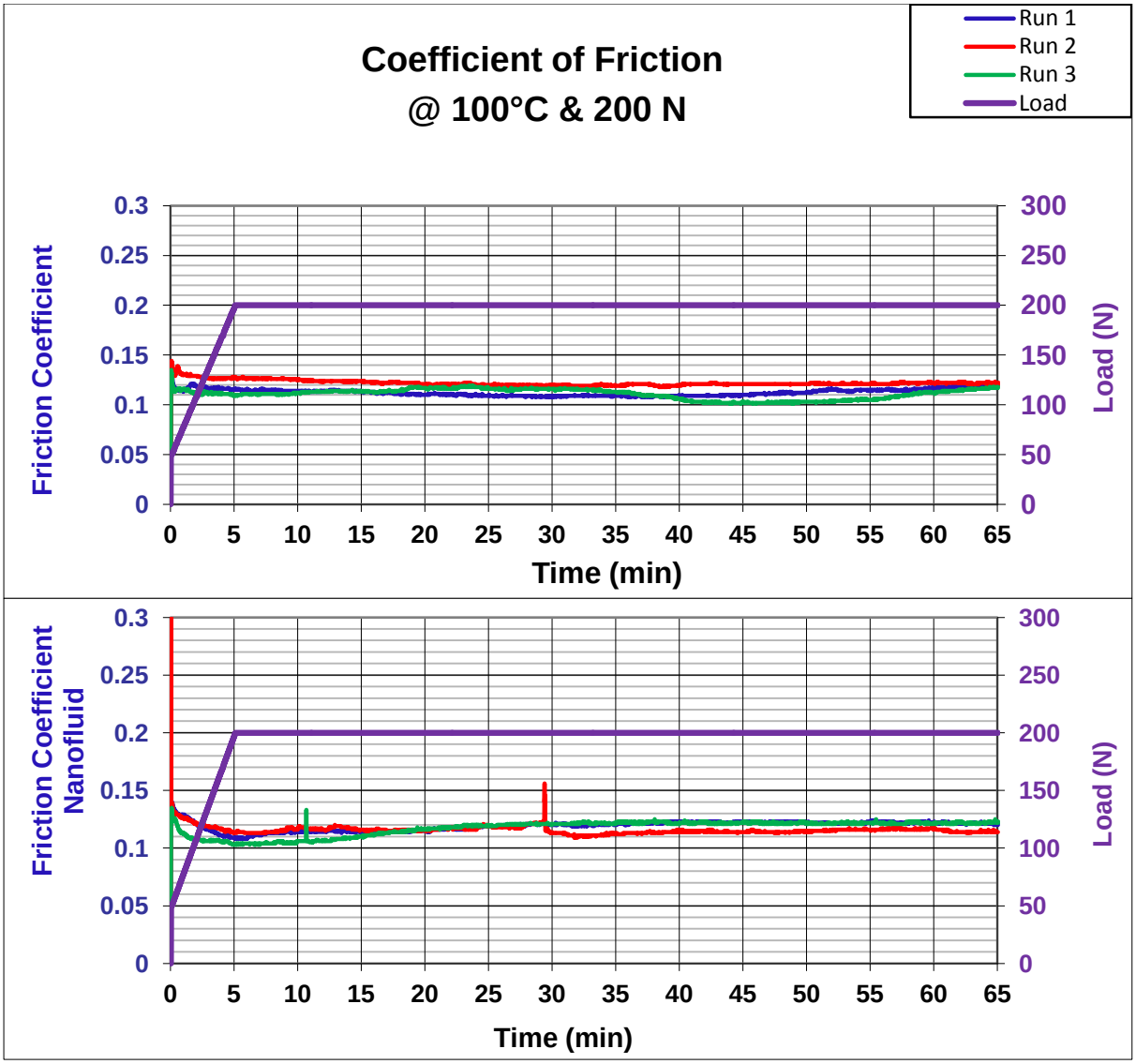

Figure 4.6.1: Coefficient of friction (COF) for the test fluid without particles (top) and for the test fluid with particles (bottom).

© University of Pretoria

Table 4.6.1: Average coefficient of friction values obtained from friction and wear testing on SRV test rig with modified test method and constant relative humidity (10%) (ASTM D6425).

	Lubricating Fluid	Nanofluid
COF_{min}		
AVG	0.098	0.107
STDEV	0.010	0.004
COF_{max}		
AVG	0.139	0.144
STDEV	0.005	0.011
COF_{15}		
AVG	0.115	0.113
STDEV	0.009	0.003
COF_{30}		
AVG	0.109	0.118
STDEV	0.010	0.003
COF_{end}		
AVG	0.119	0.119
STDEV	0.003	0.005

The standard deviation of the wear scar volume for the test fluid without particles was 15 x 10^{-4} mm^3 (Table 4.6.2) and for test fluid with particles were 8 x 10^{-4} mm^3 (Table 4.6.2). These values compare well with each other, but the addition of the particles seems to improve the repeatability of the wear volume, since the standard deviation of test fluid without particles was about twice the standard deviation for fluid with particles.

© University of Pretoria

Table 4.6.2: Average wear volume values obtained from friction and wear testing on SRV test rig with modified test method and constant relative humidity (10%) (ASTM D6425)

Wear Volume (x10-4 mm3)		
	Lubricating Fluid	**Nanofluid**
AVG	63	96
STDEV	15	8

The wear scar surfaces of both fluids are given in Figure 4.6.2. It is immediately evident that there is a smaller amount of the corrosion layer for the scars with the nanofluid (second row). This is an indication that the particles remove the corrosion layer from the surface.

It is also evident that the scars for the fluid with the particles are more uniform and consequently better repeatability for the wear scar appearance was obtained. This is probably due to the particles that remove the corrosion layers, which results in more consistent wear scar surfaces for the duration of the test.

Wear Scar Surface: Lubricating Fluid

Run 1	**Run 2**	**Run 3**
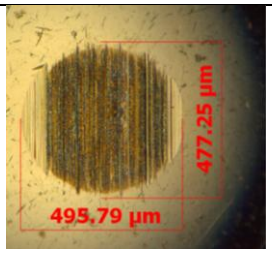	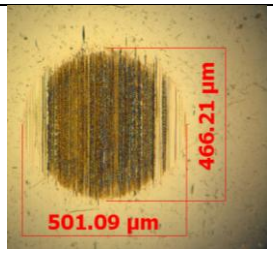	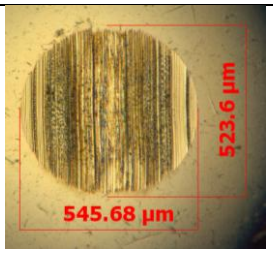

Wear Scar Surface: Nanofluid

Run 1	**Run 2**	**Run 3**
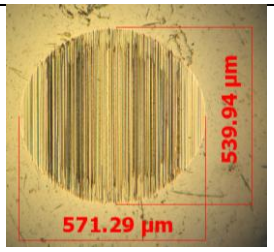	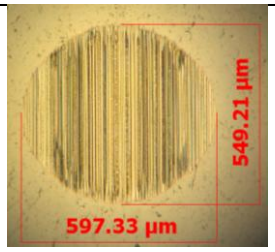	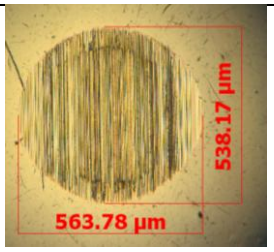

Figure 4.6.3: Wear scar surfaces of test fluid with and without particle additives.

© University of Pretoria

The corrosion products found on the wear scar surfaces are also summarized in Table 4.6.3. Greigite and goethite were found on both surfaces, which were probably formed due to the sulphurised ester in the lubricating fluid (see sections 4.4.3 and 4.5.2).

However, when boron nitride was added to the fluid, melanterite and rozenite were also found (section 4.5.2). These products were most likely formed due to oxidation of the greigite.

Raman spectroscopy of the wear scars indicated that boron nitride did not react with the environment or with the other compounds in the fluid. The presence of melanterite and rozenite, however, indicated that the corrosion layer formation was influenced by the presence of the particles.
This was most likely due to differences in the amount of corrosion products on the wear surface during the test, since the wear scar surfaces in Figure 4.6.3 indicated that the particles removed the corrosion layers.

Table 4.6.3: Products found on wear scar surfaces with Raman Spectroscopy.

Wavenumber (cm^{-1})	**Test Fluid**			
	Lubricating Fluid Scar Surface		**Nanofluid Scar Surface**	
	Substance	**Formula**	**Substance**	**Formula**
340	Greigite	Fe_3S_4	Greigite	Fe_3S_4
374	Goethite	α-FeOOH	Goethite	α-FeOOH
785			Melanterite	$FeSO_4.7H_2O$
965			Rozenite	$FeSO_4.4H_2O$
1364			Boron Nitride	h-BN

© University of Pretoria

5. Conclusions and Recommendations

5.1. Physical Properties

It was found that:

1. The lubricating fluid is consistent up to 100 °C and does not volatalize below 175 °C.
2. Size of the particles is larger than specified by the supplier, but are still smaller than 1 µm.

5.2. Particle Dispersion

It was found that:

1. Glycerol mono-stearate proved to be an adequate dispersant, as long as the temperature of the fluid was kept above 65 °C.
2. Viscosity profiles did not indicate when the optimum ratio of dispersant to particles was reached. This was probably due to the particle concentration that was too low to have any significant effect.
3. The particle size distribution determined with a Malvern Zeta sizer revealed that a ratio of 1 to 10 (particles to dispersant) provided adequate stability.
4. The dispersant does not lose its solubility in the fluid or desorb from the particle with an increase in the temperature (up to 100 °C).

5.3. Friction and Wear Testing

For the test fluid without any particle additives, it was found that:

1. The standard test method resulted in poor repeatability for the wear scar surface (WSS) and wear scar volume (WSV) when the lubricating fluid was evaluated. Also, the sudden load increase at the end of the running-in period

© University of Pretoria

caused uncertainty due to the sudden change in the measured coefficient of friction (COF) values.

2. When the test was modified by applying the load at a slower rate for the duration of the running-in period, there was some improvement in the repeatability of the wear scar volume and no sudden change was observed in the coefficient of friction. However, even though the wear volume decreased, the wear scar surfaces still varied.
3. When the relative humidity was controlled and the fluid evaluated with the modified procedure, the overall repeatability improved. This confirmed that the amount of water/moisture does indeed have an influence on the repeatability of the test. This could be due to the formation of corrosion layers that were influenced by the amount of water vapour or the test fluid itself.
4. By controlling the relative humidity, the fraction of water vapour does not remain constant. This is due to the relative humidity being a function of the atmospheric temperature, which did not remain constant during a test run.
5. It was also found that the main corrosion products formed on the surface were most likely greigite and goethite. These were probably formed due to the presence of sulphurised ester in the oil formulation. These are, however, softer than the specimens and will not cause abrasive wear.

When the hexagonal-boron nitride nanoparticles were dispersed in the lubricating fluid, it was observed that:

1. The test method and relative humidity both influenced the repeatability of the COF, WSS and WSV.
2. The addition of the particles resulted in an improvement of the repeatability of the COF, WSS and WSV, since the wear scar surfaces indicated that the particles remove the corrosion layers. This could have led to more consistent wear surfaces for the duration of the test.
3. Finally, the particles also influenced the formation of the corrosion layer, since additional products were found on the surface. These products were melanterite and rozenite.

© University of Pretoria

From these results, it is recommended that:

1. Since the dispersion is stable only at elevated temperatures (above 65 °C), other techniques for dispersing the particles must also be investigated, especially for practical applications, where the fluid will be required to have long term stability at lower temperatures.
2. The influence of the atmospheric moisture content on the lubricating fluid as well as the nanofluid must also be investigated. This will include Carl Fisher titration. It is also recommended to control the water vapour fraction in the atmosphere instead of the relative humidity, since relative humidity is a function of atmospheric temperature.

© University of Pretoria

6. References

1. Abdelmoula, M, Boursiquot, S, Ehrhardt, JJ, G'Enin, JM and Mullet, M (2002) "Surface chemistry and structural properties of mackinawite prepared by reaction of sulphide ions with metallic iron", Geochimica et Cosmochimica Acta, 66; 5: 829–836.

2. Anton Paar (2011) Instruction manual: SVM 3000/G2, Stabinger viscometer, Anton Paar GmbH, Austria.

3. Atnafu, ND, Belk, JH, Mosleh, M and Nobles, OM (2009) "Modification of sheet metal forming fluids with dispersed nanoparticles for improved lubrication", Wear; 267: 1220-1225.

4. ASTM D 2270 (1993) "Standard Practice for calculating viscosity index from kinematic viscosity at 40 and 100 °C", ASTM Int.

5. ASTM D6425 (1999) "Standard test method for measuring friction and wear properties of extreme pressure (EP) lubricating oils using SRV test machine", ASTM Int.

6. ASTM D 5707 (2005) "Standard test method for measuring friction and wear properties of lubricating grease using a high frequency, linear-oscillation (SRV) test machine", ASTM Int.

7. ASTM D7755 (2011) "Standard practice for determining the wear volume on standard test pieces used by high-frequency, linear-oscillation (SRV) test machine", ASTM Int.

8. Bando, Y, Golberg, D, Muthu, DVS, Saha,S, Sood, AK, Tang, C & Zhi, C (2006) "Comparative high pressure Raman study of boron nitride nanotubes and hexagonal boron nitride", Chemical Physical Letters; 421, 1-3: 86-90.

9. Bartz, WJ & Müller, K. "Investigations on the lubrication effectiveness of molybdenum disulphide", Wear 1972; 20: 371-379.

© University of Pretoria

10. Batchelor, AW & Stachoviak, GW (2003) *Engineering Tribology*, Butterworth-Heinemann, USA.

11. Benning, LG & Hunger, S (2007) “Greigite: a true intermediate on the polysulfide pathway to pyrite”, Geochemical Transactions; 8: I.

12. Bernard, S, Chiriac, R, Miele, P and Salles, V (2011) “Structural and thermal properties of boron nitride particles”, Journal of the European Ceramic Society; 32, 9: 1867-1871.

13. Bhimaraj, P, Burris,D, Sawyer, WG, Toney, CG, Siegel, RW and Schadler, LS (2008) “Tribological investigation of the effects of particle size, loading and crystallinity on poly(ethylene) terephthalate nanocomposites”, Wear; 264: 632–637.

14. Bhushan, B and Gupta, BK (1991) *Handbook of Tribology,* McGraw-Hill, USA.

15. Bhushan, B and Nosonovsky, M (2012) *Green Tribology: Biomimetics, Energy Conservation and Sustainability*, Springer-Verlag, Berlin.

16. Black, Al, Dunster, AW & Sanders, JV (1969) “Comparative study of surface deposits and behaviour of MoS_2 particles and molybdenum dialkyl-dithio-phosphate”, Wear; 13: 119-132.

17. Booser, ER (1997) *Tribology Data Handbook*, CRC Press LLC, US.

18. Boyd, J and O’Connor, JJ (1968) *Standard Handbook of Lubrication Engineering*, McGraw-Hill, USA.

19. Bouchard, M and Smith, DC (2003) “Catalogue of 45 reference Raman spectra of minerals concerning research in art history or archaeology, especially on corroded metals and coloured glas”, Spectrochimica Acta Part A 59: 2247-2266.

© University of Pretoria

20. Bourdoiseau, J, , Dillmann, P, Guilminot, Jeannin, M, E, Matthiesen, H, Neff, D, Refait, P, Rémazeilles,C , Sabot, R, Saheb,M and Tran, K (2010) "Microbiologically influenced corrosion of archaeological artefacts: characterisation of iron(II) sulfides by Raman spectroscopy", *J. Raman Spectrosc.*, *41*, 1425–1433.

21. Burstein, GT, Jarman, RA & Shrier, LL (1993) *Corrosion,* Butterworth-Heinemann, Boston.

22. Chang, YP, Hwang, RM, Kang, Y, Peng, DX and Shyr, SS (2009) "Tribological properties of diamond and SiO2 nanoparticles added in paraffin", Tribol. Int. 42: 911-917.

23. Chen, G, Gao, Y, Oli, Y, Xue, Q and Zhang, Z (2002) "Study on tribological properties of oleic acid-modified TiO_2 nanoparticle in water", Wear 252: 454-458.

24. Chio, CH, Muenow, DW and Sharma, SK (2006) "Raman spectroscopic investigation of ferrous sulphate hydrates", Lunar and Planetary Science XXXVII.

25. Choi, SUS, Eastman, JA, Keblinski, P and Phillpot, SR (2002) "Mechanisms of heat flow in suspensions of nano-sized particles (nanofluids)", International Journal of Heat and Mass Transfer; 45: 855-863.

26. Chu, PK and Li, L (2006) "Characterization of amorphous and nanocrystalline carbon films", Materials Chemistry and Physics 96: 253–277.

27. Chu, B & Nose, T (2012) "Light scattering", Polymer Science: A Comprehensive Reference; 2.

28. Clark, J (2012) "Giant covalent structures", http://www.chemguide.co.uk [2014, August 04].

29. Cofer, CG and Economy, J (1995) "Oxidative and hydrolytic stability of boron nitride – a new approach to improving the oxidation resistance of carbonaceous structures", Carbon; 33, 4: 389-395.

© University of Pretoria

30. Dias, AM, Gras, R, Nogueira, I & Progri, R (2002) “An experimental model for mixed friction during running-in”, Wear; 253: 541-549.

31. Erdemir, A (2008) *Nanolubricants*, John Wiley & Sons, Ltd, UK.

32. Everett, DH (1994) *Colloid Science*, Royal Society of Chemistry, Cambridge.

33. Feldman, Y, Homyonfer, M and Tenne, R (1998) **“**Nanoparticles of layered compounds with hollow cage structures (inorganic fullerene-like structures)” Chemistry of Materials; 10:11: 3225-3238.

34. Gohar, R and Rahnejat, H (2012) *Fundamentals of Tribology*, Imperial College Press, London.

35. Hamrock, BJ, Jacobson, BO & Schmid, SR (2004) *Fundamentals of Fluid Film Lubrication*, Marcel Dekker Inc, New York.

36. He-long, Y, Yi, X, Pei-jing, S, Bin-shi, X, Xiao-li, W and Qian, L (2008) “Tribological properties and lubricating mechanisms ofCu nanoparticles in lubricant”, Trans. Nonferrous Met. Soc. China, 636-641.

37. Hersey, MD (1966) *Theory and Research in Lubrication: Foundations for Future Developments*, Wiley, New York.

38. Hollier, FJ, Nieman, TA & Skoog, DA (1997) *Principles of Instrumental Analysis, Fifth Edition”* Thomson Learning, USA.

39. Horiba Ltd (2014) “Horiba Scientific: What is Raman spectroscopy?”, http://www.horiba.com [2014, July 27].

40. Huang, HD, Gan, LP, Li, CZ & Tu, JP (2006) “An investigation on tribological properties of graphite nanosheets as oil additive”, Wear; 261: 140-144.

41. Hwang, Y, Jung, WH, Lee, JK & Park, HS (2006) “Thermal conductivity and lubrication characteristics of nanofluids”, Current Applied Physics; 6S1: e67–e71.

© University of Pretoria

42. Jen, TC, Menezes, PL, Lovell, MR and Reeves, CJ (2013) “The size effect of boron nitride particles on the tribological performance of biolubricants for energy conservation and sustainability”, Tribology Letters; 51: 437-452.

43. Kalpakjian, S and Schmid, SR (2006) *Manufacturing Engineering and Technology,* United States of America: Pearson Prentice Hall.

44. Klaffke, D (1995) “On the repeatability of friction and wear results and on the influence of humidity in oscillating sliding tests of steel-steel pairings”. Wear 189: 117-121.

45. Kopeliovich, D (2012) “Boron nitride as solid lubricant”, http://www.substech.com [2012, July 26].

46. Kimura, Y, Nishikawa, H, Okada, K, Wada, T and Wakabayashi, T (1999) “Boron nitride as a lubricant additive”. Wear; 232: 199-206.

47. Kraschitz, E (2014) “Stabinger Viscometer”, http://www.anton-paar.com [2014, July 26].

48. Kumar, R, Prakash, B & Sethuramiah, A (2002) “A systematic methodology to characterise the running-in and steady-state wear processes”, Wear; 252: 445-453.

49. Lowerfriction (2014) “Lower friction” http://www.lowerfriction.com [2014, July 26].

50. Ludema, KC (1996) *Friction, Wear, Lubrication: A Textbook in Tribology*, CRC, New York.

51. Luther, GW, Peak, D & Sparks, DL (2003) “ATR-FTIR spectroscopic studies of boric acid adsorption on hydrous ferric oxide”, Geochimica et Cosmochimica Acta; 67, 14: 2551–2560.

52. Matweb LCC (1996) “Matweb: material property data”, http://www.matweb.com [2014, 25 June].

© University of Pretoria

53. Maxit, B (2009) “Particle Size Measurements of Dark and Concentrated Dispersions by Dynamic Light Scattering”, http://www.particulatesystems.com [2014, July 26].

54. McMurry, J (2004) *Organic Chemistry*, Brooks/Cole-Thomson Learning, USA.

55. Miyake, S, Miyake, S, Murakawa, M & Watanabe, S (1991) Tribologic properties of cubic, amorphous and hexagonal boron nitride films. Surface and Coating Technology; 49: 406-410.

56. Mortier, RM and Orszulik, ST (1997) *Chemistry and Technology of Lubricants*, Blackie Academic and Professional, Great Brittain.

57. Oláh, ZS, Szirmai, L and Resofszki, G (2005) “Micro and Nano Analysis of Wear Scar Surfaces- A complementary Rating Method to the Evaluation of HFRR Test results”, paper presented at The 5th International Colloquium on Fuels,TAE, 12-13 January, 2005.

58. Optimol Instruments SRV (2011) “SRV Test System Operating Manual”, Hardware.

59. Parfitt, GD (1973) *Dispersion of Powder in liquids*, Applied Science Publishers LTD, London.

60. Pashley, RM & Karaman, ME (2004) *Applied Colloid and Surface Chemistry*, John Wiley and Sons LTD, England.

61. PerkinElmer Inc (2014) “Thermogravimetric analysis: Frequently asked questions”, http://www.perkinelmer.com [2014, July 27].

62. Perry, RH & Green, DW (1997) *Perry’s Chemical Engineer’s Handbook,* McGraw-Hill, United States of America.

63. Petrovykh, D (2008) “Si(III) surface”, http://www.nanowiz.tripod.com [2014, August 04].

© University of Pretoria

64. Pugh, B (1973) *Friction and Wear: a Tribology Text for Students,* Newnes-Butterworths: London.

65. Qi, WH & Wang, MP (2004) “Size and shape depending melting temperature of metallic nanoparticles”, Materials chemistry and physics; 88: 280-284.

66. Quinn, TFJ, Rowson, DM & Sullivan, JL (1984) “Origins and development of oxidational wear at low ambient temperatures”, Wear; 94: 175-191.

67. Ralph, J (1993) “Mindat: the mineral and locality database”, http://www.mindat.org [2014, 25 June].

68. Shi, Z, Srinivasan, SG & Wynblatt, P (2004) “Melting behavior of nanosized lead particles embedded in an aluminum matrix” , Acta Materialia; 52: 2305–2316.

69. Siew, R (2013) “Photovoltaics: Raman spectroscopy monitors thin film Si PV cell manufacture”, http://www.laserfocusworld.com [2014, July 27].

70. Tadros, TF (2005) *Applied surfactants: Principles and applications,* Wiley-VCH Verlag GmbH & Co. KGaA, Weinheim.

71. Ultrasonic cleaners made in China (2014) “Jeken ultrasonic cleaner limited”, http://www.ultrasoniccleaners.en.made-in-china.com [2014, July 26].

72. US Synthetic Bearings and US Synthetic Corp (2014) “US synthetic bearings”, http://www.ussbearings.com [2014, July 22].

73. Vaughan, DJ & Rimstidt, JD (2003) “Pyrite oxidation: A state-of-the-art assessment of the reaction mechanism”, Geochemical et Cosmochimica; 67, 5: 873-880.

74. Williams, RA (1994) *Colloid and Surface Engineering,* Butterworth-Heinemann, Great Britain.

© University of Pretoria

Appendix A: Dispersions

In section 2.11 a brief introduction of dispersions was given. It only mentioned how dispersions are formed and the effects on instability as well as the techniques of stabilizing dispersions. This section of the Appendix will focus on dispersions in more detail.

Nomenclature

A:	Particle cross sectional area	meter^2
Av:	Avogadro's constant	1/mole
C:	Electrolyte concentration	mole/meter^3
cn:	Number of chains per unit area	1/meter^2
E:	Repulsive energy	joule
e:	Electric charge	Coulomb
G:	Gibbs free energy	joule/mole
H:	Hamaker constant	joule
h:	Separation distance	meter
k:	Boltzmann constant	joule/Kelvin
MV:	Molar Volume	meter^3/mole
P:	Pressure	Pascal
Rp:	Radius of pores	meter
R:	Particle radius	meter
S:	Spreading coefficient	joule/meter^2
T:	Temperature	Kelvin
V:	Force between two particles	Newton
W:	Work done by the system	joule
Z:	Valency	

Greek

δ:	Layer thickness	meter
ε:	Permittivity	Coulomb^2/Newton.meter^2

© University of Pretoria

θ: Contact angle between liquid drop and solid surface

κ: Debye-Huckel parameter 1/meter

σ: Surface tension Joule/meter^2

χ: Flory-Huggins interaction parameter

Ψ: Surface potential Volt or Joule/Coulomb

$\Omega(h)$: Number of chain configurations at separation distance equal to h

$\Omega(\infty)$: Number of chain configurations at separation distance equal to ∞

Subscripts

11: Molecules

22: Medium

A: Van der Waals attraction

a: Adhesional wetting

el: Elastic interactions

i: Immersional wetting

l: Liquid phase

min: Minimum

mix: mixture

o: Free space

R: Repulsive

r: Relative

s: Solid phase

$steric$: Steric interactions

sp: Spreading wetting

T: Total

v: Vapour phase

© University of Pretoria

A.1. Dispersion Formation: Comminution

When the molecules at a surface are considered, the resulting force acting on surface molecules is not the same as the resulting force on the bulk molecules. This is due to the surface molecules experiencing intermolecular forces from the sides and the bulk, while bulk molecules experience forces from all directions. This phenomenon gives rise to surface tension and the molecules in the bulk have less free energy than the surface molecules (Everett, 1994: 19).

Consider a particle with cross-sectional area equal to A, that is split to form two particles with the surface area between the two particles equal to $2A$, as shown in Figure A.1. The two particles are then separated to an infinite distance. Therefore, this increase in the area will result in an increase in the free energy of the system, since there are more molecules at the surface. The free energy of the system is then equal to the amount of work required to separate the two particles. This will only be true if the process of separation is isothermal and reversible. If the particles in Figure A.1 are infinitely far apart, the increase of the free energy is proportional to the surface created. This is then referred to as the surface free energy and follows the following relationship (Everett, 1994: 19-20):

$$\Delta G = \Delta W = 2A\sigma \qquad \text{(A.1)}$$

Where ΔG is the change in the Gibbs free energy, ΔW is the work done by the system and σ is the surface tension.

© University of Pretoria

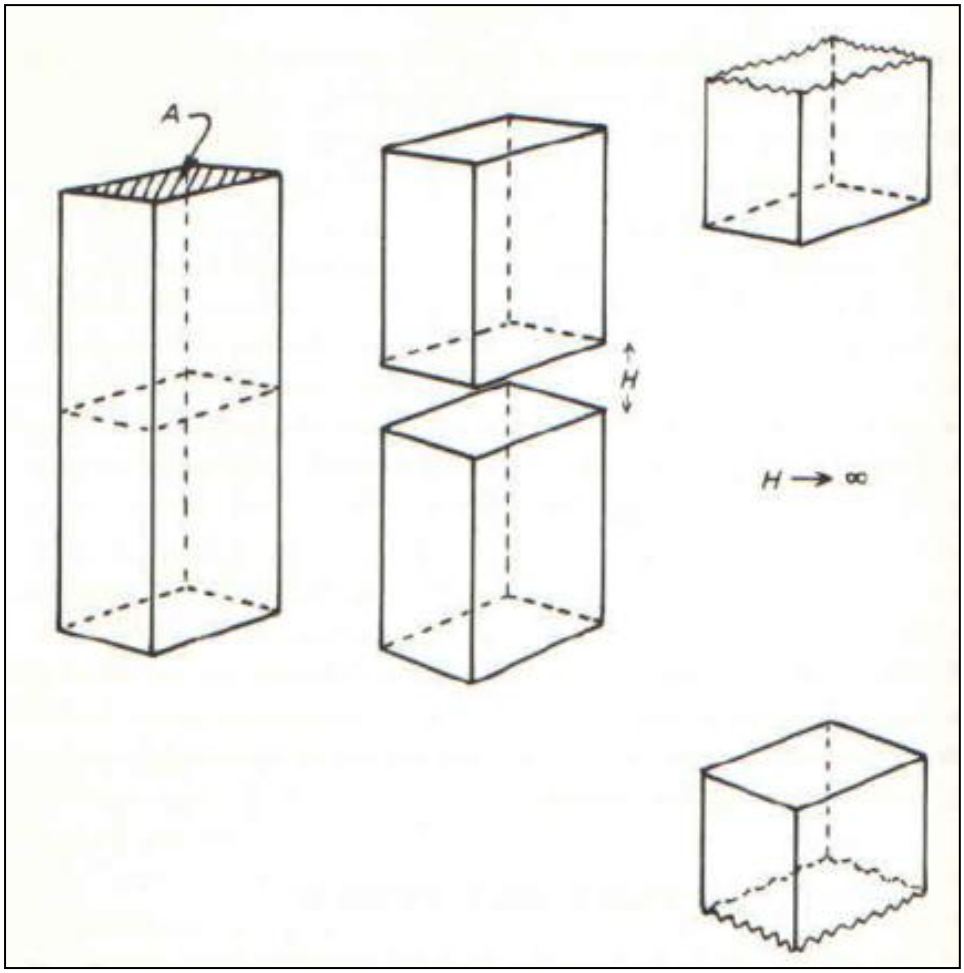

Figure A.1: Splitting of a particle with cross-sectional area of A to form two particles with the surface area between the particles equal to $2A$ and separated to an infinite distance (Everett, 1994: 20).

In Figure A2, the amount of work required is plotted as a function of the separation distance. Curve a is the amount of work required in a vacuum, and curve b is the amount of work required in a fluid medium (Everett, 1994: 20-21).

© University of Pretoria

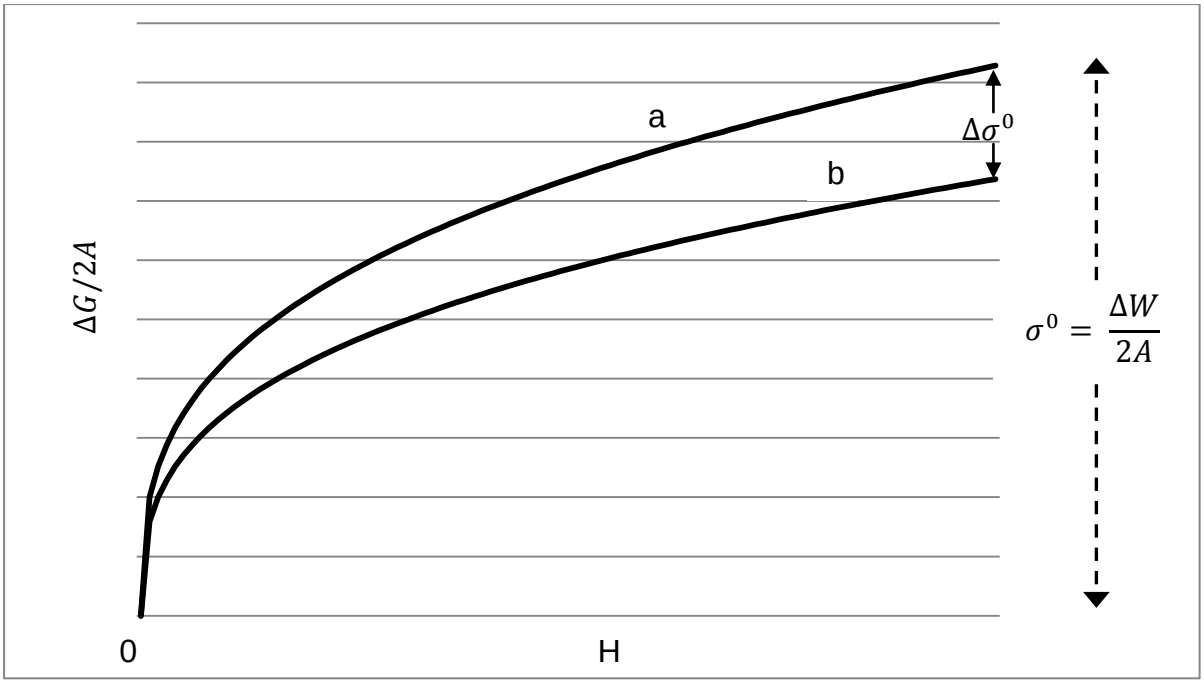

Figure A.2: Free energy per unit area of the surface area as a function of the separation distance: a.) In a vacuum b.) In a fluid medium (Everett, 1994: 21).

According to the plots in Figure A.2, the surface free energy decreases as the two particles approach one another. This is because at smaller separation distances, the surface molecules are still influenced to some extend by the intermolecular forces of the opposing surface molecules (Everett, 1994: 21).

In practice the surface area increase of a solid may be brought about by comminution. This is the process where a dispersion is made by fracturing and eroding the agglomerates that may form after wetting of a powder. This is achieved with a colloid mill (Williams, 1994: 101).

In practice it is impossible to perform comminution reversibly since some of the work is lost by friction. However, by performing the grinding in a liquid medium with a colloid mill, the surface tension is lowered (graph b in Figure A.2), since the surface molecules experience intermolecular forces from the liquid molecules. This process then requires less work (Everett, 1994: 22).

© University of Pretoria

A.2. Dispersion Formation Mechanism

The formation of dispersions can be divided into three steps:

- Wetting
- Breakdown of aggregates and agglomerates
- Dispersion stabilization (Parfitt, 1973: 2-10).

Each of these stages is distinct in their nature, but in practice they overlap. This makes it difficult to recognize the steps in a dispersion. However, in order to understand how the mechanism works they will be treated as separate stages.

A2.1. Surface Wetting

In order for a particle to be dispersed in a liquid medium, the liquid must be able to wet the particle surface. If a stationary drop of liquid is placed on a flat surface, the edge of the drop makes an angle with the surface. This angle is the contact angle, which is illustrated in Figure A.3. The contact angle is related to the balance of the surface tensions according to the following equation (Parfitt, 1973: 68):

$$\sigma_{SV} = \sigma_{SL} + \sigma_{LV} cos\theta \qquad \text{(A.2)}$$

Where σ_{SV} is the surface tension between the solid and the vapour, σ_{SL} is the surface tension between the solid and the liquid (drop) and σ_{LV} is the surface tension between the liquid and the vapour. θ is the angle between the edge of the drop and the solid surface. If the angle is larger than 90 °, the liquid will not be able to spread and consequently not be able to wet the surface. For a contact angle smaller than 90°, the surface will be wetted due to the liquid that is able to spread (Parfitt, 1973: 68-70).

© University of Pretoria

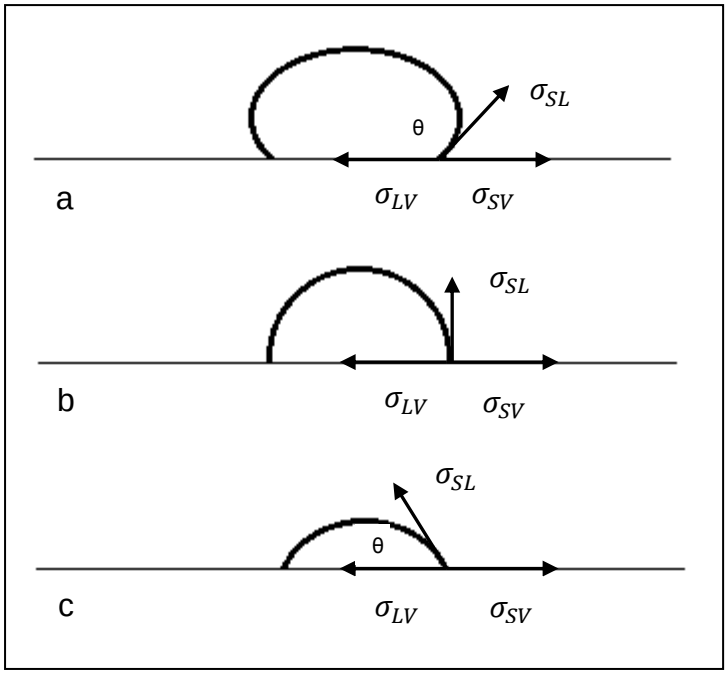

Figure A.3: Contact angle between for a drop of liquid on a surface (Parfitt, 1973: 69).

Equation A.2 describes the balance of surface tensions at equilibrium. According to Dupré's method, the work of adhesion between a solid and a liquid can be defined as (Parfitt, 1973: 68):

$$W_{SL} = \sigma_{SV} + \sigma_{LV} - \sigma_{SL} \quad \text{(A.3)}$$

Where $W_{SL}$is the work of adhesion between the solid and the liquid. By combining equation A.2 and A.3, W_{SL}can be obtained from (Parfitt, 1973: 68):

$$W_{SL} = \sigma_{LV}(1 + cos\theta) \quad \text{(A.4)}$$

Spreading or wetting can also be described by the spreading coefficient and can be determined from (Parfitt, 1973: 70):

$$S = \sigma_{SV} - \sigma_{LV} - \sigma_{SL} \quad \text{(A.5)}$$

Where S is the spreading coefficient. Equation A.5 can also be combined with equation A.2 (Parfitt, 1973: 70):

© University of Pretoria

$$S = \sigma_{LV}(cos\theta - 1) \quad \text{(A.6)}$$

In the dry state, powders usually form clusters or aggregates of primary particles. These aggregates may also be attached to other primary particles or aggregates forming agglomerates. To form a dispersion, the liquid must wet the external surfaces of the clusters as well as displace the air from the internal surfaces. In Figure A.4, some typical problems of wetting a liquid are illustrated (Parfitt, 1973: 71).

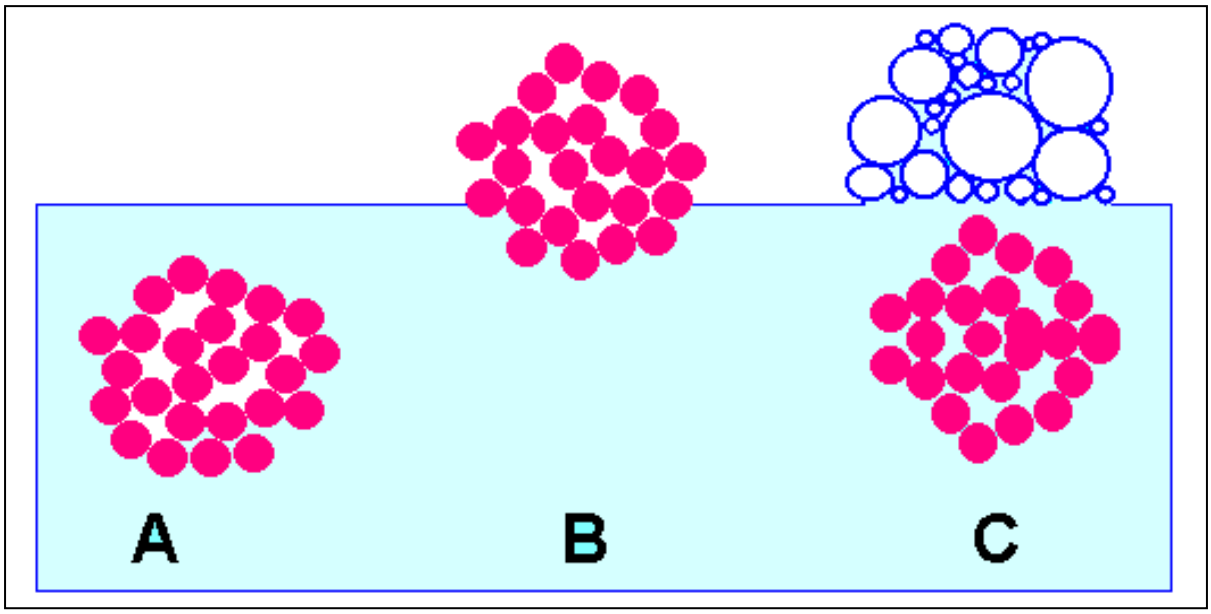

Figure A.4: Typical problems in wetting of a powder A: Air trapped inside the cluster, B: The liquid does not penetrate the pores and displace air, C: Formation of foam under the water surface. This foam is then stabilized by the wetting agent (Focke, 2011).

The process of wetting of a single particle also consists of three stages. The three stages are illustrated in Figure A.5 for a cubical particle. The three stages are adhesional wetting, immersional wetting and spreading wetting (Parfitt, 1973: 2-6).

© University of Pretoria

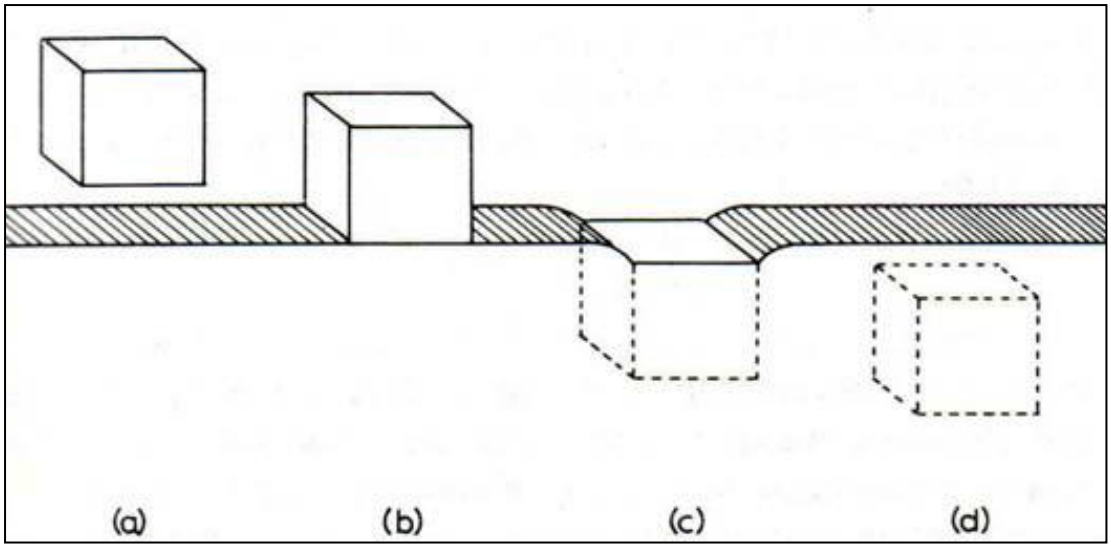

Figure A.5: Three stages of wetting of a powder. adhesional wetting: a to b, immersional wetting: b to c and spreading wetting: c to d (Parfitt, 1973: 5).

a-b: Adhesional Wetting

This is the process where one of the solid/air interfaces of the solid is replaced by a solid/liquid interface. This is shown in Figure A.4 as steps a to b. The work involved in moving from a to b (W_a) are given by (Parfitt, 1973: 3):

$$W_a = \sigma_{sl} - (\sigma_{sv} + \sigma_{lv}) \quad \text{(A.7)}$$

By substituting equation A.2 (Parfitt, 1973: 5):

$$W_a = -\sigma_{lv}(cos\theta + 1) \quad \text{(A.8)}$$

is obtained. Spontaneous adhesion will occur when $W_a < 0$. This is when the free energy of the new surface (solid-liquid) is smaller than the initial surface free energy (solid-air as well as liquid-air). The work of adhesion will be spontaneous when the contact angle (θ) is smaller than 180° (Parfitt, 1973: 5).

b-c: Immersional Wetting

This is the total immersion of the solid as shown in Figure A.4 (from b to c). The work of immersion is (Parfitt, 1973: 4):

© University of Pretoria

$$W_i = \sigma_{sl} - \sigma_{sv} \quad \text{(A.9)}$$

This is the work of replacing the solid/air interface with a solid/liquid for one of the side surfaces of the cube in Figure A.4.

If equation is A.2 is substituted (Parfitt, 1973: 5):

$$W_i = -\sigma_{lv} cos\theta \quad \text{(A.10)}$$

Immersional wetting will be spontaneous when: $W_i < 0$, i.e. when $\theta < 90$ (Parfitt, 1973: 5-6).

c-d: Spreading Wetting

This is steps c to d in Figure A.4 when the liquid spreads over the solid surface (Parfitt, 1973: 4):

$$W_{sp} = (\sigma_{sl} + \sigma_{lv}) - \sigma_{sv} \quad \text{(A.11)}$$

Again equation A.2 is substituted (Parfitt, 1973: 5):

$$W_{sp} = -\sigma_{lv}(cos\theta - 1) \quad \text{(A.12)}$$

The work of spreading is spontaneous when: $\theta = 0$ (Parfitt, 1973: 5-6).

The total work of wetting is (Parfitt, 1973: 5):

$$W_T = W_a + 4W_i + W_{sp} \quad \text{(A.13)}$$

The work of immersion (W_i) is multiplied by four, since the particle was assumed to be a cube as shown in Figure A.4 (Parfitt, 1973: 5).

© University of Pretoria

Penetration of Liquid into Pores

The penetration of the liquid into the pores is much more difficult to estimate than the wetting process. The Pressure (P) required to force the liquid into the pores is (Parfitt, 1973: 6):

$$P = -\frac{2\sigma_{lv}}{Rp} cos\theta \qquad \text{(A.14)}$$

Where Rp is the radius of the pores. This will be spontaneous only if $\theta < 90$ (i.e. $P < 0$) (Parfitt, 1973: 6-7).

A.2.2.2. STABILITY OF DISPERSIONS

The primary cause for instability of dispersions is due to *flocculation*. This is due to the Brownian motion of the particles which may bring them in close contact. When the particles come in close contact, they may form aggregates. Figure A.6 is an illustration of *flocculation* (Parfitt, 1973: 10).

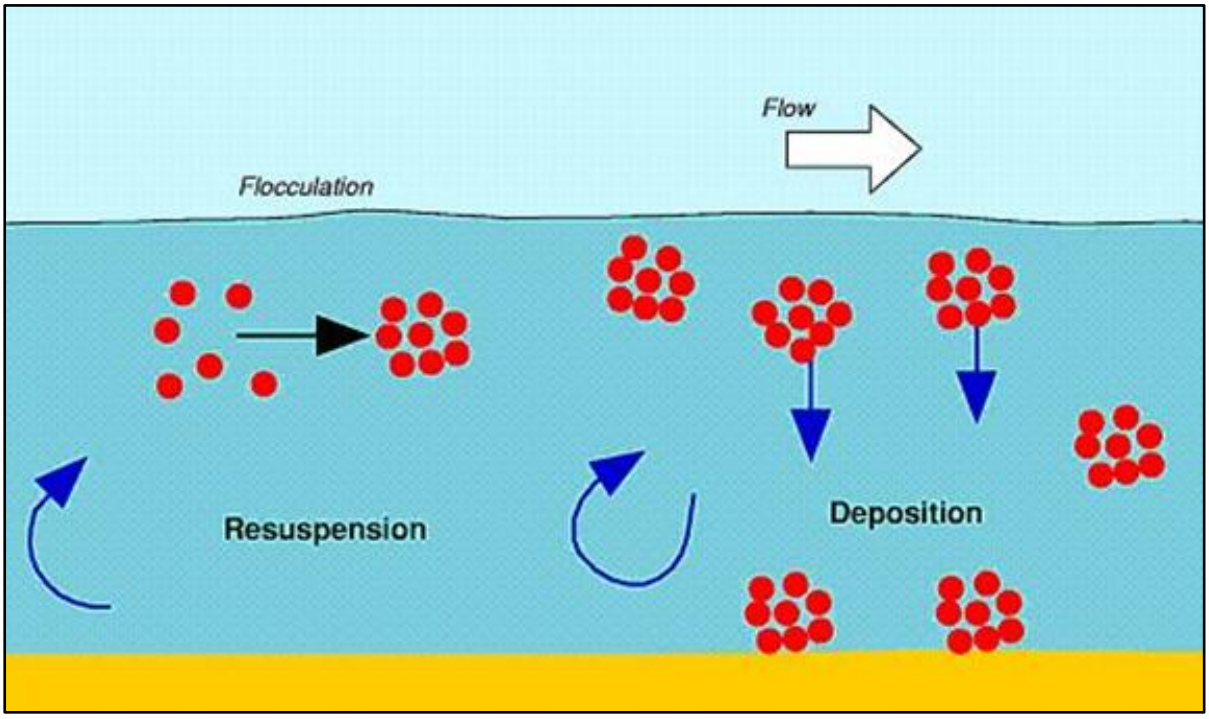

Figure A.6: Flocculation of particles that result in sedimentation (Robson et.al., 2003)

© University of Pretoria

Other causes for instability are:

- *Ostwald ripening*. This is when the solid particles are slightly soluble in the fluid medium. The solubility of the smaller particles is higher than the large particles. They dissolve and precipitate on the larger ones. The large particles will grow larger and the small particles will be eliminated (Everett, 1994: 148-149). This is shown in Figure A.7.
- *Sedimentation* (also shown in Figure A.6): When the density of the particles is larger than the density of the medium, the particles will be subjected to gravitational force and the particles will sink (Everett, 1994: 93).
- *Creaming*: This is the same as sedimentation, but the density of the particles is smaller than the medium. Instead of sinking, the particles will float (Parfitt, 1973: 93).

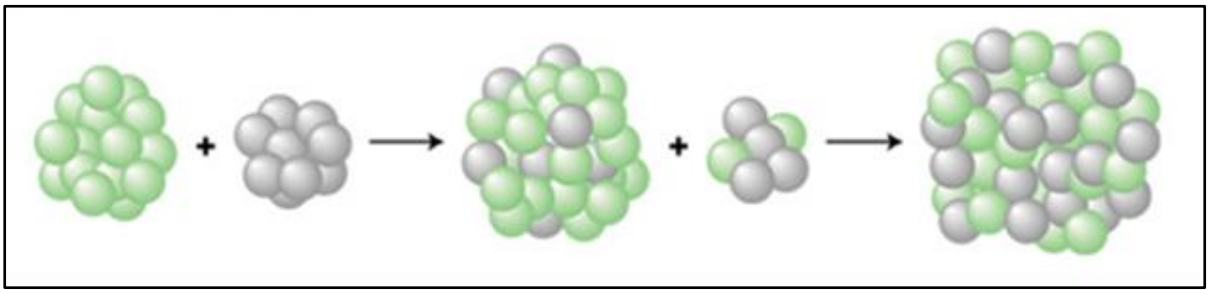

Figure A.7: Ostwald ripening (Bowker, 2002)

From these defects, it can be seen that it is important to be able to stabilize dispersions. In order to be able to stabilize dispersions, it is important to understand how the particles and the fluid medium interact and how this interaction can result in destabilization.

A.2.2.3. THE ELECTRIC DOUBLE LAYER

Particles in most colloidal dispersions in an aqueous media carry an electric charge. This charge on the particle influences the distribution of the nearby ions in the polar medium by attracting ions of opposite charge than the particle, while ions with the same charge are repulsed. This results in the formation of an electric double layer (Everett, 1994: 36-37, 41).

© University of Pretoria

The concept of the electric double layer is illustrated in Figure A.8. From this figure it can be seen that the double layer consists of an inner layer, which is known as the Stern layer. This layer contains counter-ions for the charge on the surface. Adjacent to the Stern layer is a diffuse layer. The diffuse layer contains counter-ions as well as co-ions. Co-ions are present due to thermal motion (Everett, 1994: 80-82).

The double layer forms the basis for the stabilization theory of dispersions. From this Deryaguin, Landau, Verwey and Overbeek developed the DLVO theory of flocculation (Everett, 1994: 130, Parfitt, 1973: 30). This theory is discussed in detail in the next section.

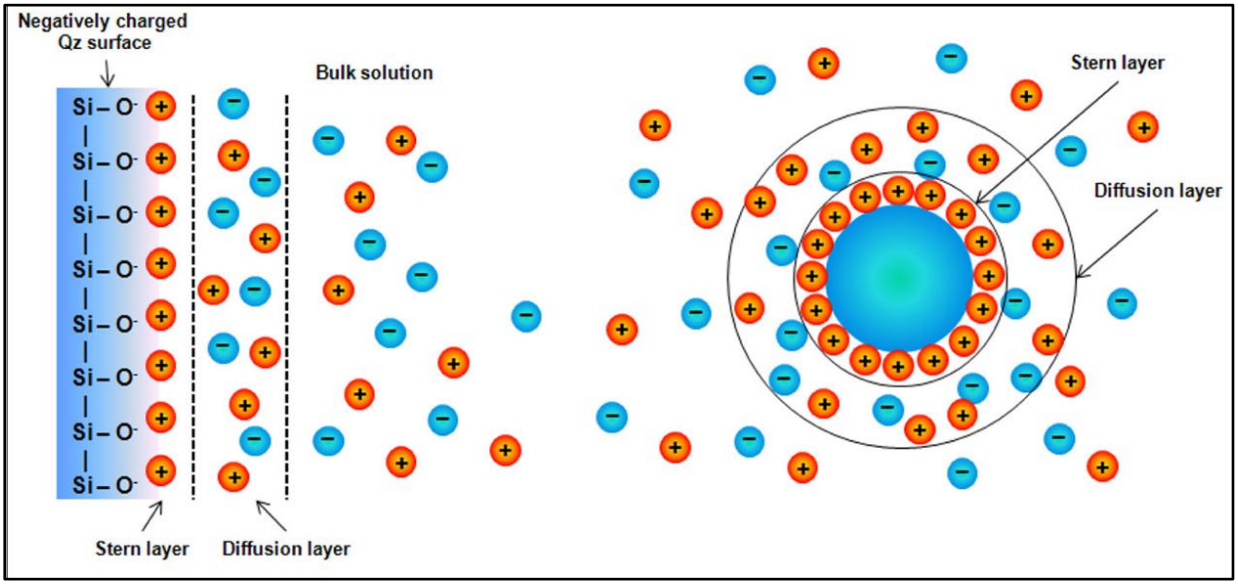

Figure A.8: The electric double layer around negatively charged quartz surface (Chin et.al., 2012).

A.2.2.4. DERYAGUIN-LANDAU-VERWEY-OVERBEEK THEORY

When two particles in a colloidal suspension approach one another, there are at least three types of forces between these two particles. These forces are (Parfitt, 1973: 13):

1. London-van der Waals attraction forces.
2. Coulombic force, either attractive or repulsive.
3. Repulsive forces due to solvation or adsorbed layer etc.

© University of Pretoria

These forces (especially 1 and 2) form the basis for the Deryaguin-Landau-Verwey-Overbeek theory. Due to these forces, four types of interactions between particles can be defined (Parfitt, 1973: 13):

Hard-sphere Interactions

For this interaction, the particles are considered as hard-spheres with the particle radius only slightly larger than the actual particle radius. The force (potential energy) between the two hard spherical particles is plotted as a function of the separation distance in Figure A.9. As the two particles approach one another to a separation distance that is smaller than the sphere radius, strong repulsion occur between the particles (Bognolo & Tadros, 2000).

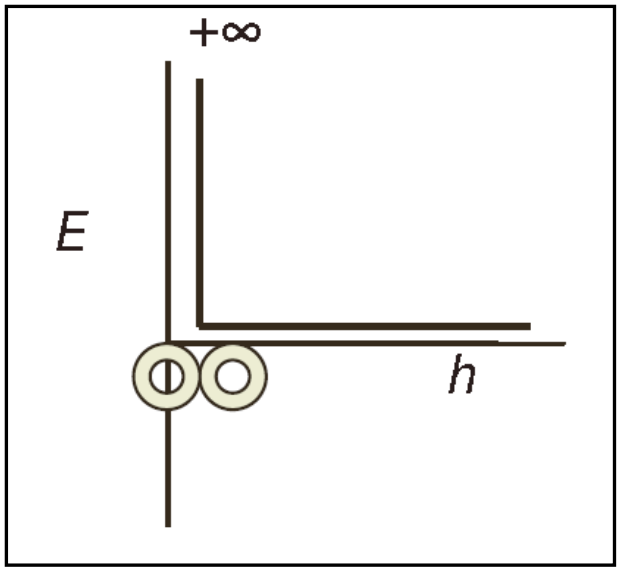

Figure A.9: Hard sphere interaction where h is the separation distance and E is the repulsive energy (Tradros, 2010: 8).

For hard sphere interactions, the suspension will change from dilute to solid over a narrow range of volume fraction. When the volume fraction exceeds the maximum hard sphere fraction of 0.6, the viscosity of the suspension increases sharply. This is due to the increase in repulsive forces between the particles (Bognolo & Tadros, 2000).

An example of a hard sphere interaction is where the suspension contains sufficient electrolyte to compress the electric double layer. This can also happen when a polar

© University of Pretoria

fluid medium such as water is replaced by a less polar fluid medium eg. benzyl alcohol (Bognolo & Tadros, 2000).

Electrostatic Interactions

For systems with low electrolyte concentrations, extended double layers around the particles are formed. Particles with similar charge will have a repulsive force on one another. The repulsive force (V_R) between particles is given in Figure A.10 as a function of separation distance (Bognolo & Tadros, 2000).

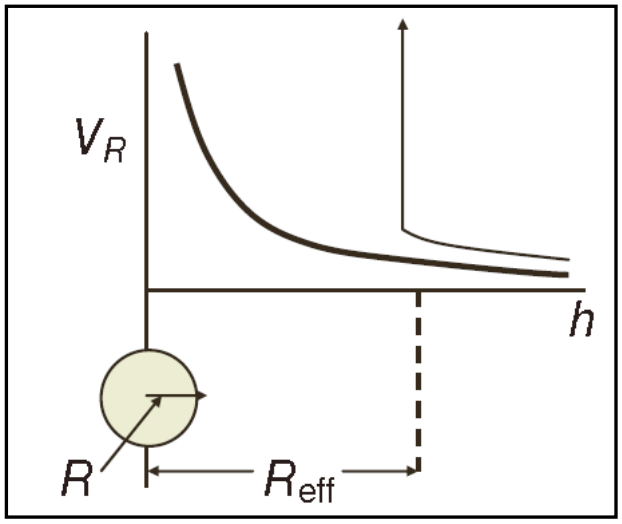

Figure A.10: Electrostatic interactions (Tradros, 2010: 8).

From this figure it can be seen that the repulsive force between the particles decays exponentially as the distance between the particles increase. The repulsive force can be determined from (Bognolo & Tadros, 2000):

$$V_R = 4\pi\varepsilon_r\varepsilon_o R^2\Psi^2 \exp[-\kappa(h-2R)]/h \qquad \text{(A.15)}$$

Where ε_r is the relative permittivity and ε_o is the permittivity of free space. R is the particle radius, Ψ is the surface potential, h is the separation distance and κ is the Debye-Huckel parameter. This parameter depends on the electrolyte concentration and the valency. The Debye-Huckel parameter can be determined from the following relationship (Bognolo & Tadros, 2000):

© University of Pretoria

$$\frac{1}{\kappa} = \left(\frac{\varepsilon_r \varepsilon_o kT}{2Z^2 e^2 Av.C}\right)^{1/2} \quad \text{(A.16)}$$

Where k is the Boltzmann constant, Z is the valency, e is the electric charge, N_A is the Avogadro's constant and C is the electrolyte concentration. The inverse of the Debye-Huckel parameter ($\frac{1}{\kappa}$) is defined as the extension of the electric double layer into the fluid medium (Bognolo & Tadros, 2000).

For low electrolyte concentrations C, $\frac{1}{\kappa}$ is relatively large. Consequently κ is small and therefore V_R decays slowly with separation distance (equation A.15). This means that the repulsive forces between particles occur at larger separation distances. If the electrolyte concentration is high, $\frac{1}{\kappa}$ will be small and V_R will decay quickly with separation distance. Repulsive forces between the particles will occur at smaller separation distances (Bognolo & Tadros, 2000).

Steric interactions

When surfactants or macromolecules adhere to a particle, layers can be formed. These molecules adsorb onto the particle to form layers. These molecules interact with one another as soon as they overlap. The interaction between two particles with layers is given in Figure A.11 (Bognolo & Tadros, 2000).

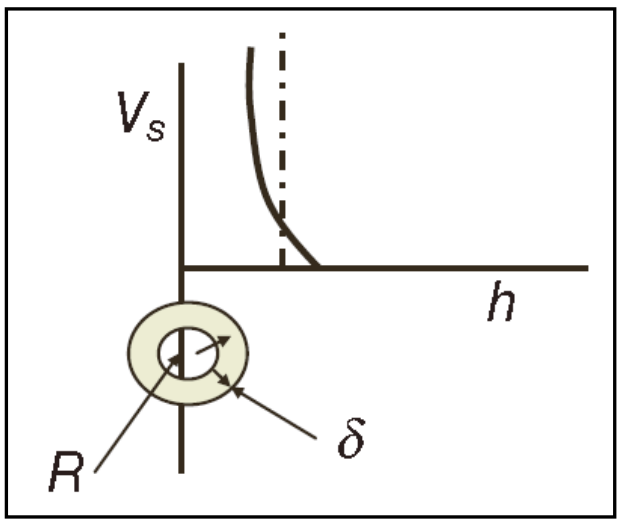

Figure A.11: Steric interactions (Tradros, 2010: 8).

© University of Pretoria

Two mechanisms contribute to this type of interaction. The first is due to the free energy gained when the surfactant or polymer molecules mix (G_{mix}). The second is due to the loss of configuration of the adsorbed molecules when the particles approach one another (elastic interaction: G_{el}) (Bognolo & Tadros, 2000).

These two types of interactions are described by equations A.17 and A.18 (Bognolo & Tadros, 2000):

$$\frac{G_{mix}}{kT} = \frac{4\pi.MV_{Pol}^2}{MV_{Sol}}.cn^2.(1/2 - \chi)(\delta - \frac{h}{2})^2\left(3R + 2\delta + \frac{h}{2}\right) \qquad \text{(A.17)}$$

Where MV_{Pol} is the molar volume of the polymer, MV_{Sol} is the molar volume of the solvent, cn is the number of chains per unit area, δ is the layer thickness and χ is the Flory Huggins interaction parameter (Bognolo & Tadros, 2000).

And:

$$\frac{G_{el}}{kT} = 2v_2 ln\frac{\Omega(h)}{\Omega(\infty)} \qquad \text{(A.18)}$$

Where $\Omega(h)$ is the number of configurations of the chain at a separation distance equal to h. $\Omega(\infty)$ is the value at infinite separation (Bognolo & Tadros, 2000).

Equation A.17 applies when two particles approach one another to a distance smaller than twice the layer thickness. From this equation it can be seen that the chain solvent interaction parameter (χ) determines if the interaction force will be repulsive or attractive. If χ is smaller than 0.5, G_{mix} will be positive and therefore repulsive. If χ is larger than 0.5, G_{mix} will be negative and the interaction force will be attractive. When χ = 0.5, the theta condition is reached. This is where the change over from attractive to repulsive (or vice versa) interaction occurs (Bognolo & Tadros, 2000).

© University of Pretoria

From equation A.18 it can be seen that G_{el} is always positive and therefore repulsive. The steric interaction between two particles (G_{steric}) with adsorbed layers is given by (Bognolo & Tadros, 2000):

$$G_{steric} = G_{mix} + G_{el} \tag{A.19}$$

Van der Waals Attraction

This type of interaction arises from the motion of electrons in a molecule leading to fluctuations in charge (London forces). For two identical particles, the attraction force is given by (Bognolo & Tadros, 2000):

$$V_A = -\frac{HR}{12h} \tag{A.20}$$

The Hamaker constant: H sums the contribution of all the atoms or molecules (H_{11}) and the medium (H_{22}) (Bognolo & Tadros, 2000):

$$H = (H_{11}^{1/2} - H_{22}^{1/2})^2 \tag{A.21}$$

From equation A.20 it can be seen that V_A increases with a decrease in the separation distance (h) and the attractive force can reach large values. This is plotted in Figure A.12 (Bognolo & Tadros, 2000).

© University of Pretoria

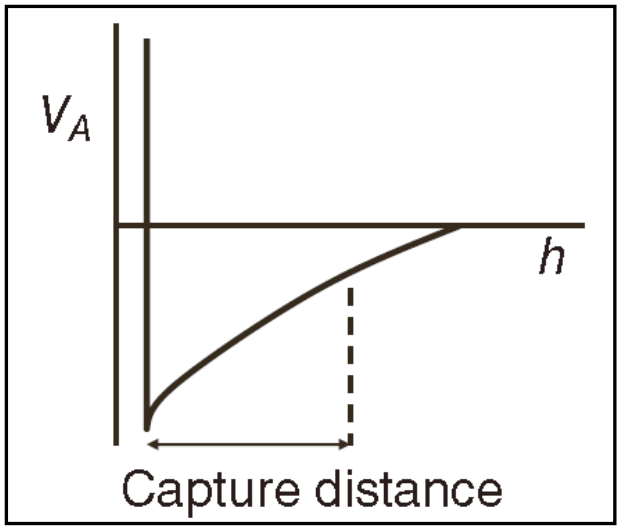

Figure A.12: Van der Waals attraction (Tradros, 2010: 8).

A.2.2.4. Theories of Colloid Stability.

As mentioned in the beginning of this section, a dispersion is stable when the total amount of particles in a dispersion remains constant and resists the formation of aggregates (Parfitt, 1973: 10 and Williams, 1994: 25). By combining the above mentioned theories, colloid stability can be obtained (Bognolo & Tadros, 2000).

Electrostatic Stabilization

This theory of stability applies to lyophobic colloids. It combines the electrostatic interaction and the Van der Waals attraction. The resultant force is (Bognolo & Tadros, 2000):

$$V_T = V_R + V_A \tag{A.22}$$

From this equation an energy-distance curve is obtained as shown in Figure A.13.

© University of Pretoria

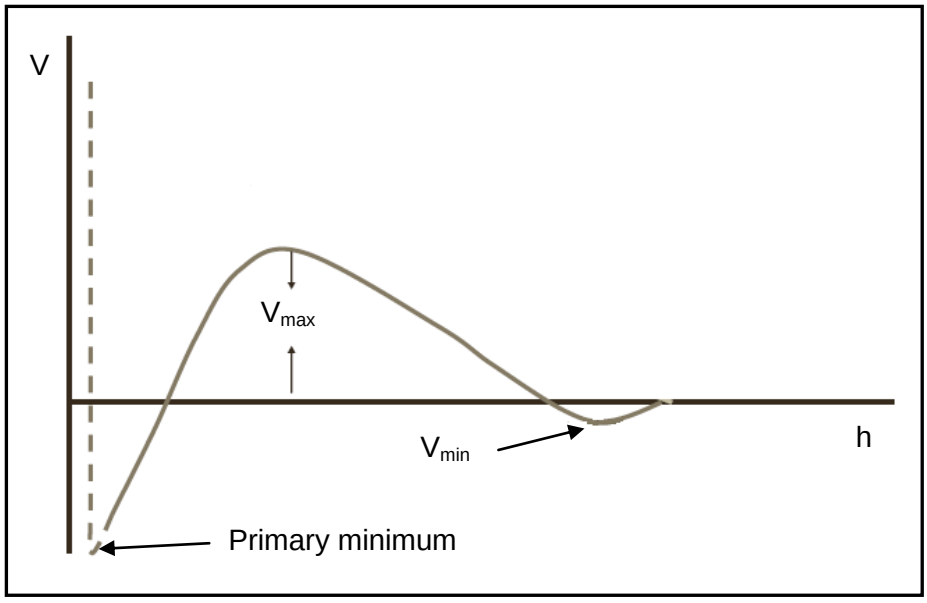

Figure A.13: Energy-distance curve for Electrostatic stabilization (Bognolo & Tradros, 2000).

The curve has two minimum values and one maximum value. V_R and V_A both decrease with an increase in separation distance. From equations A.15 ($V_R = 4\pi\varepsilon_r\varepsilon_o R^2\Psi_0^2 \exp[-\kappa(h-2R)]/h$) and A.20 ($V_A = -\frac{AR}{12h}$) it can be seen that V_R decrease exponentially and V_A decrease as an inverse power (Bognolo & Tadros, 2000).

At short separation distances, V_A is much larger than V_R and V_T is attractive (primary minimum). The same occurs at large separation distances (secondary minimum). When the distance between the two particles is intermediate, V_R is much larger than V_A and the resulting force is repulsive. Therefore to stabilize two particles, V_{max} (plotted in Figure A.13) must be as large as possible (Bognolo & Tadros, 2000).

V_{max} depend on (Bognolo & Tadros, 2000):

- The surface potential (Ψ_0)
- Particle radius R
- The electrolyte concentration (C from equation A.17)
- The Hamaker constant (H)

© University of Pretoria

To increase V_{max} value, the surface potential must be increased (equation A.15). This can be done by changing the pH of the solution. V_{max} can also be increased with a decrease in electrolyte concentration. When the electrolyte concentration is decreased, κ decreases (equation A.16). This results in a slower exponential decay and consequently an increase in V_{max} (Bognolo & Tadros, 2000).

Steric Stabilization

The theory of steric stabilization is based on the combination of steric repulsion and Van der Waals attraction. Here the interactions are represented as free energies (Bognolo & Tadros, 2000):

$$G_T = G_{Steric} + G_A = G_{mix} + G_{el} + G_A \quad \text{(A.23)}$$

Equation A.24 is the summation of equations A.17, A.18 and A.20. The interaction-distance curve for the steric stabilization mechanism is given in Figure A.14 (Bognolo & Tadros, 2000).

© University of Pretoria

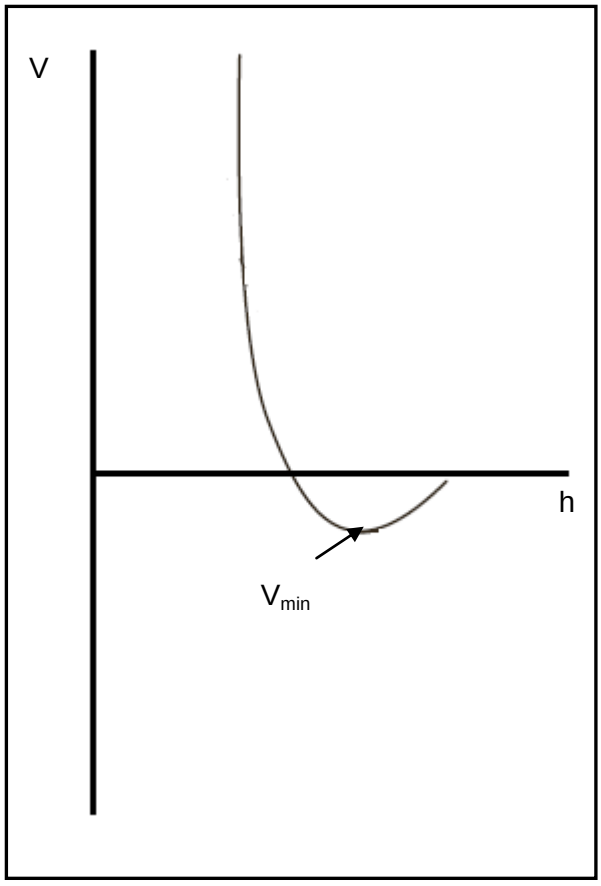

Figure A.14: Steric stabilization interaction-distance curve (Bognolo & Tradros, 2000).

The curve only forms one minimum at a separation distance equal to twice the adsorbed layer thickness. As the separation distance decreases further, the interaction increases sharply with the particles having a repulsive force on one another (Bognolo & Tadros, 2000).

G_{min} depends on the adsorbed layer thickness (δ), the particle radius and the Hamaker constant. With small particles and thick layers, G_{min} can be very small. This means that the colloid can approach thermodynamic stability (Bognolo & Tadros, 2000).

Electrosteric Stabilization

This theory combines electrostatic interactions, steric interactions and Van der Waals interactions. This normally occurs with charged particles with adsorbed

© University of Pretoria

polymers or non-ionic surfactants. This is described by equation A.25 (Bognolo & Tadros, 2000):

$$G_T = G_{Steric} + G_R + G_A \qquad \text{(A.24)}$$

The energy of interaction distance curve is given in Figure A.15. This curve has a small minimum at large separation (attractive Van der Waals force), followed by an ill-defined maximum as the separation distance decreases. This maximum is due to double layer repulsion (electrostatic interaction). As the separation distance is further decreased, the interaction increases sharply due to steric repulsion (Bognolo & Tadros, 2000).

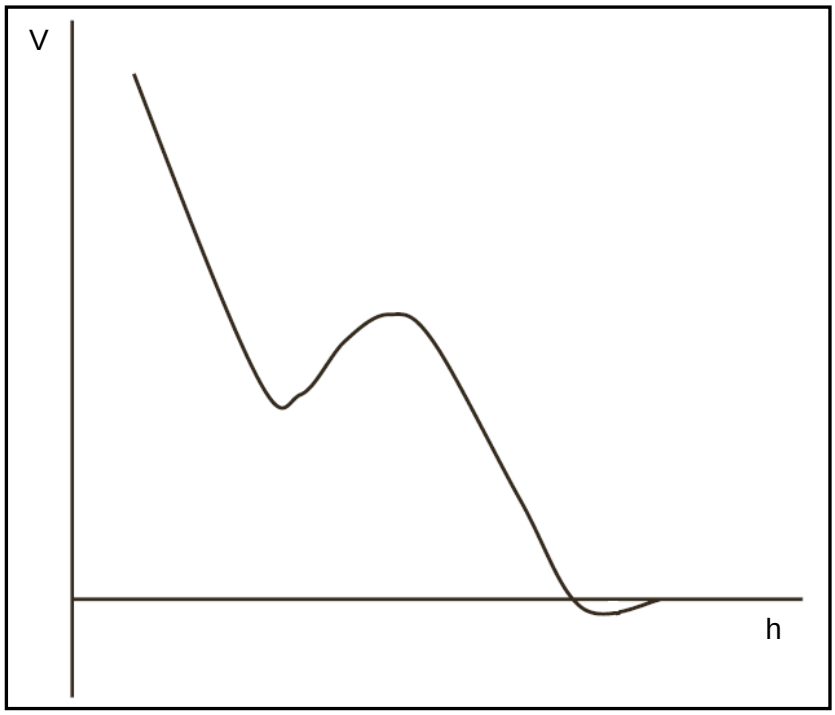

Figure A.15: Electrosteric energy of interaction-distance curve (Bognolo & Tradros, 2000).

From this discussion it can be concluded that the formation of dispersions requires understanding of the interactions of the particles with the liquid. Concepts such as the surface tension and the mechanisms involved with the formation of dispersion were covered. Finally the Deryaguin, Landau, Verwey and Overbeek (DLVO) theory

© University of Pretoria

of flocculation was discussed which forms the basis for the theories on dispersion stabilization (Bognolo & Tadros, 2000).

A.3. REFERENCES

1. Bognolo, G and Tadros, TF (2000) “Fundamental aspects of suspension stabilization and some of their applications”, Chimica & Industria.

2. Bowker, M (2002) “Surface science: The going rate for catalyst”, Nature Materials 1: 205-206.

3. Chin, SJ, Hsu, TH, Lin, KW, Lu, CL & Yen, A (2012) “Sub-20nm node photomask cleaning enhanced by controlling zeta potential”, SPIE Newsroom. DOI: 10.1117/2.1201212.004559.

4. Everett, DH (1994) *Colloid Science*, Royal Society of Chemistry, Cambridge.

5. Focke, WW (2011) “Particle suspension formulation”, Class Notes, Department of Chemical Engineering, University of Pretoria.

6. Ford, PW, Margvelashvili, N, Parslow, J, Robson, B and Webster, IT (2003) “Conceptual models of the hydrodynamics, fine sediment dynamics, biogeochemistry and primary production in the Fitzroy Estuary”,

7. Parfitt, GD (1973) *Dispersion of Powder in liquids*, Applied Science Publishers LTD, London.

8. Tadros, TF (2010) *Rheology of Dispersions: Principles and Applications,* Wiley-VCH Verlag & Co. KGaA, Weinheim, Germany

9. Tadros, TF (2013) *Emulsion Formation and Stability,* Wiley-VHC Verlag GmbH & Co., Weinhein, Germany.

10. Williams, RA (1994) *Colloid and Surface Engineering*. Great Britain: Butterworth-Heinemann.

© University of Pretoria

Appendix B: Dispersion Preparation Methodology

1. Weigh the mass of oil, particles and dispersant required in separate containers. This will minimise errors that can be made should all the materials be measured in one container.
2. Heat base fluid (correct amount), while fluid is continuously stirred (400-800 rpm).
3. Add dispersant and continue with heating and stirring until dispersant dissolves. The temperature where the dispersant dissolves will depend on the dispersant.
4. Add the particles and continue stirring (400-800 rpm), while temperature is controlled 5 °C above dissolving point of dispersant.
5. When the particles are evenly distributed, remove the container from the heating source and place it in the ultrasonic bath. The temperature of the solution (for this study water was used) in the ultrasonic cleaner must also be 5 °C above the dissolving point of the dispersant.
6. Ensure that the level of the solution (water) is the same as the dispersion level in the container.
7. Switch on the ultrasonic cleaner and sonicate the dispersion for one hour. Stir the dispersion every 15 minutes.
8. Note that the total volume of the dispersion required for friction and wear testing will not exceed 100 ml for every hour.
9. It is also important to prepare a new dispersion for every test. This to ensure that the fluid is consistent in its properties and that no aggregates and agglomerates were formed.

© University of Pretoria